CHEMICAL REVIEWS

Review

pubs.acs.org/CR

Graphene-Supported Nanoelectrocatalysts for Fuel Cells: Synthesis, Properties, and Applications

Minmin Liu,[†,‡,§] Ruizhong Zhang,[†,‡,§] and Wei Chen*[,†]

[†]State Key Laboratory of Electroanalytical Chemistry, Changchun Institute of Applied Chemistry, Chinese Academy of Sciences, Changchun 130022, Jilin, China

[‡]University of Chinese Academy of Sciences, Beijing 100039, China

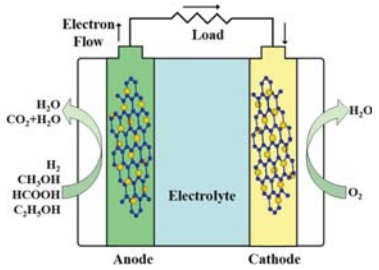

CONTENTS

1. INTRODUCTION

With the rapid increase of energy demand in people's daily life and the depletion of fossil fuel reserves, research on new environment-friendly energy sources and their practical applications has attracted increasing attention in the past decades.[1−3] Ensuring clean and efficient energy sources is one of the biggest challenges that we face in the 21st century. Among the proposed clean energy sources, fuel cells, such as proton exchange membrane fuel cells (PEMFCs), direct methanol fuel cells (DMFCs), direct formic acid fuel cells (DFAFCs), etc., have been considered a class of the most promising power sources with high energy density and high efficiency.[4−7] A fuel cell is an electrochemical device that can convert the chemical energy of a fuel into electrical energy

Received: October 6, 2013
Published: March 25, 2014

   dx.doi.org/10.1021/cr400523y | Chem. Rev. 2014, 114, 5117−5160

through chemical reactions on the interface of electrode and electrolyte. The main reactions in a fuel cell include the fuel oxidation on anode and the oxygen reduction on cathode. Among the metal catalysts for anode and cathode reactions, platinum (Pt) exhibits the highest electrocatalytic activities for electro-oxidation of small organic fuels on the anode and the oxygen reduction on the cathode. However, with Pt alone as catalyst, several obvious disadvantages largely limit its application in fuel cells. First, for small organic fuels oxidation on Pt, the self-poisoning originated from the strong CO adsorption on the surface of Pt will decrease its catalytic performance. Second, with Pt as cathodic catalyst in DMFCs, the methanol crossover from anode to cathode may reduce the ORR performance due to the mixed potentials formed from the simultaneous methanol oxidation and oxygen reduction at cathode. Third, the limited reserve in nature and the resulting high-cost hinds the wide commercialization of fuel cells. According to the annual report of the U.S. Department of Energy (DOE) in 2008, the Pt-based catalyst ink accounts for 27−43% of the cost of a direct H_2 PEM fuel cell stack.[8] The total cost of a fuel cell stack can be largely reduced by lowering the catalyst loading and using low- or non-Pt-based electrocatalysts. Therefore, how to improve the catalytic activities and lower the costs of anode and cathode catalysts are the critical issues to realize the real commercialization of fuel cells.[9]

To obtain ideal electrocatalysts for fuel cells with high catalytic performance and low price, much effort has been devoted to designing novel structured catalysts. Especially, the nanostructured materials meet excellently the requirements of a catalyst candidate with large surface area, increased surface active sites, and low metal loading. Up to now, various chemical and physical methods have been well-developed for preparing nanocrystals with desired surface facets. So far, the developed electrocatalysts can be mainly classified into the following categories: (1) The first is Pt-based nanocatalysts.[10] By incorporating transition metals into Pt, various Pt-based bimetallic and ternary nanocatalysts, such as PtRu,[11,12] PtFe,[13−17] PtNi,[18] PtCu,[19] PtCo,[20] PtMn,[21] and PtIr,[22] etc., have been designed to improve their catalytic performance and reduce the costs.[10,23] It should be pointed out that, as compared to the Pt alone catalysts, Pt-based electrocatalysts have enhanced catalytic performance and improved tolerance toward CO poisoning due to the so-called bifunctional mechanism and/or ligand effect.[24−28] (2) The second is Pd-based nanocatalysts.[29,30] Because of the similar intrinsic properties but lower cost as compared to Pt, Pd-based nanostructured materials have been constructed and used as fuel cell electrocatalysts. Moreover, in situ spectroelectrochemical investigations revealed that there is little CO poisoning during organic small molecule oxidation on Pd-based electrocatalysts, which can enhance their electrocatalytic performance. The catalytic activity of Pd-based catalysts can be effectively manipulated by alloying with different transition metals[31−37] and by fabricating different nanostructures.[38−47] (3) The third is non-noble metal nanoelectrocatalysts. To further reduce the costs of electrocatalysts, Pt- and Pd-free nanostructured materials have also been studied as catalysts, for instance, coinage metal nanoclusters,[48−52] transition metal oxides and sulfides,[53−58] transition metal macrocyclic complexes,[59,60] metal-containing porphyrin compounds,[61] carbon-supported iron- and cobalt-based catalysts,[62,63] metal nitrides,[64] and so on. (4) The final category is metal-free and heteroatom-doped carbon materials. In recent years, it has been found that single, binary, or ternary N, P, B, and S-doped carbon materials, such as graphene, carbon nanotubes (CNTs), nanofibers, exhibit enhanced electrocatalytic activity for oxygen reduction due to the conjugation between the π electrons of carbon and the lone pair electrons from dopants.[65−67] Such metal-free materials have promising applications in fuel cells as cathode catalysts with high activity, low price, and high methanol tolerance.

Besides the considerations of the catalytic activity and cost, the stability and lifetime of a catalyst are also the critical issues for its practical applications in fuel cells. When the above materials are used as fuel cell catalysts, they are usually dispersed on a catalyst support. A good catalyst support should meet some requirements, such as large surface area for catalyst dispersion, highly electric conductivity, and high electrochemical stability in acidic or alkaline electrolytes. At present, the state-of-the-art commercial catalysts are usually prepared by dispersing catalyst nanoparticles (2−5 nm) on carbon supports. However, previous studies showed that, except for the metal catalyst degradation because of the dissolution and aggregation of metal nanoparticles, the severe corrosion and oxidation of carbon support materials under the real fuel cell operating environment could also lead to the quick activity loss of the catalysts. In recent years, various catalyst support materials have been proposed to address the challenges. In addition to the traditional carbon materials, noncarbon materials, such as metal oxides, electronically conductive polymers, carbides, and nitrides, etc., have also been proposed as catalyst supports in the past decades.[68]

In the carbon material family, graphene is a new star member discovered in 2004 by Geim et al.[69] Graphene has a unique two-dimensional and single-atom thick structure with sp^2-bonded carbon atoms densely arranged in a honeycomb crystal lattice. Heteroatom-doped graphene has been found to show high electrocatalytic activity for ORR. On the other hand, graphene nanosheets (GNs) have exhibited promising wide applications as 2-D catalyst support due to the following properties. First, graphene possesses a large theoretical specific surface area (SSA) of ~2600 m^2/g, which is twice that of single walled CNTs. Second, graphene has a fully conjugated sp^2 hybridized planar structure, giving rise to ultrahigh electrical conductivity, excellent mechanical properties, and high thermoconductivity. Third, the chemically converted graphene with interlayer structure contains lattice defects (vacancies, holes) and surface functional groups (carbonyls, epoxides, hydroxyls, etc.), which can anchor and immobilize metal nanoparticles on its surface. Because of the strong metal−substrate interaction, the stability of nanocatalysts can be improved by dispersing on graphene.[70,71] For instance, by using density functional theory (DFT) and bond-order potential calculations, Fampiou and Ramasubranabuam[70] found that the surface defects in graphene support can act as strong binding traps for Pt nanoclusters, which leads to the long-term stability toward sintering of Pt−graphene composites. Moreover, the catalytic activity of the graphene-supported catalysts can be enhanced because of the increasing charge transfer from catalysts to graphene substrate. From the above, the unique properties of graphene meet very well the basic requirements of an ideal catalyst support. Therefore, notable effort has been devoted to the design of novel nanostructured catalysts dispersed on graphene support. Our recent study[72] showed that, as compared to Pt/C commercial catalyst and unsupported PtPd nanoparticles, graphene-supported PtPd alloy nanocrystals exhibited higher catalytic performance and much higher durability for methanol

dx.doi.org/10.1021/cr400523y | Chem. Rev. 2014, 114, 5117−5160

Table 1. Heteroatom-Doped Graphene Materials and Their Applications in Electrocatalysis

material	preparation method	precursor	dopant	ref
B-graphene	CVD	CH_4/B_2H_6	boron	99
		polystyrene/boric acid	boron	100
	arc discharge	graphite/H_2/B_2H_6	boron	87
	thermal annealing	GO/B_2O_3	boron	117
		graphite/H_3BO_3	boron	118
N-graphene	CVD	CH_4/NH_3	nitrogen	88, 94
		acetonitrile/NH_3	nitrogen	95
		pyridine	nitrogen	96, 98
		H_2/ethylene/NH_3	nitrogen	97
		polystyrene/urea	nitrogen	100
	arc discharge	graphite/H_2/pyridine(ammonia)	nitrogen	87
	thermal annealing	graphene/NH_3	nitrogen	105, 106
		GO/melamine	nitrogen	116
		GO/NH_3	nitrogen	107, 109, 119
		GO-silica/NH_3	nitrogen	121
		Ni(C)/B(N)	nitrogen	110
		GO/5-aminotetrazole	nitrogen	385
	pyrolysis	sugar/urea	nitrogen	115
		GO/polypyrrole	nitrogen	114
	plasma treatment	graphene/nitrogen	nitrogen	129−131
		GO/hydrogen/nitrogen	nitrogen	132
		gaphene/NH_3	nitrogen	133
		GO/H_2 and NH_3	nitrogen	134
		PMMA[a]/N_2 and H_2	nitrogen	135
	solvothermal	Li_3N/CCl_4 or $N_3C_3Cl_3/Li_3N/CCl_4$	nitrogen	140
		GO/hydrazine hydrate	nitrogen	141
	hydrothermal	GO/hydrazine/ammonia	nitrogen	142
P-graphene	thermal annealing	GO, triphenylphosphine	phosphorus	112
	pyrolysis	toluene, triphenylphosphine	phosphorus	113
S-graphene	CVD	hexane/sulfur powder	sulfur	101
	thermal annealing	GO/benzyl disulfide	sulfur	120
		GO-silica/H_2S	sulfur	121
I-graphene	thermal annealing	GO/iodine	iodine	111
B,N-graphene	thermal annealing	GO/H_3BO_3/NH_3	boron and nitrogen	122
S,N-graphene	thermal annealing	GO, melamine, benzyl disulfide	nitrogen and sulfur	123
	hydrothermal	GO, ammonium thiocyanate	nitrogen and sulfur	124
P,N-GNs	pyrolysis	GO, dicyandiamide, phosphoric acid	nitrogen and phosphorus	125

[a]PMMA: polymethylmetacrylate.

oxidation. It is anticipated that graphene-supported nanomaterials represent a promising class of electrocatalysts for fuel cells.

Despite that great efforts have been dedicated to the investigation of graphene-based nanomaterials and a number of reviews on graphene have been published,[73−81] a comprehensive overview on the graphene-based nanoelectrocatalysts for fuel cells is still absent. To keep up to date with the rapidly increasing advances in this field, it is time to review the recent progress and the challenges of the graphene-supported nanoelectrocatalysts. In this Review, we summarize first the developed synthetic techniques for the preparation of doped graphene and graphene-supported nanoelectrocatalysts. The structure-dependent properties then will be presented. In the following section, the application of graphene-based nanoelectrocatalysts in fuel cells as anode and cathode catalysts will be discussed in detail. Finally, a brief conclusion and an outlook on the development of graphene-based elecrocatalysts will be provided. We hope that this Review is helpful to push forward the advancement of this research field.

2. SYNTHESIS OF FUNCTIONALIZED GRAPHENE AND GRAPHENE-SUPPORTED ELECTROCATALYSTS

Overall, graphene-based electrocatalysts include heteroatom-doped graphene and graphene-supported nanocomposites. It is well-known that the activities of catalysts are strongly dependent on their surface properties. Especially for the graphene-supported nanocomposites, their electrocatalytic properties can be largely influenced by the composition, particle size and the exposed surface planes of the composites and the interfacial interactions between composites and graphene support. Up to now, different physical and chemical methods have been successfully used to prepare heteroatom-doped graphene and graphene-supported nanocomposites. In this section, the synthetic methods for preparation of graphene-based electrocatalysts are outlined on the basis of the catalyst composition, that is, graphene and heteroatom-doped graphene catalysts, graphene-supported non-Pt nanocatalysts, and graphene-supported Pt and low-Pt nanocatalysts.

dx.doi.org/10.1021/cr400523y | Chem. Rev. 2014, 114, 5117−5160

2.1. Synthesis of Graphene and Heteroatom-Doped Graphene Electrocatalysts

Since graphene was obtained by a manual mechanical cleavage of graphite with Scotch tape the first time, a wide range of techniques have been developed for synthesizing graphene sheets. These methods can be divided into top-down and bottom-up strategies. Top-down methods include micromechanical cleavage of highly oriented pyrolitic graphite (HOPG), intercalation/exfoliation from graphite by means of oxidation,[82,83] oxidative splitting or unzipping of CNTs via etching for the fabrication of nanoribbons,[84,85] and chemical oxidation of graphite to graphite oxide to obtain mildly oxidized graphene. Bottom-up approaches have been widely employed to fabricate large, continuous graphene or heteroatom-doped graphene films for practical applications, including arc-discharge approach,[86,87] chemical vapor deposition (CVD) on catalytically active metals,[88,89] epitaxial growth on single-crystal SiC,[90] etc. Especially, chemical dopping with foreign atoms is an effective approach to manipulate the electronic and chemical properties of graphene. Recent studies have shown that heteroatom-doped graphene materials have potential applications in fuel cells as metal-free electrocatalysts. Under certain conditions, carbon atoms in the hexagonal honeycomb lattice of graphene can be replaced by foreign atoms, such as nitrogen, boron, sulfur, etc. The most commonly used methods for the preparation of graphene, especially heteroatom-doped graphene, are summarized in Table 1 and discussed in detail below.

2.1.1. Chemical Vapor Deposition (CVD). CVD is a kind of common and popular method for controllably synthesizing various types of nanomaterials. In recent years, CVD has also been widely used as an efficient method to synthesize mono- or multilayer graphene or B-, N-, S-, and P-doped graphene nanosheets with high quality. The previous studies found that with the CVD method, the nucleation and growth of graphene occur via arranging carbon and foreign atoms on surfaces of transition metal catalysts.[89,91,92] In CVD methods, graphene sheets can be obtained by using CH_4 and hydrocarbon gases as carbon sources under high deposition temperatures (e.g., 1000 °C). Ruoff and co-workers reported a typical CVD method to grow large-area graphene films in the order of centimeters directly on the surface of copper foils using a mixture of methane and hydrogen as carbon resources at temperatures up to 1000 °C.[91] The electron microscopy (SEM, TEM) and Raman spectroscopy characterizations showed that the formed graphene films are highly uniform and predominantly single-layer products. It was found that on Cu substrate the graphene growth is a surface-catalyzed and self-limited process. In another work, Kim et al.[93] synthesized large-scale graphene films with high quality by using CVD method on thin nickel layers. More importantly, the graphene monolayer can be transferred to various arbitrary substrates while maintaining their low sheet resistance (~280 Ω per square) and high optical transparency (80%), which makes them perfect applications in electronic devices.

As for the preparation of N-doped graphene (denoted as N-graphene) with CVD method, a similar process is used except for introducing nitrogen-containing precursors as nitrogen source.[88,94−98] In the previous reports, NH_3 and other organic compounds have been used as nitrogen sources. For example, Dai and co-workers[94] developed a CVD method for synthesizing N-graphene films on nickel film. In the synthesis, Ni film was first deposited on a SiO_2/Si substrate. After the Ni film was heated to 1000 °C under argon atmosphere, a gaseous mixture with the composition of NH_3:CH_4:H_2:Ar = 10:50:65:200 was introduced, followed by a flow of NH_3 and Ar for another 5 min. After treatments with aqueous HCl solution, the N-graphene film can be transferred onto different substrates. From the digital photo image shown in Figure 1a, the as-synthesized N-graphene film is flexible and transparent. The atomic force microscopy (AFM) measurements (Figure 1b and c) showed that the formed N-graphene film is highly uniform with a smooth surface. The height analyses indicated that the N-graphene film is 0.9−1.1 nm in thickness, consisting of only one or a few layers of carbon atoms. The X-ray photoelectron spectroscopic (XPS) measurements indicated the presence of both pyridine-like and pyrrolic nitrogen atoms in the product. In addition to NH_3, liquid N-precursors such as acetonitrile and pyridine have also been used as nitrogen sources for the synthesis of N-graphene. Jin et al.[98] successfully synthesized monolayer N-graphene in centimeter-scale sheets by CVD process with pyridine as the sole source of both carbon and nitrogen. Imamura and Saiki[96] found that the substrate temperature and N-containing source materials have strong effects on the formation of N-graphene. In their study, when pyridine was used as precursor, N-graphene can be formed on a Pt(111) surface at the substrate temperature (T_s) higher than 500 °C, while nitrogen can not be doped into graphene at T_s higher than 700 °C. However, with the same substrate, only graphene but not N-graphene can be obtained by using acrylonitrile as precursor at any temperature. On the basis of the proposed N-doping mechanism of "bond breaking and bonding reforming" two processes, the weak single C−C bond in acrylonitrile is preferentially broken, resulting in the formation of CN fragments. Because of the formation of

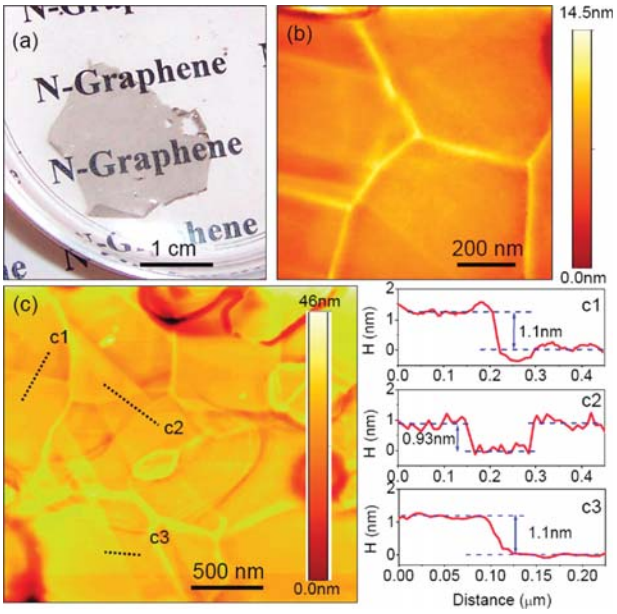

Figure 1. Characterizations of the N-doped graphene film. (a) A digital photo image of a transparent N-doped graphene film floating on water; (b,c) atomic force microscopy (AFM) images of the N-graphene film and the corresponding height analyses along the lined marked in the AFM image (c1−c3 in panel c). Reprinted with permission from ref 94. Copyright 2010 American Chemical Society.

dx.doi.org/10.1021/cr400523y | Chem. Rev. 2014, 114, 5117−5160

other molecules from CN fragments, N can not be doped into the formed graphene sheets.

In addition to nitrogen, other heteroatoms have also been successfully doped in graphene through CVD process. Cattelan et al.[99] synthesized single layer boron-doped graphene (B-graphene) on polycrystalline copper foil through CVD method by using methane and diborane as carbon and boron sources. In the synthesis, a two-step process was adoped to prepare the B-graphene. As shown in Figure 2, large graphene patches were

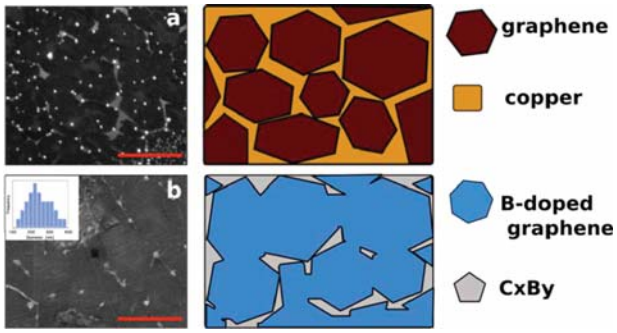

Figure 2. SEM micrographs of the boron-doped graphene synthesized by CVD method on copper polycrystalline foils and schematic diagram of the two-step growth. (a) First step of the synthesis of large graphene domains covered about 80% of the copper surface; (b) second step with the further growth of graphene islands and the nucleation of some 3D clusters of nonstoichiometric boron carbide on bare copper surface areas. Both scale bars are 3 μm. Reprinted with permission from ref 99. Copyright 2013 American Chemical Society.

first formed by exposing Cu substrate in methane and hydrogen at 1000 °C. At this stage, about 85% of the copper surface is covered by single layer graphene. In the second step, with the further growth of graphene islands and introduction of B_2H_6, nonstoichiometric boron carbides were formed on the bare Cu surface area between graphene domains, which can migrate by diffusion into the graphene patches to produce boron-doped graphene films. With CVD approach, Wu et al.[100] synthesized nitrogen- and boron-doped graphene on Cu foil substrate by using polystyrene, urea, and boric acid as C-, N-, and B-containing precursors, respectively. By changing the ratio of the precursors, the doping concentration of N can be tuned from 0.9% to 4.8% and B can be modulated from 0.7% to 4.3%. It was found that the nitrogen types vary with the doping concentration of N in graphene films. For the N-graphene with doping of about 2.1%, the N-binding configuration is predominated by pyridinic N. However, for the N-graphene with doping of about 4.8%, 60.2 at. % pyridinic N and 39.8 at. % pyrrolic N are presented in the product. Such a result indicates that the properties of N-graphene can be manipulated by controlling the doping concentration. With CVD technique, Gao et al.[101] synthesized sulfur-doped graphene sheets by using sulfur powder and hexane as the growth precursors. On the basis of the XPS, high-resolution TEM, and elemental mapping characterizations, it was proposed that S atoms tend to form linear nanodomains in graphene lattice. The S-graphene exhibited p-type semiconductor behavior.

However, it should be noted that CVD or ultrahigh vacuum (UHV) CVD techniques usually require transition metals as substrate materials. The high cost of the single crystal substrates, special synthetic instruments, and the extreme conditions, such as high temperature (1000 °C), ultrahigh vacuum, greatly limit its large-scale application.

2.1.2. Arc-Discharge Approach. In the past two decades, the arc-discharge method has been widely utilized to prepare carbon-based nanomaterials, such as carbon nanotubes and fullerenes, by evaporating carbon sources at high temperature. This method has also been used in the synthesis of graphene and heteroatom-doped graphene. The properties of graphene more or less depend on the heating modes. Wu et al.[102] developed a hydrogen arc-discharge exfoliation method for the synthesis of graphene. In the method, the presynthesized graphene oxide (GO) was rapidly heated by arc discharge in a mixed buffer atmosphere of H_2/Ar (H_2:Ar =10:90 kPa pressure) with graphite rod as cathode and a rotatable graphite cylinder as anode. The obtained exfoliated graphite was then dispersed in *N*-methylpyrolidone by ultrasonication to produce graphene sheets. The obtained graphene sheets exhibited higher electric conductivity and thermal stability than those of graphene synthesized by argon arc-discharge exfoliation and thermal exfoliation processes. The excellent properties of graphene may be ascribed to the high plasma temperature and hydrogen atmosphere, which can result in efficient exfoliation, considerable deoxygenation of GO, and defect elimination.[102] With a similar method, Rao's group[86] synthesized 2−4 layer graphene flakes by arc discharge between graphite electrodes under a relatively high pressure of hydrogen (above 200 Torr). In their study, with the presence of a mixture of H_2 and diborane or H_2 and pyridine during arc discharge, boron-doped (1−3 wt %) graphene or nitrogen-doped (0.6−1.0 wt %) graphene can be produced. Chen and co-workers[103] developed an arc-discharge method for efficient and large-scale synthesis of few-layered graphene by using a gas mixture of He/CO_2. Volotskova et al.[104] reported a one-step approach for simultaneous preparation and separation of graphene flakes and carbon nanotubes via the arc-discharge method by splitting the high-temperature growth and low-temperature separation zones and depositing nanotubes and graphene in different areas.

The arc-discharge method has also been used to synthesize N- and B-doped graphene. Panchakarla et al.[87] studied the effects of the precursors on the structure and doping degree of the N- and B-graphene. They synthesized two B-graphene samples by using graphite electrodes in the presence of H_2 + B_2H_6 (BG1) or boron-stuffed graphite electrodes (BG2). The electron energy loss spectroscopy (EELS) measurements showed that boron is bonded to sp^2 carbon in both samples. However, the XPS results indicated that the boron doping concentration in BG2 (3.1 at. %) is much higher than that of BG1(1.2 at. %). They also prepared three N-graphene samples by using graphite electrodes in the presence of H_2 + pyridine (NG1), H_2 + ammonia (NG2), and by using the transformation of nanodiamond in the presence of pyridine (NG3). The N-doping concentrations are 0.6 (NG1), 1.0 (NG2), and 1.4 at. % (NG3), respectively. The in-plane crystallite sizes of the undoped graphene, BG1, BG2, NG1, NG2, and NG3 were calculated to be 64, 30, 26, 43, 41, and 19 nm, respectively. The results indicate that the precursors can influence the structure and doping concentration of the heteroatom-doped products.

2.1.3. Thermal Annealing Method. With the presence of heteroatom-containing precursors, doped graphene can be obtained easily through high-temperature annealing graphene or graphene oxide. Up to now, N, S, I, P, and B-doped graphene have been synthesized via different thermal annealing methods.[105−115] Xia and co-workers[116] developed a catalyst-

dx.doi.org/10.1021/cr400523y | *Chem. Rev.* 2014, 114, 5117−5160

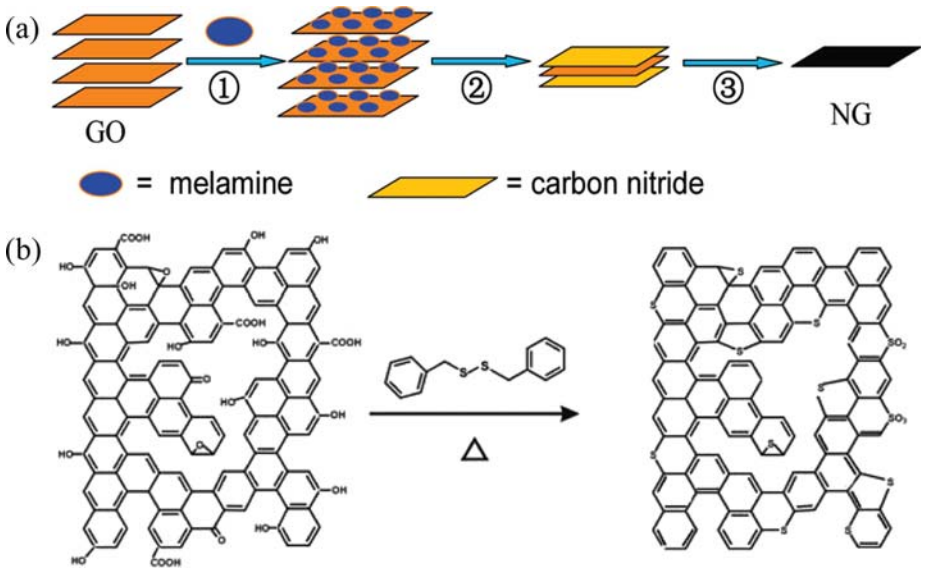

Figure 3. N- and S-doped graphene sheets synthesized by thermal annealing methods. (a) Illustration of the formation of N-doped graphene with melamine as precursor. (1) Melamine adsorption on the surface of GO with a temperature lower than 300 °C; (2) melamine condensed and carbon nitride formed at temperature lower than 600 °C; (3) carbon nitride decomposed and doped into graphene layers at temperature higher than 600 °C. Reprinted with permission from ref 116. Copyright 2011 American Chemical Society. (b) Schematic illustration of S-doped graphene synthesis by using benzyl disulfide as precursor. Reprinted with permission from ref 120. Copyright 2012 American Chemical Society.

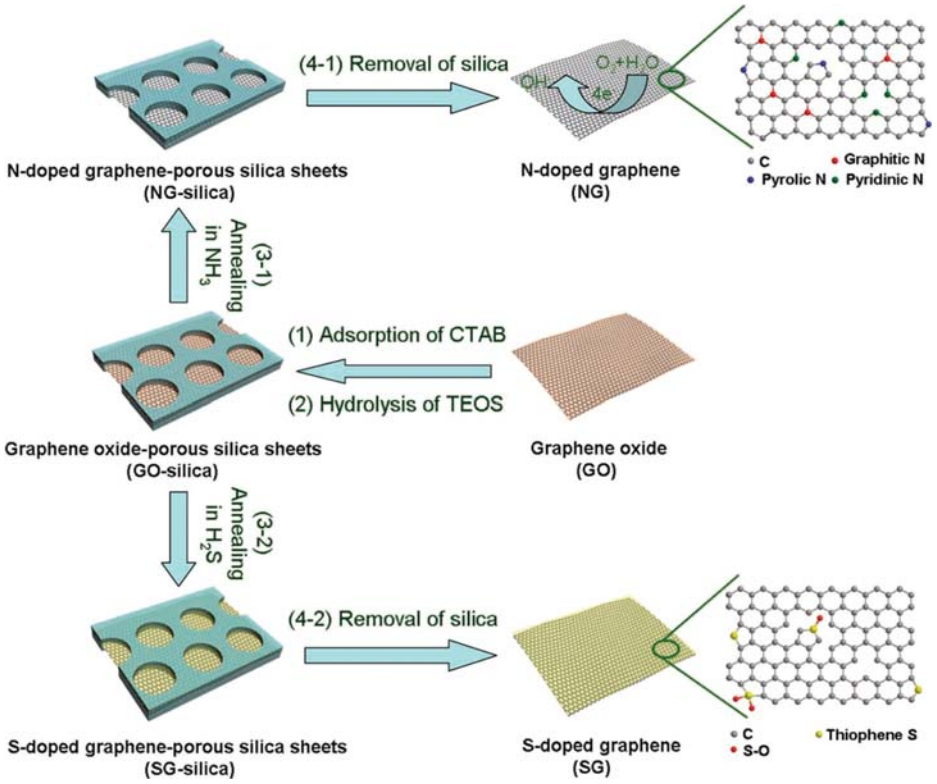

Figure 4. Schematic illustration of the synthesis of N- and S-doped graphene. (1,2) Hydrolysis of tetraethyl orthosilicate (TEOS) on GO surface with the presence of cetyltrimethyl ammonium bromide (CTAB). (3-1) Thermal annealing of GO-silica sheets in ammonia at 600, 800, 900, and 1000 °C, respectively. (3-2) Thermal annealing of GO-silica sheets in H_2S at 500, 700, and 900 °C, respectively. (4-1 and 4-2) Removal of silica by HF or NaOH solution. Reprinted with permission from ref 121. Copyright 2012 Wiley-VCH.

free synthetic method to prepare N-graphene by thermal annealing graphite oxide with melamine as the nitrogen source. As shown in Figure 3a, the method includes three steps. First, melamine molecules were adsorbed on the presynthesized GO. Melamine was then condensed to carbon nitride at high temperature (<600 °C). Finally, with the removal of oxygen

dx.doi.org/10.1021/cr400523y | *Chem. Rev.* 2014, 114, 5117−5160

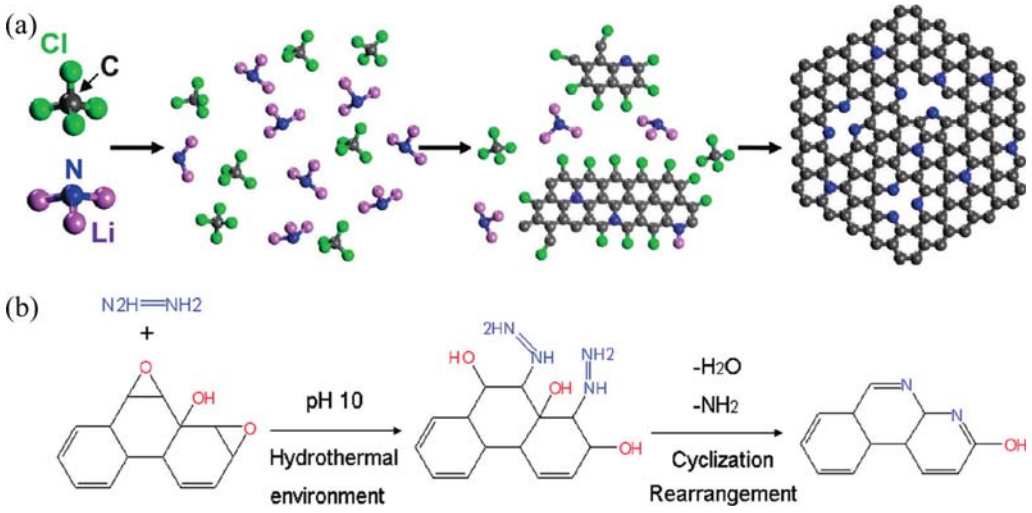

Figure 5. (a) Scheme of the proposed mechanism for solvothermal synthesis of N-doped graphene based on the reaction between CCl_4 and Li_3N. Reprinted with permission from ref 140. Copyright 2011 American Chemical Society. (b) Schematic illustration of the synthesis of nitrogen-doped graphene by a hydrothermal process. Reprinted with permission from ref 142. Copyright 2010 American Chemical Society.

groups on graphene nanosheets at high temperature, nitrogen atoms can be doped in the provided active sites. The nitrogen doping concentration can be adjusted by changing the mass ratio of GO to melamine and the annealing temperature. N-graphene with the highest nitrogen doping level of 10.1% was obtained with a GO/melamine mass ratio of 1/5 at 700 °C. Such synthetic strategy can be applied to the preparation of other heteroatom-doped graphene with appropriate precursors. For instance, a similar approach has been used to synthesize boron-doped graphene multilayers as metal-free electrocatalysts in fuel cells.[117] Boron-doped single-layer graphene was prepared by mixing boric acid and graphite and thermally treating at 2450 °C in an argon atmosphere.[118] Li et al.[119] prepared N-graphene by thermal annealing GO in ammonia atmosphere. They found that the oxygen-containing groups on GO surface are essential for the C−N formation from the reaction between GO and NH_3. In the study, the highest N-doping concentration of 5% was achieved at 500 °C. In another work, Yang et al.[120] synthesized sulfur-doped graphene through thermal annealing method at 600−1050 °C by using benzyl disulfide as precursor (Figure 3b). It was found that the S doping level decreases with increasing annealing temperature (1.53%, 1.35%, and 1.30% at 600, 900, and 1050 °C, respectively). Recently, Mullen and co-workers[121] developed a novel method to prepare N- and S-doped graphene by thermal reaction. As shown in Figure 4, sandwich-like GO-porous silica sheets were first fabricated by hydrolysis of tetraethyl orthosilicate with the presence of cetyltrimethyl ammonium bromide. The formed hybrids were then annealed at high temperature (500−1000 °C) under NH_3 or H_2S atmosphere. N- or S-graphene can be finally obtained after removal of the silica template by etching. XPS measurements showed that S and N have been doped into graphene sheets with a major form of thiophene-like S and three types of nitrogen, including pyridinic-N, pyrrolic-N, and graphitic-N. Also, the doping levels of S and N are in the ranges of 1.2−1.7% and 2.4−2.6%, respectively.

Besides single-doping, codoping of graphene has also been achieved through thermal annealing treatment. Wang et al.[122] reported a facile approach to prepare boron and nitrogen codoped graphene by thermal annealing GO in the presence of boric acid under ammonia atmosphere. Tunable B/N codoping levels can be achieved by changing annealing temperature and time. In the study, $B_7C_{87}N_6H_{26}$, $B_{12}C_{77}N_{11}H_{26}$, and $B_{38}C_{28}N_{34}H_{26}$ were obtained with the annealing times of 0.5, 1, and 2 h, respectively at the annealing temperature of 1000 °C. In another work, Liang et al.[123] successfully prepared mesoporous N-,S-dual-doped graphene (N-S-G) via heating treatment of the mixture of GO/SiO_2, melamine, and benzyl disulfide (BDS) at 900 °C. Other dual- or tridoped graphene, such as N,S-,[124] N,P-,[125] and N,S,Se-GNs,[126] have also been synthesized as ORR electrocatalysts.

2.1.4. Plasma Treatment. In recent years, substrate-free gas-phase synthesis of graphene has been achieved through plasma treatment.[127] Hazra et al.[128] reported a method to transform multilayer graphene to single-layer graphene in a hydrogen and nitrogen plasma environment. As compared to the harsh conditions, plasma treatment can be realized at relatively ambient conditions. As a kind of energy-efficient and eco-friendly alternative method to synthesize carbon materials, plasma treatment has been used to prepare heteroatom (mainly N)-doped graphene or GO.[129−133] In N_2 or NH_3 plasma atmosphere, carbon atoms of graphene may be replaced by nitrogen. Wang et al.[129] prepared N-graphene by plasma treatment of graphene nanosheets supported on glassy carbon electrode in a nitrogen atmosphere. The nitrogen percentage doped in graphene can be manipulated in the range of 0.11−1.35% by controlling the exposure time. In this study, it was also found that the plasma treatment can not only lead to the doping of nitrogen in graphene but also increase the oxygen content, which increased from ∼15% in graphene to ∼27% in N-graphene. Recently, Kumar et al.[134] reported a scalable approach to simultaneously reduce GO and introduce nitrogen into GO near room temperature by plasma treatment in a mixed gas atmosphere of H_2 and NH_3. The synthesis can produce gram-scale quantities of N-graphene with high nitrogen doping level of 5.8%. In another study, Wang et al.[135] synthesized single- or double-layer graphene sheets on copper foils through microwave plasma using polymethylmethacrylate as carbon source. N-Graphene with around 5%

dx.doi.org/10.1021/cr400523y | Chem. Rev. 2014, 114, 5117−5160

Table 2. Graphene-Supported Noble Metal Electrocatalysts and Their Applications

material	preparation method	precursor	application	ref
Pt/GNs	chemical reduction	N-GN, $H_2PtCl_6{\cdot}6H_2O$, EG	MOR	109
		GN, Pt salt, $NaBH_4$	ORR	131
		GO, H_2PtCl_6, $NaBH_4$	MOR/ORR	163, 170
		GO, H_2PtCl_6, EG	MOR	165
		GO, PDDA,[a] H_2PtCl_6, $NaBH_4$	MOR/ORR	190
	self-assembly	3D GN, K_2PtCl_4	MOR	159
	electrodeposition	3D GN, H_2PtCl_6	MOR	175
		GO, Cu foil, H_2PtCl_6	MOR	176
	microwave-assisted process	GO, H_2PtCl_6, EG	MOR	180
	impregnation/thermal reduction	GN, $Pt(NO_2)_2(NH_3)_2$, H_2/Ar	MOR/HOR	184, 458
PtPd/GNs	chemical reduction	GO, PVP,[b] $Pt(acac)_2$, $Pd(acac)_2$	MOR	72
		PVP[b]-GN, K_2PtCl_4, $PdCl_2$	MOR	200
	electrodeposition	GO, H_2PtCl_6, $PdCl_2$	MOR/EOR	202, 203
	hydrothermal	GO, K_2PtCl_4, Na_2PdCl_4, NaI, PVP[b]	MOR	204
PtAu/GNs	chemical reduction	GO, H_2PtCl_6, $HAuCl_4$, EG	FAOR	154
		PDDA[a]-GO, H_2PtCl_6, $HAuCl_4$, $NaBH_4$	FAOR	206
	electrodeposition	GN, H_2PtCl_6, $HAuCl_4$	MOR/ORR	207
	microwave-assisted process	N-GN, H_2PtCl_6, $HAuCl_4$	MOR	208
PtRu/GNs	chemical reduction	GO, H_2PtCl_6, $RuCl_3$, EG	MOR/EOR	212
		GO, $Pt(acac)_2$, $Ru(acac)_3$	MOR	216
		3D GN-CNTs, H_2PtCl_6, $RuCl_3$, EG	MOR	219
		GN-N-CNTs, H_2PtCl_6, $RuCl_3$, $NaBH_4$	MOR	220
	microwave-assisted process	PMo_{12}-GN, H_2PtCl_6, $RuCl_3$, EG	MOR	218
		GN-Vulcan C, H_2PtCl_6, $RuCl_3$	MOR	221
PtCo/GNs	chemical reduction	GO, $Co(NO_3)_2$, K_2PtCl_4, CTAB,[c] $NaBH_4$	MOR	222
		GO, H_2PtCl_6, $Co(NO_3)_2$, EG	ORR	225
		GO, H_2PtCl_6, $Co(CH_3COO)_2$, EG	ORR	226
		GO, H_2PtCl_6, $CoCl_2$, $NaBH_4$	MOR/ORR	227, 228
		CTAB[c]-GN, K_2PtCl_4, $CoCl_2$, EG	ORR	229
	electrodeposition	GN, H_2PtCl_6, $(Co(NO_3)_2$	MOR	224
PtNi/GNs	chemical reduction	PDDA[a]-GO, H_2PtCl_6, $NiCl_2$, EG	MOR	230
		GN, H_2PtCl_6, $NiCl_2$, $NaBH_4$	MOR	231
		GO, K_2PtCl_4, $NiC_4H_6NiO_4$, $NaBH_4$	ORR	233
		GO, H_2PtCl_6, $NiCl_2$, hydrazine	MOR	234
		GO, K_2PtCl_6, $NiCl_2$, PVP,[b] $NaBH_4$	MOR	236
PtFe/GNs	chemical reduction	GO, $Pt(acac)_2$ $Fe(CO)_5$	ORR	237
		GO, H_2PtCl_6, $Fe(NO_3)_3$, hydrazine	MOR	239
PtCu/GNs	chemical reduction	GN, H_2PtCl_6, $CuCl_2$, $NaBH_4$	MOR	241
PtSn/GNs	chemical reduction	GO, H_2PtCl_6, $SnCl_2$, EG	MOR	242
		GO, H_2PtCl_6, $SnCl_6$, EG	MOR	243
PtCr/GNs	chemical reduction	GO, H_2PtCl_6, $CrCl_3$, EG, Ar−H_2	ORR	244
PtAg/GNs	chemical reduction	GO, K_2PtCl_4, $HAuCl_4$, $NaBH_4$, AA[d]	MOR	245
PtPdAu/GNs	chemical reduction	GO, H_2PtCl_6, $PdCl_2$, $HAuCl_4$, EG	MOR	251
PtPdCu/GNs	chemical reduction	graphene, H_2PtCl_6, $PdCl_2$, $CuSO_4$, EG	EOR	252
Pd/GNs	chemical reduction	GO, K_2PdCl_4	FAOR/EOR	262
		GO, $PdCl_2$, $NaBH_4$	FAOR	263
		GO, pyrrole, H_2PdCl_4, $NaBH_4$	MOR	266
	impregnation/thermal treatment	GO, $H_2PdCl_4/PdCl_2$, N_2, H_2	ORR/FAOR	182, 278
	electrochemical deposition	GO, Na_2PdCl_4	FAOR	270
Pd-MnO_2/RGO	chemical reduction	GO, $KMnO_4$, EG, $(NH_4)_2PdCl_6$, $NaBH_4$	MOR	267
AuPd/GNs	electrochemical reduction	GO, $HAuCl_4$, $PdCl_2$	ORR	269
PdRu/GNs	polyol reduction	GNs, $PdCl_2$, $RuCl_3$, EG	MOR	257
PdSn/GNs	polyol reduction	GNs, $PdCl_2$, $SnCl_2$, EG	MOR	273
PdAu/GNs	galvanic displacement reaction	GO, $CoCl_2$, $C_6H_5Na_3O_7$, $NaBH_4$, $HAuCl_4$, Na_2PdCl_4	FAOR	275
PdAg/GNs	galvanic displacement reaction	GO, $C_6H_5Na_3O_7$, $AgNO_3$, $Pd(NO_3)_2$	ORR	276
PdRuSn/GNs	polyol reduction	GO, $NaBH_4$, $RuCl_3$, $PdCl_2$, $SnCl_2$, EG	MOR	277
Pd_3Y/GNs	impregnation/thermal treatment	GO, $Pd(NO_3)_2$, $Y(NO_3)_3$, N_2/H_2	ORR/EOR	281
Au/GNs	chemical reduction	GO, polyallylamine, $HAuCl_4$	ORR	303
Au/GNs	chemical reduction	GO, PTCDA,[e] N_2H_4, NH_3, $HAuCl_4$	ORR	306
Au/GNs	electrochemical deposition	GO, N_2H_4, NH_3, $HAuCl_4$	ORR	290

dx.doi.org/10.1021/cr400523y | *Chem. Rev.* 2014, 114, 5117−5160

Table 2. continued

[a]PDDA: poly (diallyldimethylammonium chloride). [b]PVP: polyvinylpyrrolidone. [c]CTAB: hexadecyltrimethylammonium bromide. [d]AA: ascorbic acid. [e]PTCDA: 3,4,9,10-perylenetetracarboxylic dianhydride.

doping concentration was then obtained by treatment in N_2/H_2 plasma. The XPS measurements showed that most of the doped nitrogen atoms are present with pyridine-like structure, which was attributed to the polycrystalline nature of graphene sheets and the easy formation of carbon vacancies by N_2/H_2 plasma treatment.

2.1.5. Solvothermal and Hydrothermal Treatments. Much work has been done to develop the solvothermal and hydrothermal approaches for the preparation of graphene and N-doped graphene.[136−139] Such method is accepted to be a green method for graphene preparation without using hazardous reducing agents. Recently, Deng et al.[140] developed a one-pot solvothermal method to prepare 1−6 layered N-graphene with gram scale production. As shown in Figure 5, N-graphene can be produced by solvothermal reaction between lithium nitride (Li_3N) and tetrachloromethane (CCl_4) at 250 °C for 10 h (denoted as NG-1) or between cyanuric chloride ($N_3C_3Cl_3$), Li_3N, and CCl_4 at 350 °C for 6 h (denoted as NG-2). It was proposed that dichlorocarbene, free −C═C−, and −C═N− groups are likely the intermediates during the change from sp^3 carbon in CCl_4 to sp^2 carbon in graphene. In comparison with the low N doping concentration in graphene with the synthetic methods mentioned above, high N doping levels at 4.5 and 16.4 at. % have been achieved in NG-1 and NG-2 products, respectively. In another work, Wang et al.[141] reported a hydrazine-assisted solvothermal method to synthesize N-graphene. By the proposed process, ∼3% nitrogen was introduced into the reduced graphene oxide (rGO).

Yoon and co-workers[142] synthesized N-graphene through a hydrothermal reduction of GO in the presence of NH_3 and hydrazine. It was found that the hydrothermal temperature has an obvious effect on the N-doping level. For instance, N-graphene with 5.21 wt % nitrogen content can be obtained at low temperature (80 °C). However, with increasing temperature, the nitrogen content decreases gradually, and only 4.01 wt % nitrogen is present in graphene at 200 °C. The XPS measurements showed that more pyridine N was incorporated into the graphene at higher temperature. On the basis of the proposed mechanism shown in Figure 5b, under hydrothermal environment, the reaction between hydrazine and epoxides may readily open the ring of epoxide and form hydrazine alcohols. During the deoxygenatino and reconstruction of the carbon network, nitrogen atoms can be incorporated spontaneously.

In addition to the methods listed above, the synthesis of high-quality and large-area graphene sheets can also be achieved by other techniques, such as epitaxial growth on single-SiC carbide or metal surface,[143−145] micromechanical exfoliation from graphite,[69,146] electrochemical methods,[147,148] microwave-assisted methods,[149] unzipping carbon nanotubes,[85,150] and so on. Currently, these methods are usually applied to the synthesis of graphene or GO but not heteroatom-doped graphene. Interestingly, recent studies showed that GO can be effectively reduced to graphene by taking advantage of the bacterial respiration.[151,152] Generally, through physical processes, high-quality graphene nanosheets can be obtained with few defects, which are suitable for the fabrication of electric devices. On the other hand, graphene sheets prepared by chemical methods usually have a number of surface defects and functional groups, which can serve as anchoring sites for metal/graphene formation.

2.2. Graphene-Supported Pt and Low-Pt Nanocatalysts

Graphene-supported noble metal nanoparticles are one class of the most widely used hybrid electrocatalysts for fuel cells. Although Pt-free catalysts have been investigated extensively in recent years, Pt and Pt-based nanocatalysts are still mainly used in practical applications due to their high catalytic performance. By depositing Pt and low-Pt nanomaterials on graphene nanosheets, high dispersity of metal nanocatalysts can be achieved. Previous studies have showed that graphene-supported Pt and low-Pt nanocatalysts exhibited enhanced catalytic activity and long-term durability. It is well-known that the catalytic performance of hybrid electrocatalysts is strongly dependent on the size, composition, shape, dispersion states of noble metal nanocrystals, and their interactions with graphene support.[14,49,153,154] Up to now, various synthetic strategies have been developed for the preparation of high-quality graphene-supported nanocatalysts.[155−159] In this section, the syntheses of graphene-supported Pt and low-Pt nanocatalysts are summarized (Table 2).

2.2.1. Graphene-Supported Pt Nanocrystals (Pt/Graphene). To prepare Pt/graphene hybrids, the most frequently used method is reducing Pt-containing precursors in the presence of graphene or graphene oxide.[160−162] By using $NaBH_4$ as reducing agent, Li et al.[163] prepared Pt/graphene nanocomposites via the coreduction of H_2PtCl_6 and presynthesized GO in water with pH = 10. With the process, Pt nanoparticles with the average diameter of 5−6 nm were dispersed on the graphene surface. In addition to the strong reducing agent, mild reductants, such as ethylene glycol (EG), sodium citrate, etc., have also been used to prepare Pt/graphene composites.[164−169] Wang and co-workers[165] reported a simple approach of depositing Pt nanoparticles (1−5 nm) onto surfaces of GO nanosheets by EG reduction at 120 °C under stirring. Modified polyol method has also been used to synthesize rGO-supported Pt nanoparticles (∼2.9 nm).[170] In the method, under the refluxing at 120 °C, $NaBH_4$ dissolved in EG was added dropwise into the mixed solution of GO and H_2PtCl_6. On the other hand, it has been found that GO and rGO themselves can serve as reducing agents. Therefore, metal nanoparticles could be directly reduced on GO or r-GO nanosheets without addition of any reducing agent. In the process, the electrons in negative-charged graphene sheets can be transferred to positive-charged metal precursors to produce zerovalent metal nanoparticles.

In addition to chemical reduction methods, Pt/graphene composites can also be prepared by other synthetic routes. As a traditional electrochemical technique, electrodeposition is a useful approach to prepare metal nanocrystals with the advantages of simplicity, free of templates, and easy shape control of metal particles.[171−174] For instance, Maiyalagan et al.[175] have successfully electrodeposited Pt nanoparticles on 3D graphene nanosheets as an anode electrocatalyst toward methanol oxidation in fuel cells. 3D graphene foams were first synthesized by chemical vapor deposition with nickel foam as the template and ethanol as precursors. The morphology and

dx.doi.org/10.1021/cr400523y | Chem. Rev. 2014, 114, 5117−5160

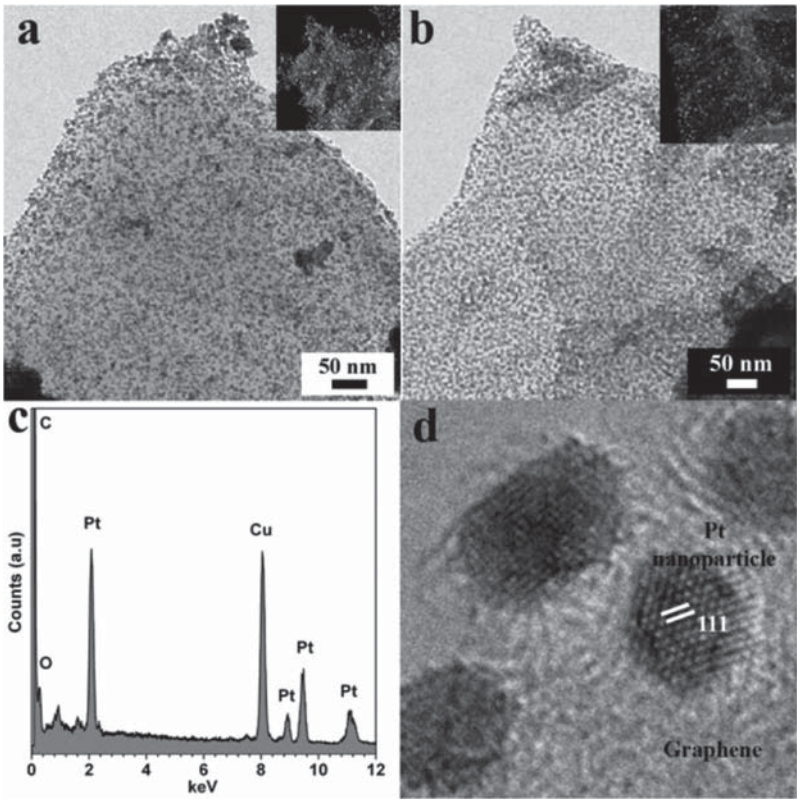

Figure 6. TEM bright-field images of (a) Pt/graphene-1 (20 mL of EG) and (b) Pt/graphene-2 (50 mL of EG) with corresponding dark-field images as insets. (c) EDS of the hybrid Pt/graphene-1. (d) HRTEM image of Pt nanoparticles dispersed on the rGO sheets. Reprinted with permission from ref 180. Copyright 2011 American Chemical Society.

size of Pt nanoparticles can be controlled by electrodeposition potential and time in H_2PtCl_6 solution. It was found that 200 pulses with the profile of 0 mV (500 ms)−1000 mV (200 ms)−0 mV (500 ms) (vs Ag/AgCl/3 M KCl) can produce spherical 10−30 nm Pt nanoparticles, which uniformly dispersed on the 3D graphene support. Recently, Liu et al.[176] developed a simple electroless deposition method to synthesize metal−graphene hybrid materials by taking advantage of the different redox potentials between a substrate and metal ions. In the synthesis, graphene sheets were first deposited on a Cu substrate by immersing a piece of copper foil into a graphene suspension. After being dried, the substrate was immersed into metal ion solution, resulting in nanoparticle-decorated graphene. In the process, due to the work function difference between Cu (4.67 eV) and graphene (4.7−5.0 eV), and the redox potential difference between Cu^{2+}/Cu and $PtCl_4^{2-}/Pt$, H_2PtCl_4 can be reduced to nanoparticles on graphene nanosheets. Moreover, the size and density of Pt nanoparticles dispersed on graphene can be tuned by changing the deposition time. Multilayer assemblies of hybrid Pt/graphene can also be obtained by repeating the graphene-coating and Pt-depositing processes.

In recent years, microwave-assisted process has also been applied to the synthesis of metal nanoparticle/graphene hybrids. Microwave irradiation can generate homogeneous and rapid heating, which has been used to prepare unsupported or supported metal nanoparticles.[177−179] Ravishankar and co-workers[180] reported a rapid method to synthesize graphene-supported Pt nanoparticles by the coreduction of GO and $PtCl_6^{2-}$ (H_2PtCl_6) using ethylene glycol as reducing agent under microwave irradiation. It was proposed that under microwave irradiation, the platinum ions were first reduced to Pt^{2+} by EG, which can reduce GO. The defect sites generated from the removal of functional groups on GO surface during the reduction process can serve as anchoring centers for the formation of Pt nanoparticles. As shown in Figure 6a and b, the produced Pt nanoparticles with sizes of 2−3 nm are uniformly dispersed on the graphene surface. The authors also studied the effect of the amount of EG on the morphology of products. By comparing Figure 6a,b and insets, larger interparticle spacing was obtained when more EG (Figure 6b) was used. Figure 6c,d clearly shows the presence of Pt nanoparticles with (111) planes.

Impregnation methods or thermal reduction process were found to be useful for the synthesis of small and even subnanometer-sized Pt clusters.[181−183] Yoo et al.[184] synthesized graphene-supported Pt nanoclusters with diameter smaller than 1 nm. In the synthesis, the mixture of presynthesized graphene sheets and $Pt(NO_2)_2(NH_3)_2$ was dispersed in ethanol and then dried in air at 40 °C for 1 h. Pt/graphene can be obtained by thermal reduction of the mixture in a hydrogen/argon stream at 400 °C for 2 h. In the mechanism study,[185] the authors found that when strong reductant of $NaBH_4$ was used instead of ethanol, no subnanometer Pt cluster but only large Pt nanoparticles were obtained. Therefore, only the gradual reduction process of Pt^{4+}, Pt^{2+}, and finally Pt^0 by weak reductant can produce tiny Pt clusters.

It should be pointed out that the experimental conditions have considerable effects on the morphologies and properties of Pt/graphene products. Although the above developed methods have been successfully applied to the syntheses of Pt/graphene

dx.doi.org/10.1021/cr400523y | *Chem. Rev.* 2014, 114, 5117−5160

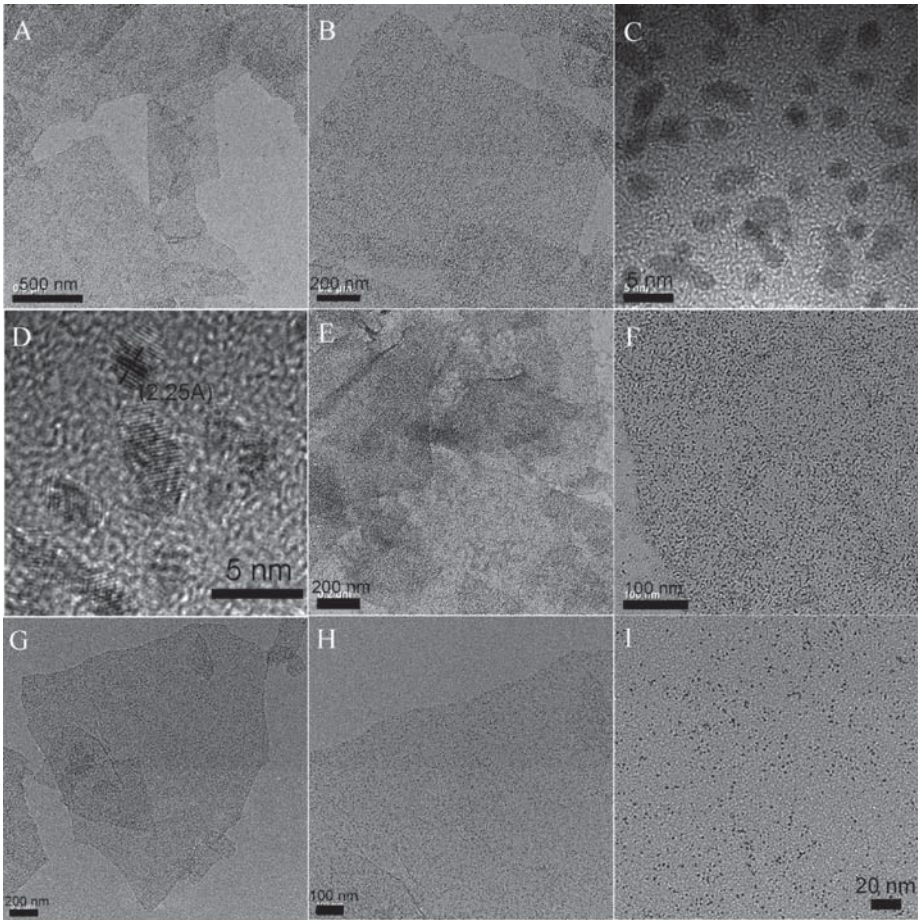

Figure 7. (A–C) TEM images of Pt/graphene (1 mL Pt precursor) at different magnifications. (D) HRTEM image of the Pt nanoparticles dispersed on graphene. (E,F) TEM images of Pt/graphene with relative high density of Pt nanoparticles (2 mL of Pt precursor) at different magnifications. (G–I) TEM images of Pt/graphene with relative low density of Pt nanoparticles (0.5 mL of Pt precursor) at different magnifications. Reprinted with permission from ref 186. Copyright 2010 American Chemical Society.

hybrids, some critical issues of the hybrids still remain, especially for their practical applications in fuel cells, including the poor distribution and aggregation of Pt nanoparticles on graphene surface, and the durability of the hybrids. To achieve the homogeneous distribution and improve the stability of Pt nanoparticles, surface-treatments of graphene by covalent or noncovalent functionalization have been proposed. Guo et al.[186] synthesized Pt/graphene hybrids by heating a water/EG solution of H_2PtCl_6 and graphene oxide in the presence of poly(methacrylic acid sodium salt) (PMAA). Figure 7A–D shows that 2.6 nm Pt nanoparticles were homogeneously dispersed on the graphene nanosheets. In this work, the PMAA plays an important role for the formation of uniform Pt nanoparticles with small size. PMAA can not only improve the stability of graphene sheets due to the strong hydrophobic interaction between them, but also stabilize the Pt nanoparticles as a protecting agent. Moreover, as shown in Figure 7E,F and G–I, the mass loading (density) of Pt nanoparticles deposited on graphene can be easily controlled by changing the ratio of Pt precursor to PMAA.

Poly(diallyldimethylammoniumchloride) (PDDA) is a widely used cationic polyelectrolyte, and it can be adsorbed on the surface of carbon nanotubes and graphene through $\pi-\pi$ and electrostatic interactions.[187] Previous studies found that PDDA can be used as a kind of unique stabilizer for controlled synthesis of Pt/graphene.[166,188,189] Graphene nanosheets with negative charge can be easily functionalized by positively charged PDDA through the electrostatic interaction, which can increase the stability of graphene in solution. On the other hand, $PtCl_6^{2-}$ ions can be confined in the positively charged surface of PDDA-functionalized graphene and then be in situ reduced to Pt nanoparticles upon the addition of reducing agents. With this strategy, controllable deposition of Pt nanoparticles on graphene was realized by Qiu et al.[190] From the TEM characterization in Figure 8, the formed Pt nanoparticles are uniformly dispersed on graphene surface. The Pt loading density can be effectively adjusted by changing the ratio of PDDA-GO to the Pt precursor. As shown in Figure 8a–f, the Pt/graphene with Pt loading from 30 to 78 wt % was obtained when the ratio of PDDA-GO to H_2PtCl_6 varies from 1:1 to 1:8.5, whereas the particle size was maintained at ~4.6 nm. In another work,[191] by using PDDA as both reducing agent and stabilizer, soluble graphene nanosheets were obtained from graphite oxide. The PDDA-functionalized graphene facilitated the in situ growth of highly dispersed Pt nanoparticles to produce Pt/graphene nanocomposites. Besides PDDA, thiolated graphene,[192] poly(sodium styrene sulfonate),[193] and perfluorosulfonic acid-functionalized graphene[194] have also

dx.doi.org/10.1021/cr400523y | *Chem. Rev.* 2014, 114, 5117–5160

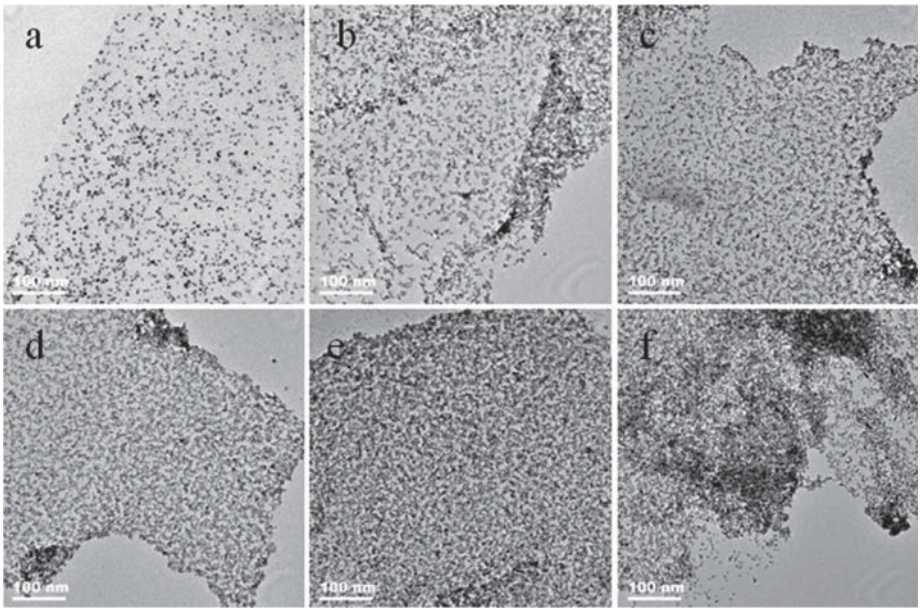

Figure 8. TEM images of the Pt/graphene-PDDA nanocomposites synthesized at different mass ratios of PDDA-GO to H_2PtCl_6: (a) 1:1, (b) 1:1.5, (c) 1:2.5, (d) 1:3.5, (e) 1:6.0, and (f) 1:8.5. Reprinted with permission from ref 190. Copyright 2011 American Chemical Society.

been fabricated to improve the dispersion of Pt nanoparticles on graphene surface and their electrocatalytic performances.

To improve the catalytic properties, especially the stability of graphene-based nanocomposites, some recent research focused on the unique interfacial construction between Pt nanoparticles and graphene nanosheets. Kou et al.[71] proposed an interesting route to deposit Pt nanoparticles and metal oxides on graphene surface to form stable metal−metal oxide−graphene triple junctions. The experimental and theoretical calculations indicated that the Pt nanoparticles supported at the Pt−indium tin oxide (ITO)−graphene triple junctions are more stable than those only dispersed on graphene. Such unique Pt−ITO−graphene junctions with large surface area, good particle distribution, and high electrical conductivity exhibited better catalytic properties than Pt/graphene and commercial Pt/C catalysts. Meanwhile, Huang and co-workers[195] found that by inserting carbon black (CB) into Pt/graphene, the formed Pt/rGO/CB hybrid structure showed greatly enhanced catalytic activity for oxygen reduction in comparison with the simple Pt/rGO hybrids. It was proposed that the presence of CB can effectively prevent the stacking of rGO sheets and thus improve the diffusion of O_2 molecules through rGO, resulting in the high electrocatalytic activity toward ORR.

2.2.2. Graphene-Supported Low-Pt Alloy Nanocrystals. Because of the low loading of Pt metal and bifunctional mechanism or the so-called ligand effect, graphene-supported Pt-based nanomaterials attract much attention. The synthetic strategies for Pt/graphene have also been applied to the preparation of Pt-based bimetallic or trimetallic nanostructure supported on GNs. Up to now, several kinds of important PtM alloys/GNs have been prepared as efficient electrocatalysts for fuel cells.

2.2.2.1. PtPd/GNs. Among the Pt-based nanostructrued materials, PtPd alloys are among the most interesting cathode catalysts because of their excellent stability and catalytic performance. In previous studies, various structured PtPd alloys have been synthesized.[196−199] To synthesize PtPd/graphene nanocomposites, methods similar to those described above for the preparation of Pt/graphene are usually used. To improve the dispersity of PtPd nanocrystals on graphene surface, GNs can be prefunctionalized with stabilizers. Guo et al.[200] reported a wet-chemical method to prepare high-quality three-dimensional Pt-on-Pd bimetallic nanodendrites supported on polyvinylpyrrolidone (PVP)-functionalized graphene sheets, which can be used as an advanced electrocatalyst toward the methanol oxidation. In this method, PVP-functionalized graphene was first obtained under the reduction of hydrazine. Pd/GNs hybrids were then synthesized using HCOOH as reducing agent at room temperature. Finally, Pt-on-Pd nanodendrites supported on GNs were produced by heating the mixture of Pd/GNs suspension and Pt precursor in the presence of ascorbic acid as reducing agent. In another work, by using PDDA-functionalized GNs as supports, PtPd alloys with controlled compositions (Pd_4Pt_1, Pd_3Pt_1, Pd_2Pt_1, and Pd_1Pt_1) have been synthesized under the reduction of EG.[201] The highly dispersed alloy particles on GNs exhibited composition-dependent catalytic activity for the ORR, higher performance from the alloys with higher Pt content. Meanwhile, a simple two-step electrodeposition method was also developed to construct PtPd/GNs nanostructures directly on electrode surface.[202,203] In the first step, graphene oxide was chemically or electrochemically reduced and deposited on a glassy carbon electrode surface. PtPd alloy nanoparticles were then electrodeposited on the graphene-modified electrode. The as-synthesized hybrid catalysts exhibited high catalytic activities and stability for alcohol oxidation in alkaline media.

The electrocatalytic activity of nanoparticles is very sensitive to the surface electronic structure and the arrangement of surface atoms. Therefore, it is of great importance to synthesize Pt-based alloy nanoparticles with specific morphology and narrow size distribution. In the reported syntheses, most produced metal nanoparticles supported on graphene are spherical. Designing and synthesizing highly active Pt−Pd alloy nanoparticles templated by graphene with desirable structures

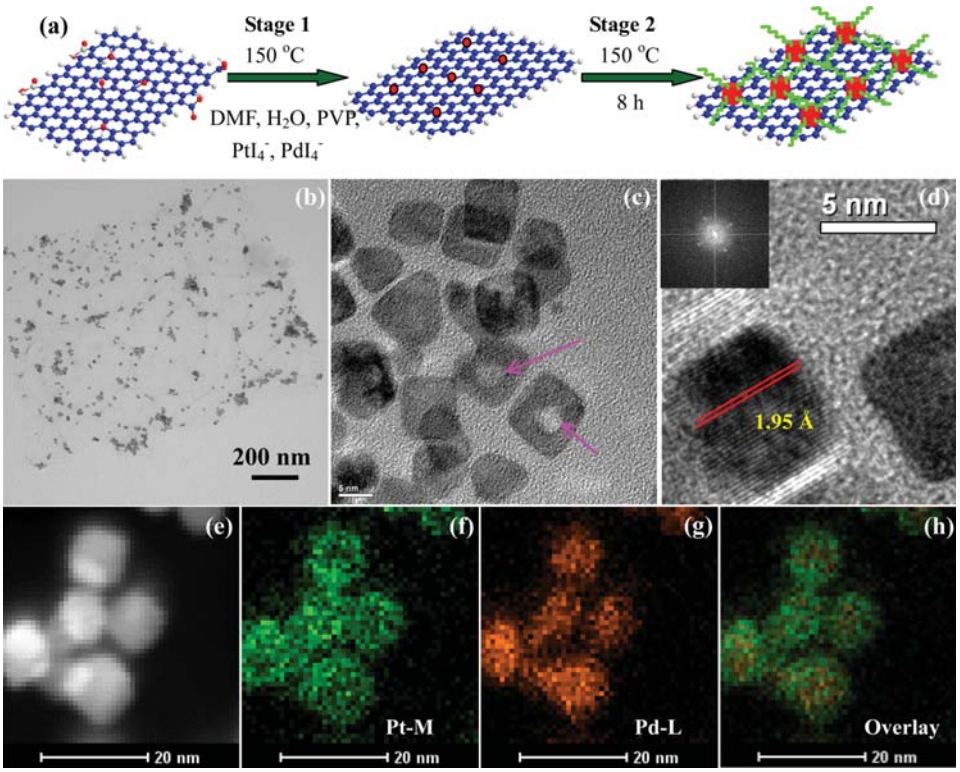

Figure 9. (a) Schematic illustration of the one-pot hydrothermal synthesis of PtPd alloy nanocubes supported on rGO. (b) TEM and (c,d) HRTEM images of the PtPd alloy nanocubes dispersed on rGO at different magnifications. The inset in (d) shows the FFT pattern of an individual PtPd nanocrystal. (e) The high-angle annular dark-field (HAADF)-STEM image of PtPd/rGO, and the corresponding elemental mapping of (f) Pt, (g) Pd, and (h) the overlay. Reprinted with permission from ref 72. Copyright 2013 American Chemical Society.

are still challenging. Recently, we developed a facile and general hydrothermal approach that could allow the one-pot fabrication of water-soluble and uniform single-crystalline PtPd alloy nanocubes supported on the reduced graphene oxide nanosheets (PtPd/rGO).[72] This method could also be used to synthesize other water-soluble Pt- or Pd-based alloy nanocrystals with desirable morphology supported on rGO. As shown in Figure 9a, the synthesis includes two steps: (1) the reduction of GO and the nucleation of nanocrystals attached onto the surface of rGO sheets because of the strong interaction between them; and (2) the nuclei grew gradually into the cubic shape under the protection of PVP. From the TEM characterizations and element mapping shown in Figure 9b–h, PtPd nanocrystals with 82% nanocubes are uniformly distributed on the rGO surface. With a similar hydrothermal method, PtPd alloy concave nanocubes can also be in situ formed on the graphene surface.[204]

2.2.2.2. PtAu/GNs. Because of the inert property of gold in acid electrolyte and its excellent catalytic activity for CO oxidation, Pt–Au bimetallic catalysts can not only improve the adsorption/dissociation of alcohol in acid media and enhance the catalytic performance toward the oxidation of alcohol fuels, but also promote the durability of the catalysts.[205] Therefore, binary PtAu nanomaterials are of special interest and importance as fuel cell electrocatalysts. Rao et al.[154] reported an EG reduction method to synthesize graphene-supported Pt–Au alloy nanoparticles with an average size of 4.5 nm. The Pt–Au alloys are well-dispersed on graphene surface and exhibit high electrocatalytic performance toward formic acid oxidation. By using PDDA-modified graphene as support, Pt–Au alloy nanoparticles with a mean diameter of 3.2 nm were also synthesized by the $NaBH_4$ reduction method.[206] With the electrodeposition method, Pt–Au nanoparticles were electrodeposited on graphene-decorated glassy carbon (GC) electrode at −0.4 V (versus SCE).[207] The composition, size, and morphology of the formed Pt–Au particles can be easily controlled by adjusting the ratio of Pt and Au precursors in the reaction mixtures. As described above, nitrogen-doped graphene exhibit higher catalytic activity and thermal stability as compared to graphene. Therefore, N-graphene may be an excellent support for the deposition of metal nanocatalysts. Zhu and co-workers[208] synthesized Pt_3Au/N-graphene with a wet-chemistry method under the assistance of microwave heating. The electrochemical measurements showed that the Pt_3Au/N-graphene nanocomposites have much higher electrocatalytic activities for methanol oxidation than do the Pt_3Au/graphene and commercial Pt/C catalysts.

2.2.2.3. PtRu/GNs. Among the bimetallic catalysts for fuel cells, PtRu alloys are considered to be the best anode catalysts for DMFCs, and they have been used in commercial fuel cells.[209,210] Besides the intrinsic catalytic properties of catalysts, the used support also plays important roles in determining their catalytic performance. The dispersion and durability of catalysts can be improved by using a good support. Carbon materials, such as carbon black, carbon nanotube, and carbon nanofiber, are the traditional supports in fuel cells for the dispersion of electrocatalysts. Because of the high electronic conductivity and large surface area, graphene has also been studied as an efficient support for PtRu catalysts.[211−214] Dong et al.[212] synthesized graphene-supported PtRu nanoparticles by using the EG

dx.doi.org/10.1021/cr400523y | *Chem. Rev.* 2014, 114, 5117–5160

reduction method, and they found that the PtRu/GNs exhibited enhanced efficiency for methanol and ethanol oxidation in comparison with the PtRu catalysts supported on Vulcan XC-72R carbon black. Under the assistance of supercritical carbon dioxide, Zhao et al.[215,216] prepared graphene-supported ultrafine PtRu nanoparticles at low temperature. With the proposed route, the PtRu nanoparticles (~2.87 nm) can be uniformly distributed on the surface-functionalized GNs. Highly dispersed PtRu nanoparticles with an average size of 1.8 nm supported on graphene were prepared by a simple surfactant-free process,[217] in which the mixture of hydrogen hexachloroplatinate(IV) hexahydrate, ruthenium(III) chloride hydrate, and graphene nanosheets was treated at 300 °C under N_2 + H_2 (4%) atmosphere. To improve the dispersion and stability of PtRu nanoparticles on graphene sheets, Li et al.[218] prepared PtRu catalyst (ca. 2.0 nm) supported on PMo_{12}-functionalized graphene nanosheet by microwave irradiation method in ethylene glycol (EG) solution. Because of the negatively charged nature of PMo_{12}, the resulted hybrid catalyst exhibited higher catalytic activity and better cycle stability for methanol electrooxidation as compared to that of the unmodified PtRu/graphene catalyst.

Before the discovery of graphene, carbon black and carbon nanotubes were the main supports for electrocatalysts. Although graphene and carbon nanotubes have excellent properties as catalyst supports, their disadvantages will be present obviously when they are used singly. For example, the surface area of graphene sheets will be decreased during the electrochemical cycling due to the aggregates of nanosheets from van der Waals force and $\pi-\pi$ interaction. On the other hand, with CNTs alone as support, only the external surface of CNTs can be efficiently utilized for dispersing metal catalysts due to the small inner diameter and the usually closed tips. Recently, several studies focused on the hybrid supports composed of graphene and CNTs. Wang et al.[219] constructed a 3-D porous GNs-CNTs architecture as support for the deposition of PtRu nanoparticles. In the carbon hybrid, CNTs act as nanospacers to efficiently decrease the face-to-face aggregation of GNs. The porous structure provides large surface area for the immobilization of PtRu nanoparticles and facilitates the electrolyte and reactant diffusion, and thus increases the catalytic performance of the catalysts. In another study, Lv et al.[220] synthesized an interesting GNs-N-doped CNTs (NCNTs) hybrid with graphene sheets grown inside the large inner cavities of the NCNTs through a one-step water-assisted CVD process. Figure 10a,b shows the TEM images of PtRu nanoparticles formed on multiwalled CNTs and GNs-NCNTs, respectively. Clearly, the aggregates of PtRu nanoparticles can be easily formed on CNTs (indicated by the circles). With the same reduction process, the produced PtRu nanoparticles in the size range of 2–4 nm are well dispersed on the GNs-NCNTs hybrid. The improved dispersion of PtRu nanoparticles was attributed to the nitrogen doping and the presence of graphene inside the carbon nanotubes.[220] Benefiting from the hybrid structure, the PtRu/GNs-NCNTs exhibited enhanced catalytic performance and better long-term operation stability for methanol oxidation as compared to CNTs-supported PtRu catalysts. Woo et al.[221] designed another graphene–Vulcan carbon hybrid as support for PtRu nanoparticles. In the sandwich structure, the Vulcan carbon serves as a nano spacer to decrease the aggregation of graphene sheets and improve the electrocatalytic activity of the PtRu catalyst.

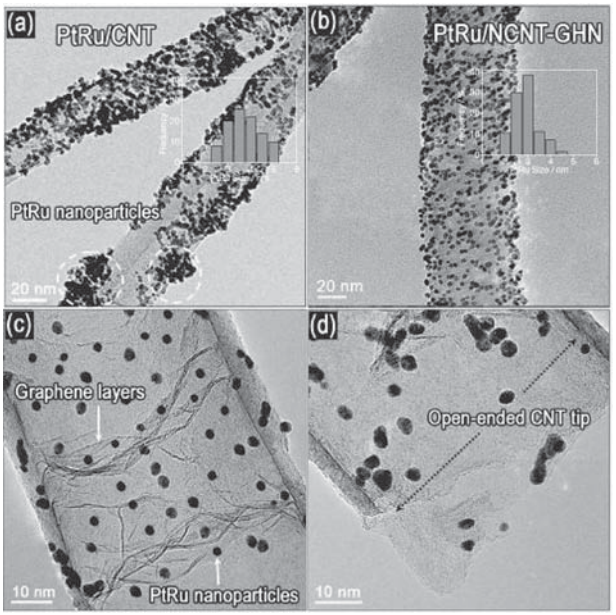

Figure 10. TEM images of PtRu nanoparticles supported on multiwalled CNTs (a) and GNs-NCNTs (b–d). The white circles in (a) show the PtRu aggregates on CNTs. The insets in (a) and (b) are the corresponding size-distribution histograms of the PtRu nanoparticles supported on CNT and NCNTs-GNs. Reprinted with permission from ref 220. Copyright 2011 Wiley-VCH.

2.2.2.4. Other Pt-Based Bimetallic Catalysts Supported on Graphene. In addition to the above Pt-based catalysts, other Pt-transition metal alloys supported on graphene have also been fabricated by the methods described above, such as PtCo/graphene,[222−229] PtNi/graphene,[230−236] PtFe/graphene,[237−239] PtCu/graphene,[240,241] PtSn/graphene,[242,243] PtCr/graphene,[244] PtAg/graphene[245] PtIr/graphene,[246] PtW, and PtMo/graphene,[247] etc. For example, Guo et al.[237] found that the annealing process can improve the catalytic activity of FePt/graphene composites for ORR. The ORR activity of FePt/graphene annealed at 100 °C for 1 h showed 2 times higher catalytic activity than that of the unannealed sample. The study demonstrated that graphene is indeed an effective support to improve the activity and durability of electrocatalysts. To avoid the aggregation and increase the stability of nanoparticles, Choi and co-workers[229] prepared PtCo nanoparticles via an EG reduction method by using hexadecyltrimethylammonium bromide (CTAB)-functionalized graphene sheets as support. Similar to the unsupported Pt-based electrocatalysts, all of the studies showed that the Pt-based bimetallic nanocomposites supported on graphene exhibited higher catalytic activities than those of single Pt catalysts because of the synergistic effect.

2.2.2.5. Ternary Metal Composites Supported on GNs. Because of the catalytic activity and stability superior to that of bimetallic alloys, ternary metal catalysts have attracted much attention in recent years. Several methods have been reported to synthesize graphene-supported ternary metal composites as efficient catalysts for fuel cells.[248−250] For instance, PtPdAu ternary alloy nanoparticles were synthesized on graphene nanosheets by a simple EG chemical reduction method.[251] As compared to the Pt/GNs and the bimetallic composites of PtPd/GNs and PtAu/GNs, the ternary nanoparticles have higher catalytic activity and stability for methanol oxidation. Qu and co-workers[252] developed a novel dual-solvothermal process

dx.doi.org/10.1021/cr400523y | Chem. Rev. 2014, 114, 5117–5160

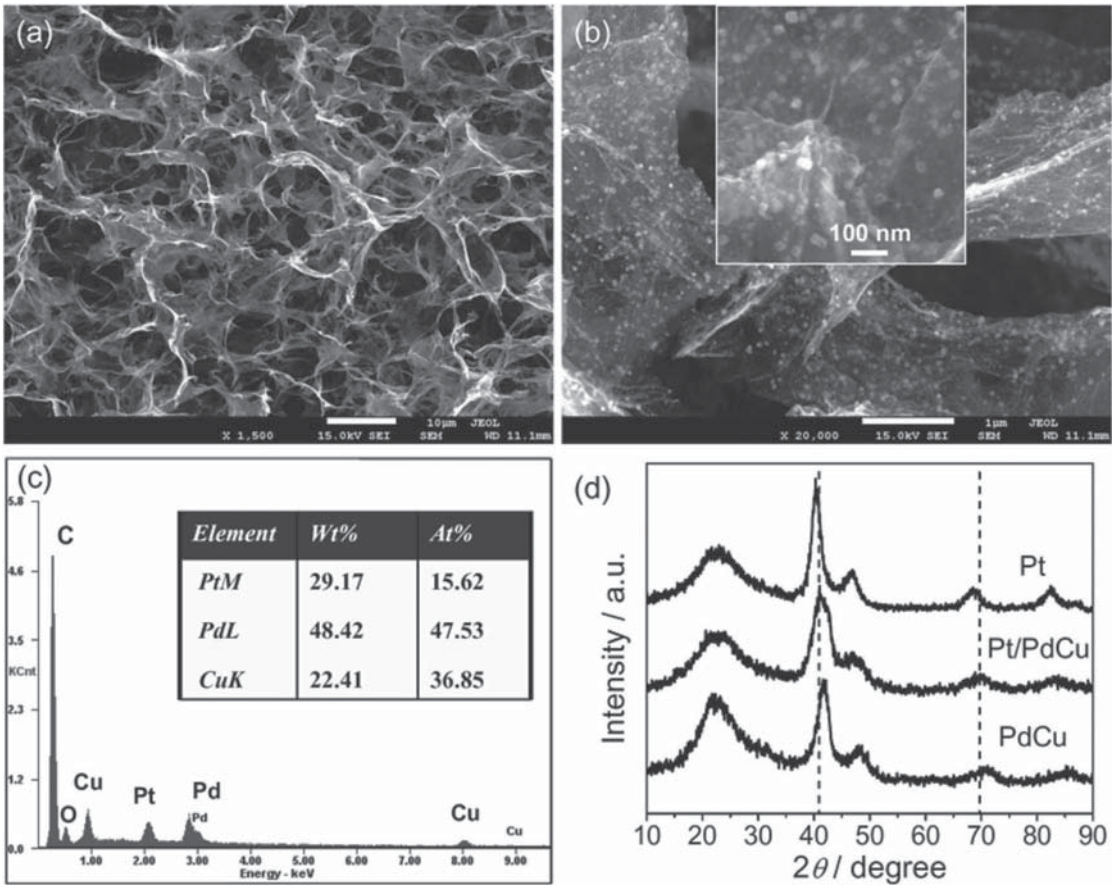

Figure 11. (a,b) SEM images of Pt/PdCu nanocrystals supported on a 3D graphene framework (3DGF). The inset in (b) is a magnified SEM image of the cubic Pt/PdCu on graphene nanosheets. (c)EDS and (d) XRD patterns of Pt, PdCu, and Pt/PdCu anchored on the 3DGF. Reprinted with permission from ref 252. Copyright 2012 Wiley-VCH.

to synthesize ternary Pt/PdCu nanoboxes supported on 3D graphene framework (3DGF), which can be used as an efficient anodic electrocatalyst for ethanol oxidation. In the reported method, hollow PdCu nanocubes on 3DGF were first synthesized by solvothermal treatment in EG at 160 °C. Ternary structure was then achieved by mixing the PdCu/3DGF with EG solution of H_2PtCl_6 and heating at 160 °C for another 3 h. As shown in Figure 11a,b, the formed Pt/PdCu nanoboxes with an average size of 30 nm are dispersed on the interconnected 3D porous network of graphene sheets. The energy dispersive spectroscopy (EDS) and XRD measurements shown in Figure 11c and d further indicate the presence of Pt/PdCu ternary nanocrystals.

2.3. Graphene-Supported Non-Pt Nanocatalysts

From above, Pt-based nanocrystals supported on graphene have been extensively studied because of their excellent catalytic properties and resistance to corrosion and oxidation. However, the high cost and limited reserve hinder the large-scale application of Pt-based catalysts and the wide commercialization of fuel cells. To reduce the cost of electrocatalysts and fuel cells, many studies on fuel cell electrocatalysts focus on the fabrication and development of nonprecious metal alternatives. Previous studies found that for graphene-supported non-Pt nanocatalysts, there exists a charge transfer process across the graphene−metal interface, which depends on the distance and the Fermi level difference between graphene and the supported catalysts. Such charge transfer may be beneficial for the enhanced catalytic activities of graphene-supported catalysts, as exampled by the catalysts of Co_3O_4/graphene,[253] Fe_3O_4/graphene,[254] Co_xS_{1-x}/graphene,[255] $MnCo_2O_4$/graphene[256] for ORR, and PdRu/graphene[257] for methanol electrooxidation, etc. Graphene-supported noble and nonprecious metal electrocatalysts and their applications are summarized in Tables 2 and 3, respectively.

2.3.1. Pd-Based Nanocatalysts/GNs. Among the potential metal catalysts, Pd stands well as the Pt substitute, because it has similar properties, lower cost, and greater resistance to CO poisoning in comparison with Pt. First-principle calculations revealed that, as compared to Pt, Pd can interact with and bind more strongly to graphene surface because more interaction states and transmission channels can be produced between Pd and graphene, and Pd tends to grow into three-dimensional structures on GNs.[258,259] During recent years, various methods have been developed to synthesize Pd-based nanocatalysts on graphene with different size, composition, and morphology. Similar to the preparation of nanocatalysts on other supports, Pd and Pd-based alloy nanocatalysts supported on graphene can be generally prepared through numerous synthetic routes, such as chemical reduction, electrochemical reduction, impregnation, and heat treatment, etc. Most of the syntheses are carried out by first preparing GO (or functionalized GO), followed by reducing GO and metal ions simultaneously with different strong or weak reducing agents,

dx.doi.org/10.1021/cr400523y | Chem. Rev. 2014, 114, 5117−5160

Table 3. Graphene-Supported Nonprecious Metal Electrocatalysts and Their Applications

catalyst	preparation method	precursor	application	ref
FeTsPc[a]/GNs	chemical reduction	GO, N_2H_5OH, FeTsPc[a]	ORR in PBS	331
Fe/N-graphene	thermal treatment	GO, cyanamide, $FeCl_3$	ORR in acid and alkaline	332
FePc[b]/N-graphene	thermal treatment	GO, ammonia, FePc[b]	ORR in alkaline	334
Fe/N-graphene	thermal treatment	GO, pentaethylenehexamine, $FeCl_3$	ORR in acid	335
FeCN/N-graphene	thermal treatment	GO, NH_3, $Fe(OAc)_2$, phenanthroline	ORR in acid	336
Fe−N/rGO	thermal treatment	GO, NH_3, N_2H_4, dicyandiamide, $FeCl_3$	ORR in acid/PBS	337, 338
$(Fe-P)_n$-MOF/rGO	solvothermal	GO, 4-(4-aminostyryl)pyridine sodium nitrite, TCPP,[c] $FeCl_3$	ORR in alkaline	340
Fe_3O_4/N-graphene	hydrothermal/heat treatment	GO, iron acetate, polypyrrole	ORR in alkaline	254
$Co(OH)_2$/graphene	electrodeposition	GO, NH_3, N_2H_4, $Co(NO_3)_2$	ORR in alkaline	348
Co_3O_4/(N−)rGO	hydrothermal	GO, $Co(Ac)_2$, NH_4OH	ORR/OER in alkaline	253
$Co_{1-x}S$/rGO	heat treatment	GO, TAA,[d] $Co(OAc)_2$	ORR in acid	255
$MnCo_2O_4$/N-rGO	solvothermal	GO, $Co(OAc)_2$, $Mn(OAc)_2$, NH_4OH	ORR/OER in alkaline	256
Co-CoO/GNs	thermal decomposition	GO, $Co_2(CO)_8$	ORR in alkaline	341
CoTAPP[e]/GNs	diazonium salt reaction	graphene, CoTAPP[e]	ORR in acid	353
Ni/GNs	chemical reduction/thermal treatment	GO, $NiCl_2$	MOR in alkaline	366
Ni−Co/GNs	chemical reduction	GO, $NiSO_4$, $Co(NO_3)_2$, NH_3, N_2H_4	EOR in alkaline	350
$Ni(Co)O_x$/GNs	chemical reduction	GO, $Ni(NO_3)_2$, $CoCl_2$, $NaBH_4$ or N_2H_4	MOR in acid	367
Ni(Cu)-α-MnO_2/GNs	hydrothermal	rGO, $MnSO_4$, $KMnO_4$, $Cu(NO_3)_2$, $Ni(NO_3)_2$	ORR in alkaline	368
$NiCo_2S_4$/graphene	solvothermal	GO, $Co(OAc)_2$, $Ni(OAc)_2$, thiourea,	ORR in alkaline	363
Cu_2O/rGO	polyol reduction	GO, copper acetate, diethylene glycol	ORR in alkaline	373
CuO/N-rGO	aqueous process	GO, NH_3, $CuCl_2$	ORR in alkaline	371
MnO_2/rGO	chemical reduction	GO, PSS,[f] $MnSO_4$, NH_3, H_2O_2, N_2H_4	ORR in alkaline	378
MnO_x/GNs	hydrothermal	GO, N_2H_4, $KMnO_4$, $MnSO_4$	ORR in alkaline	380
Ir_xV/rGO	polyol reduction	GO, $IrCl_3$, NH_4VO_3, ethylene glycol	ORR in alkaline	381

[a]FeTsPc: iron tetrasulfophthalocyanine. [b]FePc: iron(II) phthalocyanine. [c]TCPP: 5,10,15,20-tetrakis(4-carboxyl)-21*H*,23*H*-porphine. [d]TAA: thioacetamide. [e]CoTAPP: cobalt[tetrakis(*o*-aminophenyl)porphyrin]. [f]PSS: poly(sodium 4-styrene sulfonate).

such as $NaBH_4$, trisodium citrate, polyol, K[Bet_3H], hydrogen gas, hydrazine hydrate, etc. A variety of Pd/graphene composites could be prepared by these processes.[260−265] For example, Zhao and co-workers[266] synthesized Pd nanoparticles supported on polypyrrole (PPy)-functionalized GNs. In the synthesis, the PPy-graphene was first prepared by an in situ radical polymerization method with graphene, pyrrole, and $(NH_4)_2S_2O_8$ precursors, and $PdCl_4^{2-}$ was chemically reduced to Pd nanoparticles on the support by $NaBH_4$. In another case, Giovanni et al.[182] prepared Pd/graphene hybrids by thermal exfoliation method in nitrogen or hydrogen atmosphere. In a typical process, the graphite oxide presynthesized by Hofmann method was dispersed in water containing palladium(II) chloride under ultrasonication. The mixed suspension was consequently dried in a vacuum oven to yield the metal doped-graphite oxide precursor powders. The thermal exfoliation of the dry precursor was carried out at 1000 °C for 12 min. The obtained product was then flushed repeatedly with pure nitrogen and subsequently inserted into a preheated reactor in nitrogen or hydrogen atmosphere to produce Pd/graphene hybrid material.

To improve the stability and dispersion of Pd nanoparticles, graphene or GO can be modified by functional groups before deposition of Pd nanoparticles. Liu et al.[267] prepared Pd nanoparticles supported on manganese dioxide-modified rGO (MnO_2/rGO) by a chemical reduction method. The formed Pd nanoparticles are well-dispersed on the MnO_2/rGO support without aggregation, and the as-synthesized catalyst exhibited much higher electrocatalytic activity and stability as compared to the Pd/rGO, indicating the promoting effect of the MnO_2 functionalized on rGO. More recently, Chen and colleagues[268] developed a facile aqueous-based method for well-dispersion of ∼2 nm Pd nanoparticles on phosphonic acid calyx[8]arene functionalized graphene. Here, *p*-phosphonic acid calyx[8]-arene acts as both a noncovalent stabilizer for suspending 2D materials in water and also a surfactant for the decoration of Pd nanoparticles. In the chemical reduction methods, undesirable excessive reducing agents may increase the cost in mass production and contaminate the chemically reduced GO, which will also affect the electrocatalytic performance of the nanocomposite. Alternatively, electrochemical reduction is a facile and environmentally friend approach for the syntheses of Pd-based alloy nanocomposites.[269,270] For instance, Yang et al.[269] electrochemically prepared Au−Pd/GNs composites without the aid of any reducing reagent. The electrochemical reduction process can efficiently remove the oxygen-containing groups in GO, which was then modified with homogeneously dispersed AuPd nanoparticles in a good size distribution.

Nanomaterials with clean surface are very beneficial for their applications as active catalysts in fuel cells. However, nanocrystal surface is usually protected by stabilizer to keep them from agglomeration, which may heavily block their surface catalytically active sites and therefore lower the catalytic performance. Chen et al.[262] successfully prepared ultrafine Pd nanoparticles monodispersed on GO surface through a surfactant-free process. By taking advantage of the difference between the reduction potential of $PdCl_4^{2-}$ and the oxidation potential of GO, Pd nanoparticles can be spontaneously produced on GO without the presence of additional reducing agent. From the TEM images shown in Figure 12, Pd nanoparticles with a uniform size of ∼3.5 nm are monodispersed on the surface of GO, although no additional stabilizer was used. It was suggested that the strong anchoring effect between the Pd nuclei and the GO surface plays a key

dx.doi.org/10.1021/cr400523y | *Chem. Rev.* 2014, 114, 5117−5160

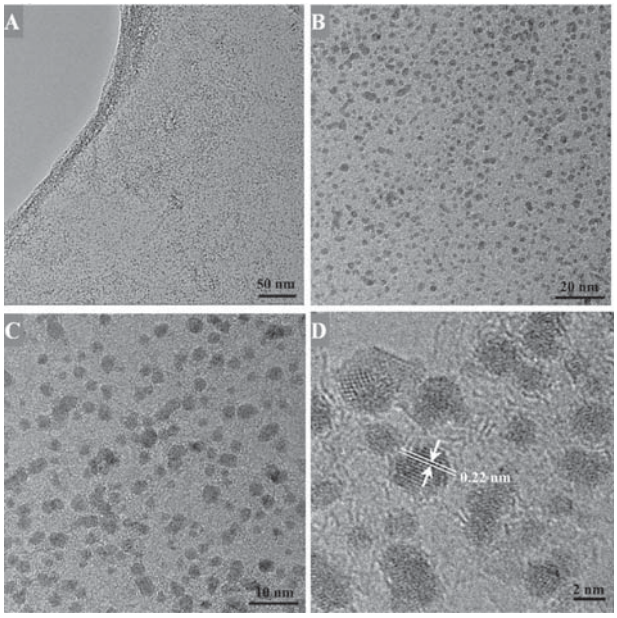

Figure 12. TEM images (A–C) at different magnifications and HRTEM micrographs (D) of Pd nanoparticles supported on GO. Reprinted with permission from ref 262. Copyright 2011 American Chemical Society.

role during the formation of Pd nanoparticles. Recently, highly dispersed Pd nanoparticles supported on graphene were also successfully synthesized by a one-step electrochemical codeposition approach.[270] The as-synthesized hybrid composite provides a "clean" surface as a result of the reductant- and surfactant-free synthesis process. The electrochemical studies showed that the clean Pd/graphene materials have desirable catalytic performance for formic acid oxidation.

Similar to the Pt-based nanocatalysts, interesting behaviors have also been exhibited by the Pd-based alloys, which often provide better electrocatalytic properties than the pure metal alone due to the synergistic effect. On the basis of the density functional theory, Wang and Balbuena[271] predicted that ORR catalytic activity could be enhanced by coupling a metal M (M = Co, Ni, Cr, V, and others) with low occupancy of d-orbitals with another metal M′ (such as M′ = Pd, Au, and Ag) with fully occupied d-orbitals. The enhancement arises from decreasing the Gibbs free energy of the electron transfer steps with alloying. Meanwhile, previous studies indicated that palladium alone exhibits inert behavior toward alcohol oxidation in acidic medium, while it is highly catalytically active in alkaline solution.[30,272] To improve the catalytic performance, Pd-based nanostructures have been designed by alloying Pd with other metals. Pd-based alloys supported on graphene could be prepared by chemical reduction procedure.[257,273,274] For instance, Chai and co-workers[275] prepared a novel hollow AuPd alloy nanostructure with a rough surface via a facile one-pot simultaneous reduction of Au(III) and Pd(II) with $NaBH_4$. The produced hollow nanospheres were then assembled on ionic liquid-grafted graphene sheets by electrostatic interaction to form AuPd/graphene hybrid nanomaterials under mild conditions. Recently, our group successfully synthesized PdAg nanorings supported on GNs by two steps.[276] In the first step, Ag nanoparticles supported on graphene nanosheets (Ag/GNs) were prepared by refluxing an aqueous mixture of silver nitrate and GO with sodium citrate as the reducing agent. In this process, the oxy-functional groups on GO surface can act as nucleation sites and facilitate seeding and growth of the silver nanoparticles. Taking advantage of the different standard reduction potential between Ag^+/Ag (+0.7991 V vs NHE) and Pd^{2+}/Pd (+0.915 V vs NHE), PdAg nanorings can be obtained through a galvanic replacement reaction between the Ag nanoparticles and Pd^{2+} on GNs. From the HRTEM images shown in Figure 13a,b, the highly crystalline ring-shaped

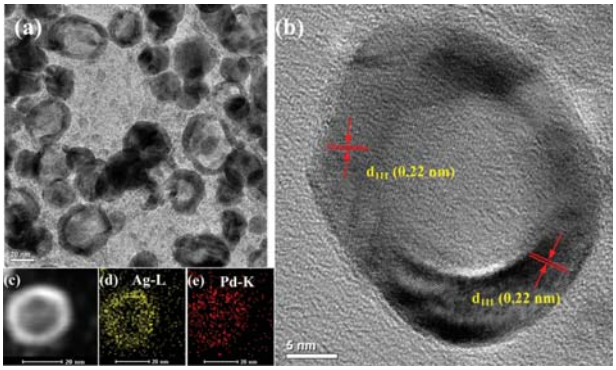

Figure 13. (a,b) HRTEM images of PdAg nanorings supported on GNs at different magnifications. (c) High-angle annular dark-field (HAADF) micrograph of single PdAg nanoring, and (d,e) the corresponding elemental mapping of Ag and Pd. Reprinted with permission from ref 276. Copyright 2013 Wiley-VCH.

nanocrystals can be observed clearly. The elemental mapping shown in Figure 12c–e indicates that Ag and Pd are evenly distributed in the shell of nanorings.

In addition, Pd-based ternary alloy composites supported on GNs have also been prepared via chemical reduction procedures. Awasthi[277] reported a graphene-supported ternary Pd–Ru–Sn nanoalloy with a face centered cubic structure by a microwave-assisted polyol reduction method. Briefly, GNs, $RuCl_3$, $PdCl_2$, and $SnCl_2{\cdot}2H_2O$ were dispersed in ethylene glycol under ultrasonication. Ternary Pd–Ru–Sn/GNs composites were obtained by keeping the resulting mixture in a microwave oven for 5 min at 800 W power with a solution pH of 10. Meanwhile, impregnation and heat treatment (hydrogen atmosphere) provide simple, low-cost, high-efficient synthetic routes to synthesize highly dispersed Pd and Pd-based nanoparticles on GNs.[278−280] Seo and co-workers[281] synthesized GNs-supported Pd and Pd_3Y nanoparticles through the impregnation method combined with a heat treatment under hydrogen gas. Both experimental and ab initio density functional theory calculations showed that the alloying with Y can significantly modify the electronic structures of Pd atoms. The up-shifted d-band center and thus enhanced bond strength of Pd–O in Pd_3Y/GNs make the Y-modified bimetallic Pd alloys good electrocatalysts for ethanol oxidation but not for ORR.

2.3.2. Au- and Ag-Based Nanocatalysts/GNs. Although Pt- and Pd-based nanomaterials are the most active catalysts, further exploring other noble metals, such as Au, Ag, and their alloys, as advanced catalysts is of significance in both fundamental research and practical applications in fuel cells. Bulk coinage metals are quite inert and show poor catalytic activity due to the filled d bands and thus the high activation barriers. Interestingly, it has been found that Au, Ag, and Cu

dx.doi.org/10.1021/cr400523y | Chem. Rev. 2014, 114, 5117–5160

nanoclusters exhibit enhanced catalytic activities, which can be mainly ascribed to the high fraction of low-coordinated surface.[48,49,51,282−284] However, the small size and high surface energy of metal clusters may induce their aggregation or dissolution during the practical applications as catalysts. Therefore, deposition of metal clusters on a stable support can improve their electrochemical stability. In recent years, increasing studies have been carried out on the Au- and Ag-based nanocatalysts supported on graphene.[285−297] Among the used preparation methods, the most convenient way to prepare graphene-loaded Au or Ag nanocatalysts is based on the reduction of metal precursors' solution in the presence of graphene. Goncalves et al.[298] prepared Au nanoparticles grown on graphene surface using a simple chemical method in aqueous medium. The study showed that the presence of oxygen functionalities at the graphene surface provide reactive sites for the nucleation and growth of gold nanoparticles; no gold nanoparticles can be formed at the totally reduced graphene surfaces. Pasricha et al.[299] developed a facile method to prepare Ag/GNs through the reduction of metal precursors in graphene dispersion. In the synthesis, silver nanoparticles were first deposited on GO sheets via chemical reduction of silver ions in KOH aqueous solution. The formed Ag-GO films were then subjected to hydrazine treatment to remove the oxygen functionalities to reduce the defects and restore the sp^2 network. Ye's group[300] used mixed reducing agents of EG and $NaBH_4$ to prepare Ag/graphene composites. The mixed reductants can not only keep the mild reaction environment, but also enhance the reducing strength to speed up the reaction. Moreover, by controlling the strength of the reducing agents, the chemical reduction of GO to graphene and the formation of Ag nanoparticles can be achieved simultaneously. Recently, Li and colleagues[301] reported a novel method for synthesizing a cylindrical piece of Au/graphene hydrogel with 1.08 cm in diameter and 1.28 cm in height through the self-assembly of Au/graphene sheets under hydrothermal conditions with GO as the graphene precursor, chloroauric acid as Au precursor, and triethylenetetramine as a reductant. Such 3D nanocomposites can improve the stability and the catalytic activity.

Metal nanoparticles produced by chemical reduction methods usually exhibit poor dispersion on GNs, and the hydrophobic GNs tend to aggregate through van der Waals interactions. With the assistance of positive charge polyelectrolyte and surfactant, noncovalent functionalization of GNs could be easily realized, which is favorable for the generation of Au or Ag nanoparticles uniformly dispersed on surface of GNs.[188,302−304] Of them, Zhang et al.[305] reported a facile one-pot method for synthesizing high-quality single-layer Ag-graphene composite by using commercially available poly-(*N*-vinyl-2-pyrrolid one) (PVP) as reductant and stabilizer. The size and loading of Ag nanoparticles can be tuned by changing the reaction time and the ratio between the precursors of $AgNO_3$ and GO. In another work, Li et al.[306] synthesized 3,4,9,10-perylene tetracarboxylic acid (PTCA)-functionalized graphene/Au-ionic liquid through a chemical reduction route. In the first step, the conjugated ring of PTCA can interact with graphene sheets through the $\pi-\pi$ stacking and hydrophobic forces, and the −COOH groups on PTCA can separate the exfoliated graphene sheets and serve as uniformly distributed sites for nucleation of Au nanoparticles. The synthesized amino-terminated ionic liquid can interact with the −COOH of PTCA/graphene and in situ reduce $HAuCl_4$ to Au nanoparticles. The resulting hybrid nanocomposites showed high electrocatalytic activity for ORR. Different from the usual in situ growth of metal nanoparticles on graphene sheets from the corresponding metal salts, Huang et al.[307] demonstrated a facile method to synthesize Au/GO(or rGO) composites just by mixing GO (or rGO) and presynthesized gold nanoparticles with surface functionalized by 2-mercaptopyridine. Through the noncovalent $\pi-\pi$ stacking and other molecular interactions, Au nanoparticles can be assembled on GO or rGO with controlled size, size distribution, and morphology. Cho et al.[292] reported an interesting procedure to synthesize gold nanostructures with well-defined shapes deposited on unfunctionalized rGO. First, a $HAuCl_4$ layer was coated on an rGO film supported on glass. The dried $HAuCl_4$ layer was reduced to gold nanocrystals with EG vapor at high temperature. The shape of the Au nanostructures can be tuned by changing the loading of $HAuCl_4$, triangular nanoplates produced at low Au loading, and hexagonal and pentahedron nanoplates formed at high Au loading.

In addition to the traditional chemical reduction method, other synthetic strategies, such as electrochemical deposition,[290,308,309] photochemical synthesis,[310] and thermal reduction,[182] have also used to synthesize Au (or Ag)/graphene composites. Fu and co-workers[311] prepared Au/graphene nanocomposites by electrochemically reducing GO and Au (III) in ionic liquid, while Zhao et al.[312] synthesized a novel 3D hybrid film composed of electrochemically reduced graphene oxide (ERGO)/silver nanoparticle via an electrochemical route. The formed nanocomposite has layer-by-layer structure decorated by Ag nanoparticles as separators. Electrochemical sensor fabricated from the nanocomposites demonstrated fast, stable, and reliable detection of hydrogen peroxide, which could be ascribed to the enlarged surface area of the 3D layered structure. Zhang's research group[310] developed a photochemical method for the one-pot synthesis and in situ assembly of fluorescent Au nanodots (AuNDs) on rGO sheets. In the method, the surface of rGO was prefunctionalized with 1-octadecanethiol (ODT), which served as template for the in situ synthesis and assembly of AuNDs. By using an electrostatic self-assembly and thermal annealing method, Zhou and co-workers[313] fabricated transparent and conductive Ag nanoparticles/rGO multilayer film. In the procedure, Ag nanoparticles with surface capped by poly-(diallyldimethylammonium-chloride) were first synthesized. Monolayer composite of Ag nanoparticles/GO was prepared by immersing a pretreated and hydroxylated quartz substrate in the silver and GO colloid solution successively. Multilayer composites can be synthesized by repeating the adsorption cycles. The obtained films were thermally reduced to Ag nanoparticles/rGO.

Graphene is an ideal support for dispersion of metal nanoclusters, even for the naked particles, which is very beneficial for their application as electrocatalysts. Tang and co-workers demonstrated a simple strategy to grow Au nanoclusters with clean surface on rGO sheets without any additional protecting and reducing agents.[50] In a typical reaction, 1.8 nm gold nanoclusters can be formed on rGO sheets by mixing $HAuCl_4$ and presynthesized rGO solution. From the SEM and TEM images shown in Figure 14, the produced Au nanoclusters with monodisperse size are uniformly dispersed on the surface of rGO sheets, and no clusters can be formed outside the rGO. According to the proposed mechanism, negative-charged rGO can adsorb

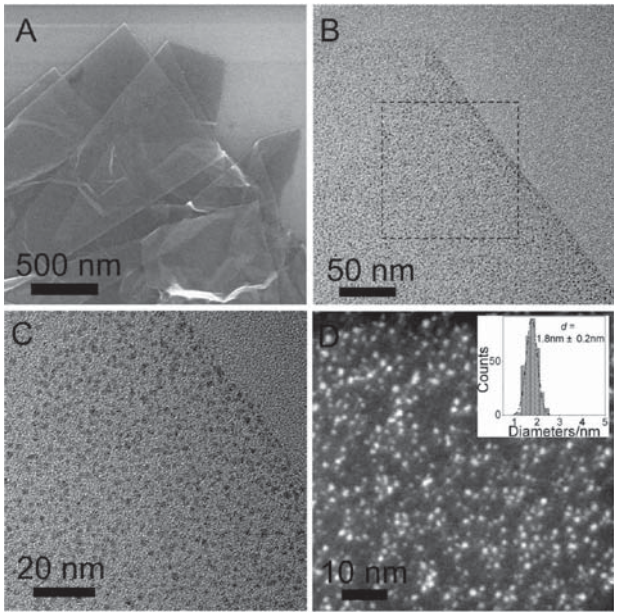

Figure 14. (A) SEM, (B,C) TEM, and (D)HAADF of Au nanoclusters supported on reduced GO. Inset in (D) is the size histogram of gold clusters with an average diameter of 1.8 ± 0.2 nm. Reprinted with permission from ref 50. Copyright 2012 American Chemical Society.

strongly the positive Au(III) ions, and most Au(III) ions may coordinate with the heteroatoms (N) at the defects of rGO sheets. Because of the electron-donor property of rGO sheets, the anchored Au(III) ions can be reduced to clusters on the surface of rGO. The prepared Au/rGO hybrid exhibited excellent electrocatalytic performance for ORR with onset potential comparable to that of commercial Pt/C catalyst.

The above syntheses are based on chemical processes. Recently, Chen and co-workers[314] reported a physical method for depositing aerosol Ag nanocrystals onto GO sheets by using electrostatic force directed assembly (ESFDA) technique. Figure 15 shows the schematic diagram of the preparation of aerosol Ag nanocrystals and the subsequent ESFDA process. Ag nanoparticles were synthesized with physical vaporization of Ag wire by using arc plasma source kept between a tungsten cathode and a graphite anode. The produced aerosol was carried by inert gases to an electric field between two electrodes. One electrode is the grounded metal tubing for

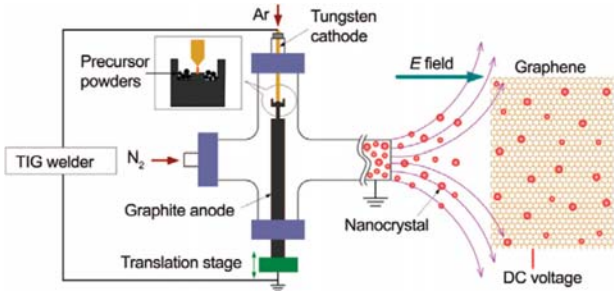

Figure 15. Schematic diagram of the synthesis of Ag aerosol nanocrystals using a mini-arc plasma reactor and the subsequent deposition of the Ag nanocrystals onto GO sheets through electrostatic force directed assembly (ESFDA) technique. Reprinted with permission from ref 314. Copyright 2009 Springer.

introducing the Ag aerosol. Another electrode composed of TEM grid containing GO sheets was applied with a direct current voltage. When a DC voltage was applied to the GO/TEM grid, the oppositely charged Ag aerosol nanocrystals can be assembled onto the GO surface.

2.3.3. Fe-Based Nanocatalysts/GNs. Advantages in low cost, recycling capability, and excellent catalytic activity of Fe-based nanomaterials dispersed on carbon supports render them good elecrocatalyts for the ORR in fuel cells. FeN_x and FeC_x materials, including macrocycles and chelates supported on carbon materials, exhibited excellent catalytic activities for ORR in acidic media.[63,315−321] In the early days, the iron-based catalysts were prepared by depositing macrocycles on a carbon support and pyrolyzing the product in inert atmosphere. In 1989, Yeager and co-workers[322] found that the compounds can be obtained from simple N- and metal-containing precursors. From then on, Fe-based catalysts have been successfully synthesized through high-temperature pyrolysis of iron complexes or procedures of iron salts and nitrogen-rich compounds.[323−330] Since the discovery of graphene in 2004, monolayer or multilayer graphene or its oxide has been widely utilized as supports for FeN_x catalysts.

Noncovalent functionalization of GNs with iron tetrasulfophthalocyanine (FeTsPc) was achieved not only to prevent the aggregation of GNs but also form an efficient electrocatalyst with the maximum power density close to that of Pt/C cathode.[331] Parvez et al.[332] developed a cost-efficient synthesis of N-doped graphene (NG) by using cyanamide as a nitrogen source, with which high and controllable nitrogen contents can be realized after pyrolysis. They found that the NG decorated with 5 wt % Fe nanoparticles exhibited enhanced catalytic performance for ORR with $4e^-$ transfer process, large current density, superior stability, and high tolerance to methanol crossover in both alkaline and acidic solutions. Among the FeN_4 macrocycles, iron(II) phthalocyanine (FePc) attracted much attention due to its best catalytic performance for ORR.[333] However, the poor electron conductivity and easy aggregation largely limit its practical application in fuel cells. Recently, Hou and co-workers[334] studied the ORR catalytic activities of FePc supported on GO, rGO, and N-doped GNs(N-GNs) and found that the FePc/N-GNs exhibited the best catalytic performance for ORR. It should be noted that most of the N-doped graphene and nonprecious catalysts supported on graphene are only catalytically active in alkaline media, which limits their application in acidic fuel cells. Therefore, developing efficient FeN_x/GNs catalysts working in acidic solutions is very important for their practical applications. Recently, Kamiya et al.[335] reported a one-pot synthesis of graphene sheets modified by iron and nitrogen in a much shorter heat-treatment period (45 s) as compared to the long-duration heat treatment in the pyrolysis-based methods (~a couple of hours). In the electrocatalytic studies in 0.5 M H_2SO_4, it was found that the synthesized Fe−N/graphene exhibited much enhanced catalytic activity for ORR as compared to the N-graphene and Fe-graphene. This study suggests that the atomic iron coordinated with N, that is, Fe−N/graphene hybrid, served as the active reaction center for ORR. In another study, Tsai and co-workers[336] reported carbon-containing iron nitride nanoparticles (FeCN) supported on N-GNs, which were synthesized through a chemical impregnation and thermal treatment process. As compared to the N-GNs, FeN, and FeN/C, the FeCN/N-GNs showed superb performance in ORR with the highest stability and

dx.doi.org/10.1021/cr400523y | Chem. Rev. 2014, 114, 5117−5160

almost four-electron transfer reaction. The Fe−N−C catalytic active sites in the FeCN/N-GNs may be responsible for its enhanced catalytic activity. Through a thermal treatment of a mixture of iron salt, graphitic carbon nitride (gC_3N_4), and rGO, Fe−N-GNs nanostructures have also been successfully prepared and showed promising ORR activities.[337−339]

Recently, Jahan et al.[340] fabricated a hybrid metal organic framework (MOF) by reacting the pyridine-functionalized graphene with iron-porphyrin, which possesses high electrocatalytic activity for ORR. The synthetic routes to make graphene-porphyrin MOF are shown in Figure 16. In the first

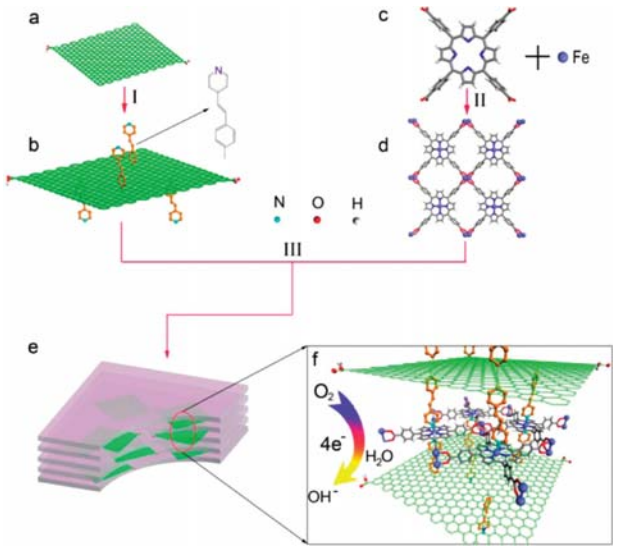

Figure 16. Schematic of the chemical structures and synthetic routes to prepare graphene-porphyrin MOF: (I) G-dye synthesized from rGO sheets via diazotization with 4-(4-aminostyryl) pyridine, (II) $(Fe-P)_n$ MOF synthesized via reaction between TCPPs and Fe ions, and (III) $(G\text{-dye-FeP})_n$ MOF formed via reaction between $(Fe-P)_n$ MOF and G-dye. Reprinted with permission from ref 340. Copyright 2012 American Chemical Society.

step, through diazotization with 4-(4-aminostyryl) pyridine, rGO was functionalized by donor-π-acceptor dye molecules terminated with pyridinium moieties. Meanwhile, MOF structure ($(Fe-P)_n$ MOF) was constructed via the reaction between 5,10,15,20-tetrakis (4-carboxyl)-21*H*,23*H*-porphyrin (TCPP) and Fe^{3+} ions. Finally, $(G\text{-dye-FeP})_n$ MOF was formed through the reaction between G-dye and $(Fe-P)_n$ MOF. In the synthesis, the addition of rGO can change the crystallization process of iron−porphyrin in the MOF, and therefore increase its porosity, enhance the electrochemical charge transfer rate of iron-porphyrin, and show efficient four-electron ORR activity.

Besides iron complexes, iron oxide is also a class of effective alternative catalysts for ORR. By depositing on graphene support, the degradation of metal oxide catalysts suffering from the dissolution, sintering, and agglomeration in electrochemical operation can be significantly improved. Recent studies also revealed that the synergetic chemical coupling effects between graphene sheets and metal oxides are beneficial to their electrocatalytic activities.[253,341] Wu et al.[254] synthesized three-dimensional Fe_3O_4/N-graphene networks via hydrothermal assembly and thermal treatment route. In the study, the novel 3D N-doped graphene aerogels can provide rich macroporosity and multidimensional electron transport pathways, which is very beneficial for their application as catalyst supports. Actually, the electrochemical studies showed that the 3D Fe_3O_4/N-graphene hybrid exhibited a more positive onset potential, higher cathodic current density, lower H_2O_2 yield, and higher electron transfer number for the ORR in alkaline electrolyte in comparison with the Fe_3O_4 nanoparticles supported on N-doped carbon black or N-doped graphene sheets.

2.3.4. Co-Based Nanocatalysts/GNs. Cobalt-based nanostructures supported on graphene have been proven to be a class of efficient electrocatalysts for ORR and have attracted tremendous attention in both experimental and theoretical scientific communities.[342,343] From density functional calculations, Mao et al.[344] found that after optimization the center of the hexagonal ring in graphene sheets is the most stable site for Fe, Co, Ni to stay, and the system of Co adatom on graphene exhibits metallic electronic structure. Recently, Olson and co-workers[345] studied the selectivity of Co-based ORR catalysts in the presence of methanol and formic acid by using experimental and theoretical analyses. It was found that noncompetitive reaction adsorption process is present in the mixed methanol/O_2 because O_2 is preferentially adsorbed on the Co−N_x type sites, whereas the adsorption of methanol mainly occurs on graphitic type surface sites. However, there exists a competitive reaction adsorption process for the formic acid/O_2 mixture as both O_2 and formic acid have a tendency to be adsorbed on the Co−N_x type sites. As efficient ORR electrocatalysts, Co_3O_4/GNs nanostructures have been studied recently from their electronic structures to their ORR catalytic performances. Wang et al.[346] studied the chemical, electronic, and structural properties of Co_3O_4 nanocrystals supported on N-doped graphene sheets (Co_3O_4/N-GNs) by spatially resolved X-ray absorption near edge structure (XANES) spectroscopy and chemical imaging. The authors found that due to the strong covalent interaction between graphene sheets and Co_3O_4, the Co^{3+} in the hybrid was partially reduced to Co^{2+}, and the reduction varies spatially on and among individual Co_3O_4 nanocrystal-graphene sheets. Meanwhile, nitrogen sites on graphene were found to be the major and important anchoring sites for Co_3O_4 nanocrystals in addition to the carbon and possibly oxygen sites.

Deposition of Co and Co-based nanoparticles onto graphene sheets as efficient electrocatalysts has been demonstrated theoretically and experimentally in recent years. The reported methods include pulsed laser deposition, chemical deposition, wet chemical and heat treatment, electrodeposition, etc. The various types of physical and chemical methods can provide different configurations and spaces to synthesize graphene-supported Co-based nanomaterials with desired morphology and tunable properties. As an important electrochemical active material, a great deal of interest has been focused on $Co(OH)_2$ material. Zhu and co-workers[347] designed a facile and straightforward soft chemical strategy to deposit $Co(OH)_2$ nanoparticles on graphene sheets at a low temperature (approximately 83 °C) in a water−isopropyl alcohol system by utilizing Na_2S as a precursor. Wu et al.[348] fabricated graphene−cobalt hydroxide composite by casting graphene suspension on a GC electrode first and subsequent electrodeposition of $Co(OH)_2$ from $Co(NO_3)_2$ solution. The hybrid exhibited efficient four-electron O_2 reduction at lower overpotential as compared to the two successive two-electron processes of ORR on only graphene modified GC electrode.

dx.doi.org/10.1021/cr400523y | *Chem. Rev.* 2014, 114, 5117−5160

Cobalt oxides (sulfides) are promising alternative electrocatalysts, but metal oxides frequently suffer from dissolution, sintering, and agglomeration during their electrochemical operation, which can result in catalyst degradation. When Co oxides are deposited on graphene nanosheets, the low intrinsic electrical conductivity of metal oxides can be remarkably improved, which favors their electrocatalytic activities. Meanwhile, the synergetic chemical coupling effects between graphene and the metal oxides (sulfides) are also beneficial to the enhanced electrocatalytic activity of the hybrid nanomaterials. The composites of flexible and electrically conductive graphene anchored with nanostructured Co_3O_4 particles can efficiently utilize the combinative merits of nanosized Co_3O_4 and graphene.[349] On the other hand, the functional groups presented on the surface of GO, such as −OH, −COOH, and epoxides, can interact with metal precursors and thus facilitate the nucleation and formation of oxide nanoparticles. Dai's group has synthesized a series of nanocomposites consisting of Co_3O_4,[253] $Co_{1-x}S$,[255] and $MnCo_2O_4$[256] nanocrystals grown on GNs as excellent ORR electrocatalysts. For instance, controlled nucleation of Co_3O_4 on GO sheets was achieved by the slow hydrolysis $Co(OAc)_2$ in ethanol/H_2O system and subsequent hydrothermal reaction.[253] It was found that the catalytic performance of the hybrid can be greatly enhanced by adding NH_4OH during synthesis to afford N-doping in graphene. Similar to ORR catalyzed by a commercial Pt/C catalyst, the obtained Co_3O_4/N-doped graphene favored the efficient four-electron oxygen reduction process. They also successfully fabricated well-defined $MnCo_2O_4$/graphene nanocomposite using the similar synthetic protocol mentioned above.[256] The produced nanocomposites showed high electrocatalytic activity and long stability in alkaline media and therefore may be advanced electrocatalysts with low-cost for energy conversion and storage. The $Co_{1-x}S$/GNs hybrids synthesized via a low-temperature solution-phase reaction followed by a high-temperature annealing step also showed unprecedented high ORR catalytic performance among all of the studied cobalt chalcogenide catalysts in acid medium.[255]

Recently, Sun and co-workers[341] synthesized Co nanoparticles assembled on graphene sheets with a layer of CoO formed on the surface of Co (Co-CoO/GNs). By controlling the oxidation extent, a series of Co-CoO/GNs were obtained with different particle size and thickness of CoO shell. The results demonstrated that the optimized Co-CoO/GNs hybrid has a comparative activity and better stability than the commercial Pt/C and may serve as a promising alternative catalyst for the ORR in alkaline solutions. The authors also found that the thickness of the CoO layer has an effect on the catalytic activity of the Co-CoO/GNs, and the hybrid with a 1 nm CoO shell exhibited the best activity. In addition to monometallic Co nanoparticles, bimetallic materials of cobalt and other metals were also reported as advanced non-noble electrocatalysts. For instance, Wang et al.[350] synthesized non-noble Ni−Co/graphene electrocatalysts through a simple solution synthesis method by using hydrazine hydrate as a reducing agent and ethylene glycol as a solvent. As compared to the Ni/graphene catalyst, the Ni−Co/graphene has higher catalytic activity and better stability for ethanol electrooxidation.

Carbon-supported cobalt/nitrogen (Co−N/C) materials have attracted increasing attention due to their promising catalytic activity toward the ORR, along with the utilization of abundant, inexpensive precursor materials. Previous studies indicated that the high temperature heating treatments during catalyst synthesis can remarkably enhance the electrocatalytic activity as well as the stability of the Co−N/C materials.[351,352] Similarly, graphene functionalized with transition metal macrocycle compounds have been fabricated as good alternatives to Pt-based catalysts. Kim et al.[353] prepared cobalt[tetrakis(*o*-aminophenyl)porphyrin] (CoTAPP) covalently anchored carbon nanomaterials (graphene, single-walled carbon nanotubes (SWCNTs), and multiwalled carbon nanotubes (MWCNTs)) via diazonium salt reactions and compared their electrocatalytic activity for the ORR. It was found that among the materials, graphene anchored with CoTAPP exhibited the most efficient electrocatalytic performance for ORR, further illustrating the advantage of graphene as carbon support.

2.3.5. Ni-Based Nanocatalysts/GNs. Nickel is a kind of low cost, relatively abundant material that is used extensively in numerous industrial applications. Among non-noble metals, Ni is a versatile catalytic material due to its electrochemical stability and resistance to poisoning. Ni can be easily converted to $Ni(OH)_2$, and the Ni^{2+}/Ni^{3+} redox centers show high catalytic activity toward oxidation of alcohols in alkaline media.[354,355] As one of the alternatives of Pt, many Ni-based catalysts, such as pure nickel,[356−358] nickel alloys,[359−363] nickel complexes,[364] and nickel hydroxides,[365] have been successfully performed to fabricate new anode and cathode catalyst systems.

As compared to other carbon materials, graphene is more suitable to immobilize guest nanoparticles due to the large contact area from its planar structure. In recent years, chemical reduction and heat treatment have been used to synthesize Ni-based materials supported on graphene. For example, Zhang and co-workers[366] prepared Ni nanoparticles anchored on graphene nanosheets by reducing GO and Ni^{2+} ions in one pot with hydrazine and the following heat treatment at high temperature (300−700 °C). The Ni/GNs obtained at 500 °C demonstrated the highest activity and stability for methanol electrooxidation in an alkaline electrolyte due to its small size and surface oxygen species. In another study, Elzatahry et al.[367] synthesized nickel oxide and cobalt oxide−graphene nanocomposites and investigated their electrocatalysis for methanol oxidation in acidic media. Recently, Lambert et al.[368] reported an interesting work on the simple syntheses of graphene-Ni-α-MnO_2 and graphene-Cu-α-MnO_2 nanowire blends. The specific activities and half-wave potentials of the hybrid materials for ORR exhibited values comparable to that of the commercial 20% Pt/C benchmark catalyst. However, the poor electrical conductivity of nickel oxides, hydroxides, and its oxidized NiOOH form may restrict their catalytic performance to some extent. Therefore, much work has been focused on using different additives to improve the electrocatalytic property of nickel, among which ethanol electrooxidation by Pd−Ni,[37] Cu−Ni,[369] and Ni−Zn[370] in alkaline solution has been reported.

2.3.6. Other Non-noble Nanocatalysts/GNs. Besides the Pt-free nanomaterials supported on graphene mentioned above, other non-noble nanocatalysts/GNs have also been investigated as electrocatalysts for fuel cells.[371,372] Yan et al.[373] reported a facile method to prepare ∼4 nm Cu_2O nanoparticles dispersed on rGO by reducing copper acetate with diethylene glycol as both solvent and reducing agent. The Cu_2O/rGO composite exhibited high ORR activity and excellent tolerance to CO and methanol in alkaline medium. MnO_x nanomaterials have also been found to be efficient ORR electrocatalysts.[374−376] Cheng

dx.doi.org/10.1021/cr400523y | *Chem. Rev.* 2014, 114, 5117−5160

et al.[377] found that the catalytic activities of MnO_2 for ORR in alkaline solution depend strongly on the crystallographic structures, with the order of α- > β- > γ-MnO_2. Gao and co-workers[378] synthesized MnO_2/rGO composites by a polymer-assisted chemical reduction method and found that the hybrid has excellent catalytic property for ORR in alkaline media with a $4e^-$ process. In another work,[379] Mn_3O_4 nanoparticles were anchored in the ionic liquid-modified rGO nanosheets by a facile solution-based growth mechanism. Lee et al. found that the hybrid with a higher Mn_3O_4 (52.5%) content showed ORR catalytic activity with the inefficient two-step, two-electron pathway. The ORR mechanism of the hybrid with a lower Mn_3O_4 (19.2%) content, however, is similar to a Pt/C catalyst with a one-step, four-electron pathway. Here, the ionic liquid can not only improve the conductivity of the hybrid, but also enhance the electrocatalytic activity of the system. In the following study, Wu et al.[380] synthesized graphene-supported manganese oxides (MnO_x) with different crystalline structures and morphologies. The authors found that the catalytic activities of the hybrid materials for ORR vary in the sequence: α-MnO_2 nanowire > amorphous MnO_x nanoparticles > β-MnO_2 microprism. The α-MnO_2 nanowire exhibited the highest catalytic property for four-electron reduction of O_2 in 0.1 M KOH solution and highest durability among the materials.

As an important transition-metal catalyst, Ir-based binary and ternary alloys have been studied as anode and cathode electrocatalysts for fuel cells. Recently, we synthesized iridium−vanadium bimetallic nanoclusters dispersed on rGO nanosheets through a facile "surfactant-free" method (Figure 17a) and studied their electrocatalytic activities for ORR in alkaline electrolyte.[381] As shown in Figure 17b and c, the as-synthesized IrV nanoclusters are uniformly dispersed on rGO sheets, and each IrV cluster has high-quality single-crystalline nature. The overall average core diameter of the clusters is 2.02 ± 0.02 nm, and the EDX showed the presence of both Ir and V. The electrochemical studies showed that the IrV/rGO hybrids exhibited composition-dependent catalytic activity for ORR and the Ir_2V/rGO clusters displayed the highest catalytic performance.

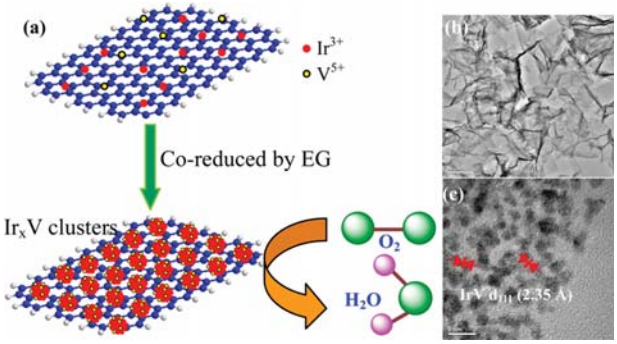

Figure 17. (a) Schematic illustration of the synthesis of IrV nanoclusters and their application for the oxygen reduction reaction. (b,c) HRTEM images of the Ir_2V bimetallic nanoclusters assembled on rGO sheets at different magnifications. The scale bars are 500 and 5 nm, respectively, in (b) and (c). Reprinted with permission from ref 381. Copyright 2013 Royal Society of Chemistry.

2.4. Graphene-Supported Metal-Free Electrocatalysts

Metal-based hybrids have exhibited significantly high electrocatalytic activities in the aforementioned studies as anode and cathode catalysts. However, the metal-based electrocatalysts often suffer from some disadvantages, such as high cost, poor durability in strong acid or base, and so on. Therefore, developing fully metal-free electrocatalysts is of great importance for the wide commercialization of fuel cells. Graphene-supported metal-free electrocatalysts and their applications are summarized in Table 4. As discussed above, heteroatom-doped graphene is one of the most studied metal-free nanocatalysts for oxygen reduction reaction (ORR) in fuel cells.[382−389] Although it is still a challenge to determine the exact active sites of heteroatom-doped graphene, many researchers have proved that the heteroatom doping can induce the charge redistribution of graphene. It was proposed that the dopant (regardless of whether it has a higher (like N, S) or lower (like B) electronegativity than carbon) could create charged sites favorable for O_2 adsorption, and thus induce the intramolecular charge transfer. Recently, carbon hybrid materials combining heteroatom-doped graphene with carbon nanotube (CNT) have been reported as an important class of metal-free nanocatalysts.[390] For example, Yu and co-workers[391] designed a mildly hydrothermal process to synthesize the hybrid composite of nitrogen-doped carbon nanotube supported on nitrogen-doped graphene (NG-NCNT) by using graphene oxide (GO), oxidized multiwalled carbon nanotube (OCNT), and ammonia as precursors. In the work, the authors demonstrated that the nanocomposite has synthergistically enhanced electrocatalytic activity for ORR, and the activity is much higher than those of the NG, NCNT, and the directly mixed product of GO and OCNT. In another case, Jin et al.[392] successfully fabricated the selenium-doped CNT/graphene composites (Se-CNT-graphene) through a facile thermal annealing process using CNTs, GO, and diphenyl diselenide (DDS) as precursors. The structure characterizations demonstrated that an interpenetrating network between CNTs and graphene has been formed, which can effectively accelerate reactant, ion, and electron transport and therefore synergistically improve the ORR catalytic activity. These studies suggest that fabrication of carbon hybrid materials will open a unique strategy to obtain novel metal-free catalysts with high activity, low cost for fuel cell applications.

In recent years, carbon nitride (CN) has attracted much attention in the studies of metal-free catalysts.[393−398] As a kind of carbonaceous material enriched with nitrogen content including pyridinic and graphitic nitrogen moieties, carbon nitride has been theoretically and experimentally considered to have high electrocatalytic activity for ORR. However, the low electrical conductivity ($<10^{-2}$ S/cm) of CN materials significantly hampers the electron transfer as electrocatalysts for fuel cells. To overcome the disadvantage, Yang et al.[399] successfully fabricated the graphene-based carbon nitride (G-CN) nanosheets by using graphene-based mesoporous silica nanosheet as template, and ethylenediamine and carbon tetrachloride as precursors. Through the synthetic process, the produced thin G-CN nanosheets not only exhibited high surface areas, high nitrogen content, but also showed improved electrical conductivity. These excellent properties are very favorable for the adsorption of oxygen molecules on the surface of G-CN catalysts, and can lead to the rapid diffusion of electrons during the ORR process. Accordingly, the electrochemical measurements indicated the outstanding electro-

dx.doi.org/10.1021/cr400523y | Chem. Rev. 2014, 114, 5117−5160

Table 4. Graphene-Supported Metal-Free Nanocatalysts and Their Applications

catalyst	preparation method	precursor	application	ref
rGO	electrochemical reduction	GO	ORR in acid	147
B-GNs	thermal annealing	GO, B_2O_3	ORR in alkaline	117
N-rGO	thermal annealing	GO, amines, EDC[a]	ORR in alkaline	436
N-GNs	CVD	CH_4, NH_3	ORR in alkaline	94
		H_2, ethylene, NH_3	ORR in alkaline	97
	solvothermal	Li_3N, CCl_4 or $N_3C_3Cl_3$, Li_3N, CCl_4	ORR in alkaline	140
	pyrolysis	GO, polypyrrole	ORR in alkaline	114
		sugar, urea	ORR in alkaline	115
N−C-GNs	hydrothermal	GO, melamine, formaldehyde, phenol	ORR in alkaline	433
N-GQDs	solution chemistry	benzene derivatives,	ORR in alkaline	434
		N-containing carbon fiber	ORR in alkaline	383
N-GNs	thermal annealing	graphene or GO, NH_3	ORR in alkaline	384
		GO, melamine	ORR in alkaline	116
		GO, silica, NH_3	ORR in alkaline	121
		N-containing polymer, rGO	ORR in alkaline	384
		GO, 5-aminotetrazole	ORR in alkaline	385
P-GNs	pyrolysis	toluene, triphenylphosphine	ORR in alkaline	113
	thermal annealing	GO, triphenylphosphine	ORR in alkaline	112
S-NGs	thermal annealing	GO, benzyl disulfide	ORR in alkaline	120
		graphene, CS_2	ORR in alkaline	386
		GO, H_2S	ORR in neutral or alkaline	387, 388
I-NGs	thermal annealing	GO, iodine	ORR in alkaline	111
B,N-GNs	thermal annealing	GO, H_3BO_3, NH_3	ORR in alkaline	122
S,N-GNs	thermal annealing	GO, melamine, benzyl disulfide	ORR in alkaline	123
	hydrothermal	GO, ammonium thiocyanate	ORR in alkaline	124
P,N-GNs	pyrolysis	GO, dicyandiamide, phosphoric acid	ORR in acid	125
N-CNTs, graphene	pyrolysis	Ni, rGO, pyridine	ORR in alkaline	389
N-graphene, N-CNTs	hydrothermal	CNTs, GO, ammonia	ORR in alkaline	391
rGO, CNTs	electrostatic interactions	GO, PDAC[b], MWNTs	ORR in alkaline	390
Se-GNs, CNTs	thermal annealing	CNTs, GO, diphenyl diselenide	ORR in alkaline	392
Se,S,N-GNs, CNTs	thermal annealing	CNTs, GO, DCDA,[c] DDS,[d] DDSe[e]	ORR in acid	126
CN, GNs	thermal annealing	rGO, polypyrrole	ORR in alkaline	398
	pyrolysis	GO, tetraethylorthosilicate, ethylenediamine, carbon tetrachloride	ORR in alkaline	399
	hydrothermal	GO, phenol, melamine,	ORR in alkaline	433
anthraquinone, GNs	electroreduction	GO, Fast Red AL salt	ORR in PBS (pH 7.0)	400
EDOT, rGO	redox-mediated synthesis	GO, EDOT[f]	ORR in alkaline	401
functionalized G nanoplatelets	ball milling	graphite, hydrogen, carbon dioxide, sulfur trioxide	ORR in alkaline	403
TDMAC, rGO	physicochemical process	GO, TDMAC,[g] $NaBH_4$	ORR in alkaline	404
amino, GNs	solvothermal	GO, ammonia	ORR in alkaline	493

[a]EDC: *N*-ethyl-*N*′-(3-dimethyl aminopropyl)carbodiimide methiodide. [b]PDAC: poly(diallyldimethylammonium chloride). [c]DCDA: dicyandiamide. [d]DDS: diphenyldisulfide. [e]DDSe: diphenyldiselenide. [f]EDOT: ethylenedioxythiophene. [g]TDMAC: tridodecylmethylammonium chloride.

catalytic activity, long durability, and high selectivity when the G-CN nanosheets were employed as metal-free catalysts for ORR.

In addition, it has also been demonstrated that through the intermolecular charge transfer between graphene and modified molecules, net positive charge can be created on carbon atoms of graphene, which could be an effective way to develop metal-free electrocatalysts.[400−403] For instance, through a simple physicochemical process, Ahmed et al.[404] synthesized reduced graphene oxide with surface functionalized by tridodecylmethylammonium chloride (TDMAC-RGO). In the synthesis, TDMAC was modified onto the surface of graphene nanosheets during the reduction of GO into RGO (by sodium borohydride) in the presence of TDMAC. Here, the quaternary ammonium salt, TDMAC, could create net positive charge on the carbon atoms of graphene sheets via the intermolecular charge transfer. Such TDMAC-functionalized/adsorbed RGO catalysts showed enhanced electrocatalytic activities toward ORR. This study suggests that the surface modification of graphene by certain molecules could be a general approach to design graphene-based metal-free ORR catalysts.

However, it should be noted that Pumera and co-workers[405] recently found that some so-called graphene-based "metal-free" electrocatalysts probably contain trace metal impurities, which are actually responsible for the improved ORR catalytic activities. In the report, the authors demonstrated that trace levels of manganese oxide modified on glassy carbon electrode and doped in graphene can effectively enhance the ORR catalytic performance. Therefore, in the electrocatalytic studies with graphene-based metal-free catalysts, it is of importance to confirm the real metal-free samples by careful elemental analysis.

dx.doi.org/10.1021/cr400523y | *Chem. Rev.* 2014, 114, 5117−5160

3. STRUCTURAL CHARACTERIZATION AND PROPERTIES OF GRAPHENE-SUPPORTED NANOELECTROCATALYSTS

3.1. Structural Characterization

Because the catalytic activities of graphene-supported nanomaterials are strongly dependent on their size, composition, morphology, and surface properties, various characterization techniques have been applied to their structural analyses. Moreover, detailed structural characterizations are needed for deeply understanding the structure−property−catalytic activity correlations, which further provide the fundamental basis for structural optimization and synthesis of nanomaterials for applications in electrocatalysts. For instance, it has been found that the electrocatalytic activities of metal nanoparticles are dependent on their structures, such as the core size, shell thickness, etc.[14,22,49,341,381] On the basis of the structural characterizations and electrochemical measurements, the dependence of catalytic performance on structure can be determined, which could give experimental feedback for further goal-directed synthesis. In this section, we briefly summarize the commonly used techniques for structural characterization of graphene-supported nanocatalysts, mainly including X-ray (XRD, XPS, EDX) spectroscopy, electron microscopy (TEM, HRTEM, SEM), ultraviolet and visible spectroscopy, infrared spectroscopy, thermogravimetric analysis, and so on.

3.1.1. Electron Microscopy (TEM, HRTEM, SEM, and STEM). For metal nanocrystals, the particle size and exposed facets represent two of the most important parameters in the regulation of their electronic and catalytic properties. Transmission electron microscopy (TEM) and scanning electron microscopy (SEM) have traditionally been used to directly obtain the morphology information of the supported nanoparticles and graphene nanosheets. However, there is around a 0.2 nm size uncertainty for TEM measurement, and more or less melting effects of tiny nanoparticles under electron beam heating could occur during imaging. Therefore, TEM can not be used to identify the actual size of small nanoclusters supported on graphene and the internal atomic structure of graphene nanosheets. High-resolution TEM (HRTEM) is a powerful tool in the study of size and crystalline structure of relatively small metal nanocrystals. On the other hand, HRTEM can not only resolve the interesting structural features of graphene, such as individual carbon atoms, defects, adatoms, etc, but also can generate defects and edge reconstruction due to the high-energy electrons.[406,407] Recently, Gomez-Navarro and co-workers[408] reported the very clear atomic structure of a single layer rGO nanosheet by using phase-contrast HRTEM. As shown in Figure 18, the hexagonal lattice of the well-crystallized graphene sheet can be seen clearly. From the different color labeled in Figure 18b, except for the graphene facet, the various defects and deformations, such as disordered carbon networks, trapped carbonaceous adsorbates, and heavy atoms, isolated pentagon−heptagon pairs and clustered defects can also be identified. The number of layers of graphene flake can be detected from the nanobeam electron diffraction in TEM.[409]

Scanning transmission electron microscopy (STEM) has also been used to investigate the morphology, crystal structure, and composition distribution of graphene and graphene-based hybrids. By using the high-angle annular dark field (HAADF) mode, the atomic information of graphen-based hybrids can be identified. For example, Pasricha et al.[299] prepared Ag-graphene-based hybrid and observed clearly the dispersion of Ag nanoparticles (bright) on graphene (dark) through the atomic-number contrast between Ag and carbon. Similarly, other graphene hybrids, such as Au nanoclusters, and PdAg nanorings supported on GNs have also been studied by HAADF-STEM.[50,276]

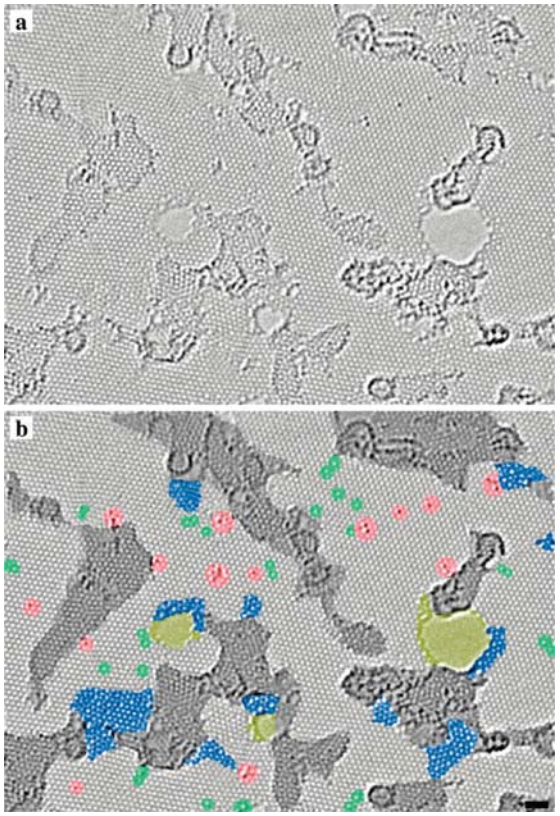

Figure 18. (a) Aberration-corrected TEM image of a single layer rGO nanosheet with atomic resolution. (a) Original image and (b) with color labeled to highlight the different features. The defect-free crystalline graphene area is displayed in the original light gray color. Contaminated regions are shaded in dark gray. Blue regions are the disordered single-layer carbon networks, or extended topological defects. Red areas highlight individual ad-atoms or substitutions. Green areas indicate isolated topological defects, that is, single bond rotations or dislocation cores. Holes and their edge reconstructions are colored in yellow. Scale bar 1 nm. Reprinted with permission from ref 408. Copyright 2010 American Chemical Society.

3.1.2. Scanning Probe Microscopy (AFM and STM). Scanning probe techniques, including atomic force microscopy (AFM) and scanning tunneling microscopy (STM), are the most important tools for the structural characterization of solid surface with atomic resolution. The morphology of a sold surface can be mapped by AFM based on the strong interatomic forces between atoms of the surface and sharp probe tips at a very short distance. There are contact, noncontact, and tapping imaging modes in AFM measurements. AFM with a tapping mode is widely used to measure the thickness of graphene sheets on different substrates. The typical thickness of a pristine graphene is around 0.34 nm. Meanwhile, the thickness of a single graphene oxide nanosheet increases to around 1−1.5 nm, possibly due to the various functional group or adsorbed molecules present on the surface of GO.[410,411] Practically, the measurement of exact thickness of graphene

dx.doi.org/10.1021/cr400523y | Chem. Rev. 2014, 114, 5117−5160

from AFM is still challenging, and repeated analyses on different substrates should be performed. To get the correct layer information, other characterization methods, such as Raman spectroscopy, should also be used to correlate the AFM measurements. On the other hand, STM can also be used to obtain the lattice structure and surface morphology of graphene at atomic resolution. Wintterlin and co-workers[412,413] studied the growth mechanism of graphene on Ru (0001) substrate by in situ high temperature STM. They found that the large terraces on Ru (0001) surface that resulted from low pressure and high temperature can produce highly ordered graphene layers. For nanoparticles deposited on graphene sheets, AFM and STM can be used to characterize the size and distribution of particle on the graphene surface.

3.1.3. Raman Spectroscopy. Raman spectroscopy is a powerful tool for characterizing ordered and disordered crystal structures of carbon materials, and there have been many studies on Raman spectra of graphene sheets.[414−416] From the Raman spectrum, the bonding configuration of carbon atoms in graphene sheets can be detected. As shown in Figure 19, the three typical Raman spectral peaks are the G band at around 1580 cm^{-1}, the D band at around 1350 cm^{-1}, and the 2D band at 2700 cm^{-1}.[414] The G band is from sp^2 carbon atoms domains, corresponding to the first-order scattering of the E_{2g} mode. The D-mode is a disorder-activated Raman mode and is related to the vibrations of sp^3 carbon atoms of disordered graphene nanosheets. D band is usually observed at graphene edge. The pervious studies showed that the position and shape of the second-order 2D-band are sensitive to the layers of graphene sheets.[414,417] On the basis of this, the 2D band can be used to evaluate the number of layers of a multilayer graphene. It can be seen from Figure 19b,c that the Raman spectra of graphene change significantly with the number of layers. Monolayer graphene exhibits a single sharp 2D band from the $2D_{1A}$ component. For bilayer graphene, the 2D band becomes broader and up-shifted in comparison with that of the single layer. From the 2D band of two-layer graphene shown in Figure 19e, the 2D band can be fitted to four components, $2D_{1B}$, $2D_{1A}$, $2D_{2A}$, and $2D_{2B}$, and the $2D_{1A}$ and $2D_{2A}$ have higher intensity than the other two. In double-layer graphene, the interaction between layers can lead to the splitting of π and π^* electronic bands into four peaks. Similarly, as indicated in Figure 19d, the D band of monolayer graphene exhibits a single sharp peak, while in bulk graphite the band splits into two peaks of D_1 and D_2. With the further increase of the number of graphene layers (Figure 19b,c), the intensity of $2D_1$ band decreases. For graphene with more than five layers, the Raman spectrum resembles that of the bulk graphite. Although multilayer non-AB stacked graphene also shows a single 2D peak,[418] the monolayer graphene can be distinguished from the full-width at half-maximum (fwhm). The fwhm of multilayer non-AB stacked graphene is 50 cm^{-1}, which is twice that of single layer graphene.

The Raman spectrum of graphene is also sensitive to the heteroatom doping and surface decoration of metal clusters.[419,420] Increasing the electron doping concentration or decreasing the hole doping concentration in graphene can lead to the decrease of 2D band position, which can be used to identify the doping type, that is, electron or hole doping. The intensity ratio of the D- and G-bands (I_D/I_G) has been widely used to evaluate the quality of graphene nanosheets.

3.1.4. X-ray Photoelectron Spectroscopy (XPS). XPS is a powerful tool to investigate the oxidation states, chemical composition, and the nature of the bonds in graphene-supported composites. Moreover, the surface chemistry of nanocomposites can also be studied from XPS results. For example, in a recent report, the oxidation states of Ir and carbon of Ir_2V nanoclusters supported on rGO nanosheets were studied by XPS measurements.[381] As shown in Figure 20a, the peaks at 61.43 and 64.35 eV in the Ir 4f photoelectron

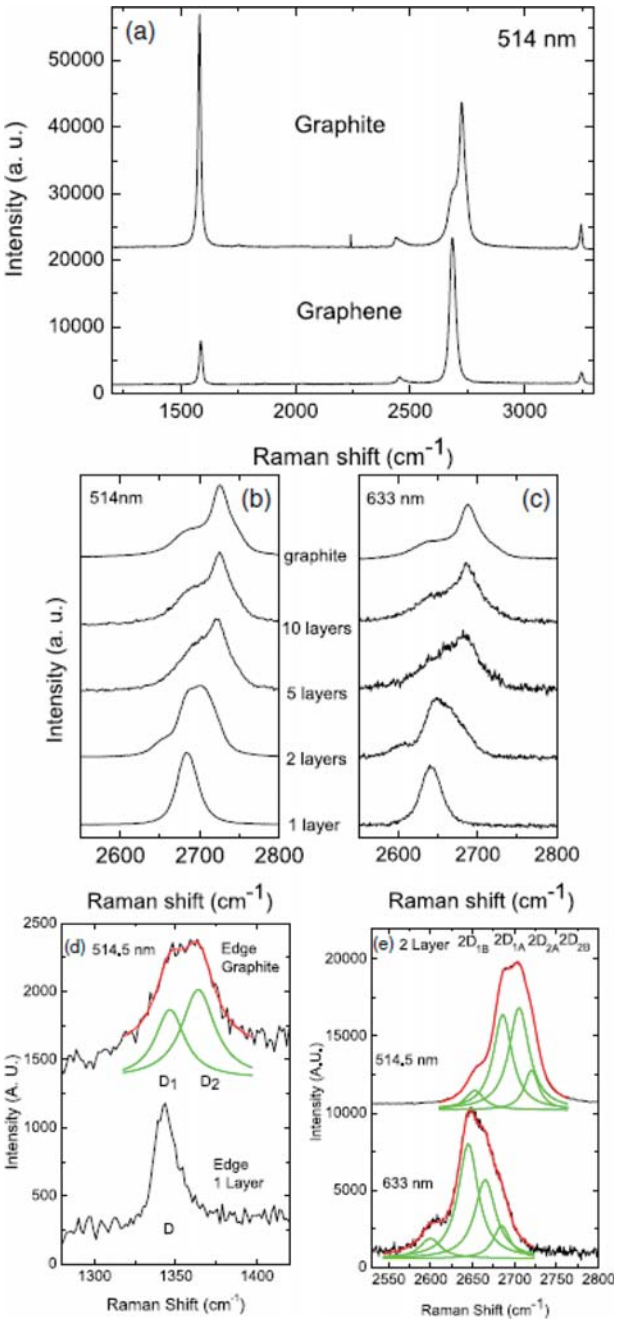

Figure 19. (a) Raman spectra of graphene and graphite. (b) Evolution of the Raman spectra at 514 nm with the number of layers of graphene. (c) Evolution of the Raman spectra at 633 nm with the number of layers of graphene. (d) Comparison of the D band at 514 nm from single layer of graphene and bulk graphite. (e) The four components of the 2D band in two-layer graphene at 514 and 633 nm. Reprinted with permission from ref 414. Copyright 2006 American Physical Society.

dx.doi.org/10.1021/cr400523y | Chem. Rev. 2014, 114, 5117−5160

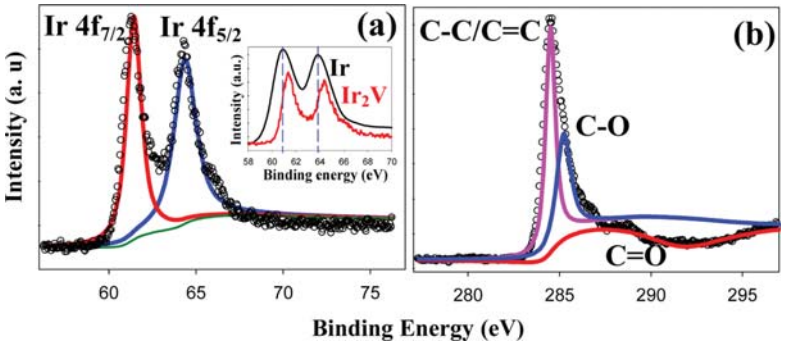

Figure 20. (a) Ir 4f and (b) C 1s XPS spectra of Ir_2V nanoclusters supported on rGO sheets (Ir_2V/rGO). The inset in (a) shows the Ir 4f XPS spectra from Ir and Ir_2V nanoclusters supported on rGO. Reprinted with permission from ref 381. Copyright 2013 Royal Society of Chemistry.

spectrum could be assigned to the binding energies of Ir $4f_{7/2}$ and Ir $4f_{5/2}$ of metallic Ir^0. Moreover, by comparing the Ir 4f XPS spectra from Ir/rGO and Ir_2V/rGO samples (Figure 20a, inset), Ir $4f_{7/2}$ and $4f_{5/2}$ shift from 60.90, 63.90 eV on Ir/rGO to 61.43, 64.35 eV on Ir_2V/rGO, respectively, exhibiting upshift of Ir 4f binding energy from Ir to Ir_2V nanoclusters (0.53 and 0.45 eV for Ir $4f_{7/2}$ and Ir $4f_{5/2}$, respectively). Such results strongly suggest the electronic interactions between Ir and V atomic orbitals, resulting in electron transfer from Ir to V. From the deconvoluted C1s XPS spectrum shown in Figure 20b, the three fitted peaks can be assigned to the binding energies of carbon in C═C/C−C, C−O (epoxy/hydroxyls), and C═O (carbonyl/ketone), respectively. The predominant intensity of C═C/C−C indicates that graphene oxide has been reduced to graphene by the ethylene glycol reduction treatment. These results clearly indicate that XPS measurements can provide valuable information about the bond structure of nanoparticles and the surface interaction between graphene support and the metals. On the other hand, from the ratio of the corresponding XPS peak intensities, the formula of metal nanoparticles or the average composition of alloy nanoparticles can also be identified.

3.1.5. X-ray Diffraction (XRD). XRD is usually used to study the crystal structure and evaluate the crystal size of nanomaterials based on the Debye−Scherrer equation. By XRD characterization, the formation of GO and rGO can be identified. When graphite powder is used as precursor for the synthesis of GO, there is a typical sharp diffraction peak at 2θ = 26.4° from the original graphite with the corresponding *d*-spacing of 3.38 Å. However, the XRD pattern of GO product shows no diffraction peaks of the parent graphite but a new broad peak at around 2θ = 10.7° (*d*-spacing of 8.27 Å).[421] The increased interlayer distance can be attributed to the hydroxyl and epoxy groups between the carbon sheets introduced and inserted by the oxidation course, which can lead to the decrease of van der Waals forces between the graphite sheets in the exfoliated GO. With $NaBH_4$ as reducing agent to obtain rGO, the diffraction peak position from GO will change with the concentration of $NaBH_4$. Shin et al.[422] reported that with the concentration of $NaBH_4$ increasing, the diffraction peak first shifted to 2θ = 9.5° and then to 9.1°. When the concentration of $NaBH_4$ further increased (150 mM), the peak of the large interlayer distance disappeared completely, and a broad peak near 2θ = 23.9° (*d*-spacing of 3.73 Å) became evident. The XRD pattern change reflects the formation of GO and the reduction process of GO to rGO. Moreover, for bimetallic or multimetallic nanoparticles supported on graphene, their XRD pattern can also reveal the crystal structures and whether the nanoparticles have alloy structure or not.[45,72,276]

3.1.6. UV−Vis Spectroscopy. Because of the different characteristic UV−vis absorption, graphene and its oxide can be identified from their UV−vis absorption spectra. For graphene, there is a characteristic adsorption peak at around 268 nm, and the ultraviolet absorption exhibits linear enhancement with the number of layers.[423] As for graphene oxide, there are two main absorption peaks in the UV−vis absorption spectrum.[424] The peak located around 230 nm and the shoulder peak around 300 nm are assigned to the $\pi-\pi^*$ transitions of aromatic C═C bonds and the $n-\pi^*$ transitions of C═O bonds, respectively. On the other hand, metal nanoparticles exhibit unique optical characteristics with an exponential decay of the absorption profile with increasing wavelength. Meanwhile, the UV−vis absorption of coin metal nanoparticles (Au, Ag) is dominated by plasmon resonance peaks at around 420 and 520 nm for Ag, Au nanoparticles, respectively. During the deposition of metal nanoparticles on GO through chemical reduction method, the UV−vis absorption change can be observed clearly. For instance, during the deposition of Ag nanoparticles on graphene nanosheets by the chemical reduction process, there are two absorption peaks for the original GO at 226 and 305 nm.[425] After the formation of Ag nanoparticles on graphene, the characteristic surface plasmon resonance absorption of Ag nanoparticles can be observed at 391 nm. Meanwhile, the absorption peak at 226 nm from GO red-shifted to 245 nm, and the shoulder peak at around 305 nm almost disappeared. The UV−vis absorption change indicated that after the chemical reduction process, Ag nanoparticles have been successfully deposited on graphene, and GO has also been reduced to rGO. Such study clearly indicates that UV−vis absorption measurements can provide valuable qualitative information about formation of nanomaterials on graphene and their interaction.

3.1.7. X-ray Absorption Near-Edge Structure (XANES). XANES, also named near-edge X-ray absorption fine-structure (NEXAFS), is a kind of powerful and nondestructive method to investigate the chemical bonding, local electronic structure, and interactions of graphene and adsorbates.[372] XANES analysis can also provide the structure information of the doped graphene, such as oxygen-containing groups.[107,426−429]

By using NEXAFS and other characterization techniques, Zhao et al.[428] studied the individual nitrogen doping in monolayer graphene and confirmed the presence of nitrogen in graphene. As compared to pristine graphene, two new peaks (400.7 and 408 eV) from the graphitic N were observed in the

dx.doi.org/10.1021/cr400523y | *Chem. Rev.* 2014, 114, 5117−5160

N K-edge NEXAFS spectrum of N-doping graphene. For the graphene-supported Co_3O_4 catalyst, Dai and co-workers[253] found that the C K-edge peak intensity of Co_3O_4/N-rGO around 288 eV showed an obvious increase as compared to the N-rGO, indicating the interaction between Co_3O_4 and GO with the possible formation of Co−O−C and Co−N−C bonds in the hybrid. On the other hand, from the O K-edge NEXAFS, there is an obvious decrease of the unoccupied O 2p-Co 3d hybridized state and an increase in the Co L-edge NEXAFS. The strong coupled interactions between graphene sheets and Co_3O_4 nanocrystals and the modified chemical bonding environment may lead to the enhanced electrocatalytic activity of Co_3O_4/N-rGO for ORR.

3.1.8. Other Characterization Methods. Besides the above techniques, other normally used characterization approaches have also been applied to the graphene-based materials. Energy dispersive X-ray (EDX) spectroscopy is also an efficient chemical tool for qualitative and quantitative element analysis of graphene-based materials. For monometallic or bimetallic nanoparticles supported on graphene sheets, EDX can be used to determine the composition of the composites.[430] Thermogravimetric analysis (TGA) is a widely used technique to characterize the thermal stability and the loading amount of metal in graphene-based composites.[72,431] In addition to Raman spectroscopy, the functional groups present on graphene (such as hydroxyl, carbonyl, carboxylic, and epoxy) can be characterized by Fourier transform infrared spectroscopy (FTIR) technique.[432] The change of surface chemistry of graphene can also be detected during the various reactions. Electron energy loss spectroscopy (EELS) is a very effective method for measuring electronic and optical properties of graphene-based nanomaterials. Combined with scanning transmission electron microscopy, the local chemistry and electronic structure of graphene can be analyzed through EELS.[410]

3.2. Catalytic Properties

3.2.1. Intrinsic Catalytic Properties of Heteroatom-Doped Graphene. In recent years, it has been found that the heteroatom-doped graphene exhibited excellent electrocatalytic activity toward oxygen reduction reaction (ORR). For instance, N-, P-, or S-doped graphene sheets or graphene quantum dots have been studied as metal-free catalysts for ORR.[94,113,120,433−436] Mullen reported that the N- or S-doped graphene exhibited excellent catalytic performance for ORR with long durability and high selectivity.[121] Qiao's group found that the N,S- and N,B-dual doped graphene showed higher ORR catalytic activity than that of N-, S-, or B-singly doped graphene.[123,437] All of these investigations indicated that the catalytic activity of graphene can be significantly enhanced through heteroatom doping. Besides the experimental studies, much effort has also been devoted to the mechanism explanation of the enhanced ORR catalytic properties of doped graphene by different theoretical calculations.

The density functional theory (DFT) calculations showed that the electrocatalytic activity of heteroatom-doped graphene is strongly dependent on the electron spin density and atomic charge density distribution on atoms.[438−441] The catalytically active sites in doped graphene are usually the carbon atoms with high spin density. The doping of N, P, or B in graphene introduces unpaired electrons and causes local high spin density, resulting in high electrocatalytic performance for the ORR. According to the study from Zhang and Xia,[438] the N-graphene containing either pyridine or pyrrole structure has electrocatalytic property for ORR with four-electron process. It was found that, as compared to atomic charge density, spin density is the more important factor in determining catalytically active sites. Qiao and co-workers studied the synergistic effect of dual doping of B, N or S, N in enhancing the ORR performance by DFT calculations.[123,437] For N-doped graphene, due to the greater electronegativity of N atoms (3.04) than that of C (2.55), the ORR activity mainly originates from the surrounding C atoms with high charge density. For S-doped graphene, there was negligible charge transfer between C and S because of their similar electronegativities. The positively charged S atoms were considered to be the catalytic centers. When graphene is dual-doped by N and S, as shown in Figure 21, the C1 has the maximum spin density (0.43), indicating

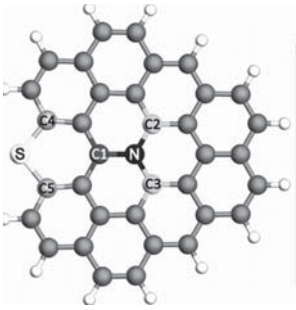

Atom Number	Spin Density	Charge Density
C1	0.43	0.23
C2	-0.03	0.28
C3	-0.03	0.28
C4	0.16	-0.22
C5	0.16	-0.22
N	0.06	-0.88
S	0.09	0.21

Figure 21. Spin and charge density of a graphene network (gray) dual-doped by N (black) and S (white). The table shows the spin and charge density of different C sites, S, and N. Reprinted with permission from ref 123. Copyright 2012 Wiley-VCH.

enhanced ORR catalytic activity. Moreover, due to the asymmetrical spin and charge density induced by dual-doping, other C sites (C2−C5) with high positive spin or charge density are also catalytically active. In the B,N dual-doped graphene, the authors analyzed the catalytic properties with the energy of HO_2 adsorption (E_{ad}), which is the rate-determining step of the ORR.[437] The results showed that the dual-doped graphene exhibited higher E_{ad} than that from singly doped B- and N-graphene, suggesting the improved ORR catalytic activity of the dual-doped graphene. Interestingly, it was also found that in singly doped N-graphene, only the graphitic N atom can induce the HO_2 adsorption at the adjacent C atom, and 2-fold-coordinated pyridinic N dopant has a tendency to suppress the ORR. However, in the dual-doped graphene the inactive pyridinic N can improve the adsorption of HO_2 on the active B dopant, whereas graphitic N decreases the activity of B.

Recently, Dai and co-workers[122] theoretically studied the ORR activities of N,B codoped graphene with different doping concentrations. From the first-principles calculations of energy gap between the highest-occupied molecular orbital (HOMO) and the lowest-unoccupied molecular orbital (LUMO), the N and B doping can result in a smaller energy gap than pure graphene and thus lead to improved catalytic activity. However, overdoping of B and N can result in significantly increased energy gap, lowering the catalytic capability of the materials. Meanwhile, the calculations showed that the pure and highly doped graphene do not have spin density at all. In contrast, graphene with modest N- and B-doping level exhibited relatively high spin and charge density. This study indicates that the energy bandgap, spin, and charge density strongly depend on the doping level, and only the modest doping can

dx.doi.org/10.1021/cr400523y | Chem. Rev. 2014, 114, 5117−5160

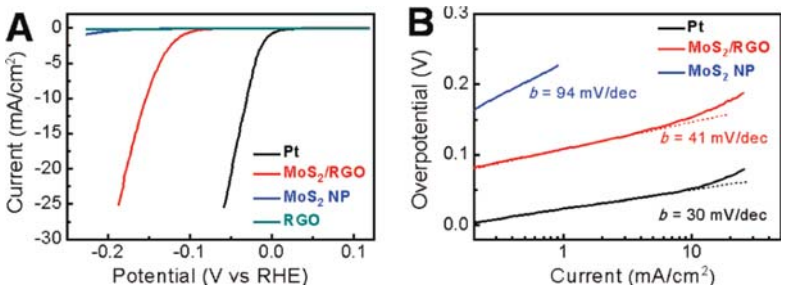

Figure 22. (A) Polarization curves of the hydrogen evolution reaction (HER) from MoS_2 nanoparticles supported on rGO and other catalysts. (B) Corresponding Tafel plots recorded on glassy carbon electrodes with a catalyst loading of 0.28 mg/cm^2. Reprinted with permission from ref 443. Copyright 2011 American Chemical Society.

enhance the electrocatalytic activity of graphene toward ORR. In another work, Kong and Chen[441] found that not all of the heteroatom doping can enhance the activity of graphene. P-substituted graphene exhibited a weak capacity of HO_2 adsorption and poor catalytic activity, which was ascribed to the large structural distortion and weakened spin density with P doping in graphene.

3.2.2. Catalytic Properties of Graphene-Supported Nanoelectrocatalysts. The enhanced electrocatalytic activities of graphene-supported nanocomposites might be partly due to the isolated sp^2 hybridized bonds (π electrons) and the strong interaction (charge transfer) between metal nanoparticles and graphene nanosheets. Johll and colleagues[442] investigated the interaction of graphene with transition-metal cluster by the plane-wave-based DFT program. They found that the charge transfer from the adsorbed clusters to graphene sheets can change the population of d and s orbitals of the metal atoms. Meanwhile, the binding energy between metal clusters and graphene depends on the adsorption site, adsorption configuration, and the composition of clusters. Dai and co-workers[443] studied the electrocatalytic activities of free MoS_2 nanoparticles and rGO-supported MoS_2 nanoparticles (MoS_2/rGO) for the hydrogen evolution reaction (HER). From the polarization curve shown in Figure 22, the prepared free MoS_2 nanoparticles and rGO alone exhibited little HER activity. However, the MoS_2/rGO showed only a small overpotential (~0.1 V) and large cathodic current density. Moreover, the MoS_2/rGO exhibited a Tafel slope of 41 mV/decade, which is very close to that obtained from commercial Pt catalyst (30 mV/decade) but much smaller than that from free MoS_2 nanoparticles (94 mV/decade). The enhanced electrocatalytic performance of MoS_2/rGO was attributed the strong chemical and electronic coupling between rGO sheets and MoS_2, which can improve the dispersion of small MoS_2 particles and afford an abundance of accessible catalytically active edge sites for the HER. On the other hand, the electronic coupling can also promote the electron transfer from the less-conducting MoS_2 particles to electrode, which was reflected from the impedance measurements.

Okamoto theoretically studied the interface interaction between graphene and Pt_{13} or Au_{13} clusters by density-functional calculations.[444] It was found that introducing a carbon vacancy into a graphene sheet can enhance the interaction between the metal clusters and graphene sheets, and the stability of the metal clusters on graphene with carbon vacancies is higher than that on defect-free graphene. Moreover, CO and H chemisorption energies become smaller on the graphene-supported metal clusters than on the clusters without carbon support. On the basis of DFT, it was also found that single-carbon-vacancy defect in graphene can significantly improve the catalytic activity of Au_8 and Pt_4 clusters supported on graphene.[445] For example, with Au_8 supported on defect-free graphene sheet, the reaction barrier of CO oxidation is around 3.0 eV, whereas the reaction barrier greatly reduced to around 0.2 eV on defective graphene. In another work, Groves et al.[446] studied the binding energy between a single Pt atom and nitrogen-doped graphene by DFT. The authors found that the N doping in graphene can increase the binding energy of C−Pt bond. Although the nitrogen atoms do not bond with Pt atom directly, the more N atoms and the closer they are to the C atom, the stronger is the binding energy of the C−Pt bond. For N-graphene, the N doping disrupts the delocalized double bond in pure graphene sheets, and therefore the C−Pt bond in N-graphene focuses on 2s/6s orbitals rather than 5d/2p orbitals. Such results suggest that the increased binding energy of Pt to N-graphene can effectively improve the catalytic stability of Pt/graphene catalysts. As an important kind of catalyst, Akturk et al.[447] studied the adsorption of Au_nPt_n nanoclusters on graphene surface by DFT. The calculations showed that the adsorption of Au_nPt_n nanoclusters on graphene can largely change the electronic properties, including the composition-dependent Fermi level and band gap.

At present, high overpotentials of ORR on most cathodic electrocatalysts arise mainly because of the sluggish electron-transfer kinetics caused by the strong adsorption of O on catalysts. Therefore, weakening the adsorption energy can improve the ORR efficiency. Recently, Liu et al.[448] studied the electronic structures of MPd_{12} (M = Fe, Ni, Cu, Zn, Pd) nanoparticles supported on defective graphene substrates and their reactivity for O adsorption by first-principles-based calculation. The defective graphene can provide anchoring sites for nanoparticle adsorption by forming strong metal−substrate interaction. The strong metal−graphene interaction can not only enhance the stability but also further tune the averaged d-band center of the deposited alloy nanoparticles, resulting in a strong effect on the O adsorption. As shown in Figure 23, as compared to the free MPd_{12} particles, lower adsorption energies were obtained for O adsorbed on the MPd_{12}/SVG composites. Because O adsorption on these composites is weakened, the ORR kinetics over these composites may be promoted, and they are thus expected to have both enhanced stability and superior catalytic performance for ORR.

These theoretical calculations have predicted that metal nanoparticles supported on graphene could generate excellent catalytic activity by the increased charge transfer from the

dx.doi.org/10.1021/cr400523y | Chem. Rev. 2014, 114, 5117−5160

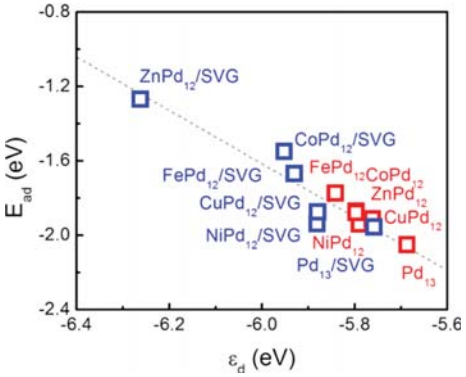

Figure 23. Calculated O adsorption energies (E_{ad}) on free MPd12 and MPd_{12} supported on single vacancy graphene (MPd_{12}/SVG) plotted versus d-band center with respective to vacuum (ε_d). Reprinted with permission from ref 448. Copyright 2013 American Chemical Society.

clusters to the substrates, while their stability could be simultaneously improved due to the hybridization between metal particles and sp^2 dangling bonds at the defect sites of graphene. The theoretical studies are useful in explaining the experimental results and helpful for the future design of graphene-based nanocatalysts.

3.3. Other Unique Properties

Besides the above catalytic properties, graphene nanosheets also possess unique electronic, optical, mechanical, thermal, and electrochemical properties. Carbon materials exhibit strong mechanical strength. For instance, diamond is the hardest natural material, and carbon nanotube has excellent tensile strength. As for graphene, the Young's modulus of graphene has been measured by AFM.[449] From the experimental evaluation, the Young's modulus and fracture strength of a defect-free graphene are 1.0 TPa and 130 GPa, respectively,[450] which suggests that graphene is the strongest material ever measured. Meanwhile, the electronic property of graphene is very important for its application in electrochemistry. The previous studies showed that the electron mobility in suspended single layer graphene can reach around 2×10^5 $cm^2/(V{\cdot}s)$ at room temperature,[451] which is higher than that of all other materials, including metals and carbon nanotubes.

Graphene-based catalysts have also been widely used in electrochemical sensors and enzyme biosensors.[424,425,452] Graphene-based biosensors exhibit good sensitivity and selectivity toward the detection of glucose, H_2O_2, DNA, small biomolecules, cholesterol, Hb, heavy metal ions, and poisonous gaseous molecules.[453] Graphene quantum dots (GQDs) possess strong quantum confinement and edge effects when their size is less than 10 nm, which induce new physical properties. GQDs have been applied in many fields, such as photovoltaics, bioimaging, light emitting diodes, sensors, and so on.[454,455] On the other hand, due to the high specific surface areas (theoretically 2620 m^2/g), excellent electron conductivity, and other properties, functionalized graphene or graphene-supported metal oxide composites have been used as advanced electrode materials in electrochemical capacitors and lithium ion batteries.[456]

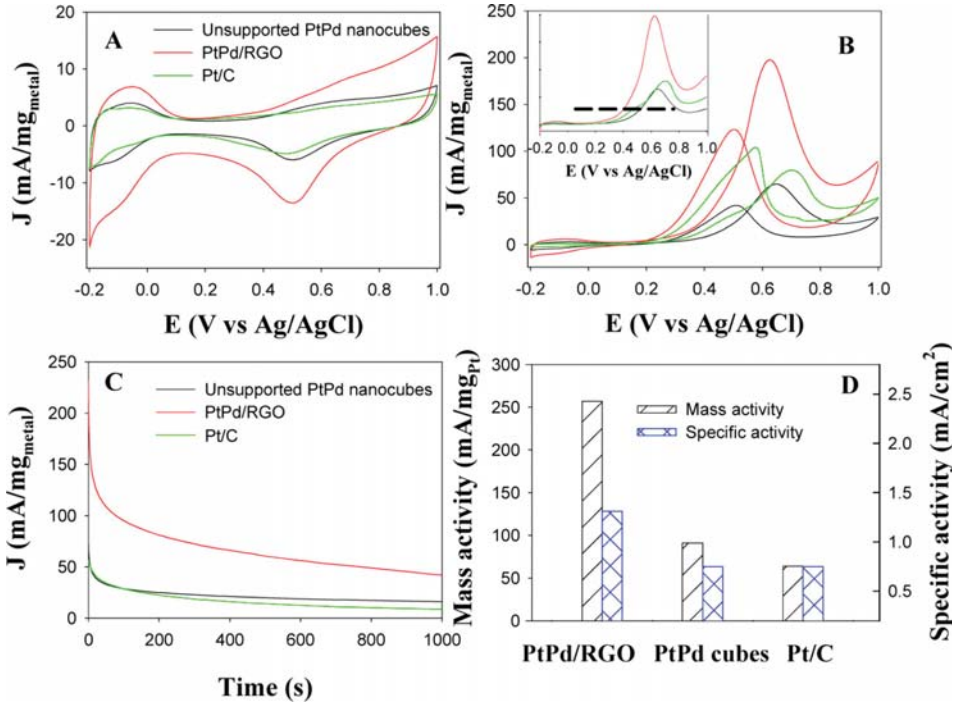

Figure 24. CVs of the unsupported and rGO-supported (PtPd/rGO) PtPd alloy nanocubes, and the commercial Pt/C catalysts in (A) 0.1 M $HClO_4$ solution, and (B) 0.1 M $HClO_4$ + 1.0 M CH_3OH solution. (C) Chronoamperometric curves of methanol oxidation at 0.62 V in 0.1 M $HClO_4$ + 1.0 M CH_3OH solution after the CO stripping treatment. Potential scan rate 50 mV/s. All currents were normalized to the total mass of noble metals (Pt and Pd). (D) Comparison of mass and specific activities of the three catalysts for methanol oxidation. Reprinted with permission from ref 72. Copyright 2013 American Chemical Society.

dx.doi.org/10.1021/cr400523y | *Chem. Rev.* 2014, 114, 5117−5160

4. APPLICATIONS OF GRAPHENE-SUPPORTED NANOELECTROCATALYSTS

4.1. Electrooxidation of Small Organic Molecules at Anode of Fuel Cells

4.1.1. Methanol Oxidation Reaction (MOR). Direct methanol fuel cells (DMFCs) have attracted persistent attention due to their high energy density and low environmental pollution as compared to traditional energy sources. Meanwhile, among various fuel candidates, methanol has been considered as one of the most appropriate fuels for the direct alcohol fuel cells because of its low molecular weight, simplest structure, and very high energy density. The process of MOR includes the methanol adsorption and the subsequent dissociation into adsorbed intermediates.[457] According to the dual-pathway mechanism, CO is a kind of poisoning intermediate species, which can largely reduce the catalytic activity of catalysts, especially Pt-based catalysts. To eliminate the CO poisoning to catalysts, oxygen-containing surface species (e.g., OH) formed on adjacent catalyst sites are usually needed to remove CO adsorbed (CO_{ad}) on the catalyst surface. Therefore, to catalyze the methanol oxidation efficiently, catalysts with multiple active sites are required for the adsorption of methanol and formation of OH species. Interestingly, Sharma et al.[179] found that the presence of oxygen groups on the graphene or rGO support can promote the oxidation of CO_{ads} formed on the active Pt sites via the bifunctional mechanism. By comparing the catalytic activity for methanol oxidation, the rGO-supported Pt nanoparticles with different size and loading exhibited higher catalytic performance than the commercial Pt/C catalyst. Because of the unusual catalytic properties, graphene-supported nanomaterials have attracted more attention in the catalytic applications for MOR over the past years.[163,165,174,175,184,458−460]

To reduce the cost and improve the electocatalytic performance of nanocatalysts, Pt-based nanomaterials supported on graphene have also been extensively investigated for MOR. Up to now, small Pt-based alloy nanoparticles well dispersed on graphene have been reported, and they displayed superior electrocatalytic activities toward methanol oxidation, such as PtRu/GNs,[212,218,461] PtPd/GNs,[72,200,202] PtNi/GNs,[234,236] PtFe/GNs,[239] PtSn/GNs,[243] etc. Among the Pt-based anode electrocatalysts for DMFCs, Pt−Ru alloy exhibits the best electrocatalytic activity because PtRu alloy can reduce CO poisoning effectively. The adsorption of hydroxyls on the oxophilic Ru facilitates the removal of residual CO-like species adsorbed on the Pt surface and thus releases the occupied active sites. The experimental results from different research groups demonstrated that PtRu nanoparticles supported on graphene show much higher catalytic activity for methanol oxidation as compared to commercial PtRu/C catalyst.[212,461,462] It is believed that the unique properties of graphene, such as large surface area and excellent electron conductivity, play key roles for the enhanced catalytic performance of PtRu/graphene for MOR. Recently, we studied the catalytic activities of rGO-supported PtPd nanocubes (PtPd/rGO) for methanol oxidation in acid electrolyte.[72] As shown in Figure 24, as compared to the unsupported PtPd alloy nanocubes and commercial Pt/C catalyst, the PtPd/rGO exhibited enhanced electrocatalytic performance with increased electrochemically active surface area, more negative onset potential, and larger current density of MOR. Moreover, the PtPd/rGO exhibited high stability during the methanol oxidation. This study indicates that graphene sheets are an excellent catalyst support for enhancing the catalytic performance and improving the stability of catalysts.

It has been well-documented that the catalytic activities of alloy nanoparticles are strongly dependent on their compositions. Ji et al.[202] found that graphene-supported PtPd nanoparticles with a molar ratio of 1:1 have the highest activity for electrocatalytic oxidation of methanol. Cai and coworkers[234] reported that the Pt−Ni/graphene nanocatalysts with a molar ratio of 1:1 exhibited the highest catalytic activity toward methanol oxidation as compared to Pt/Ni supported on single-walled carbon nanotubes and Vulcan XC-72 carbon black. Multimetal alloy catalysts supported on graphene have also been reported for MOR. Feng et al.[245] synthesized Au@PtAg nanorods/graphene hybrid materials via the self-organization of Au@PtAg nanorods on graphene. The composites showed higher catalytic activity with improved stability toward MOR than that of pure Au@Pt and Au@AgPt alloy nanorods. As carbon materials, carbon nanotubes and graphene have exhibited their potential applications as catalyst supports in fuel cells. In recent studies, carbon nanotube and graphene hybrids have been investigated as cosupports for electrocatalysts. Jha et al.[463] studied the catalytic properties of nanostructured PtRu dispersed on graphene-carbon nanotube (CNT) hybrid support. The electrochemical measurements showed that the PtRu nanoparticles supported on the hybrid support have higher activity toward methanol oxidation as compared to either PtRu/CNT or PtRu/graphene. In another work, PtRuMo nanoparticles supported on graphene−CNT nanocomposites (PtRuMo/G-CNTs) were also studied as anode catalysts for MOR. It was found that the catalytic activity and stability of the PtRuMo/G-CNTs catalyst are higher than those of PtRuMo/GNs and PtRuMo/CNTs catalysts. In these studies, the hybrid GNs-CNTS supports not only prevent the graphene from restacking and thus provide more electrochemically active surface area, but also enhance the electronic conductivity and the mass transport, resulting in enhanced catalytic performance for MOR.

Pd is a promising alternative to Pt due to its properties similar to those of Pt but much lower cost and higher abundance. Moreover, as anode electrocatalysts for fuel cells, Pd-based materials have much higher CO-tolerance as compared to Pt. In addition to Pt-based nanomaterials, Pd-based nanocatalysts supported on graphene have also been studied in both acidic and alkaline solution. Zhao and coworkers[266] investigated the activity of Pd/GNs-PPy catalysts for MOR in alkaline condition. The forward peak current density of MOR on Pd/GNs-PPy (359.8A/g Pd) is much higher than that of Pd/GNs (265.8A/g Pd) and Pd/C (205.3A/g Pd), indicating that Pd/GNs-PPy composite has the highest activity for methanol oxidation. Previous studies showed that OH_{ads} species can be produced at relatively lower potentials on Ru sites, which is beneficial for methanol oxidation at low onset potential. Awasthi et al.[257] studied the Pd−Ru bimetallic nanoparticles dispersed on graphene nanosheets as anode catalysts for MOR. By comparing the CVs shown in Figure 25, the 40%Pd−5%Ru/GNs catalyst has significantly negative onset potential and the greatest oxidation current for methanol oxidation as compared to the Pd alone catalysts supported on graphene or carbon nanotubes. Moreover, it was found that the content of Ru in the bimetallic nanoparticles has an obvious effect on the catalytic performance, and the best activity was obtained at 5% Ru.

dx.doi.org/10.1021/cr400523y | Chem. Rev. 2014, 114, 5117−5160

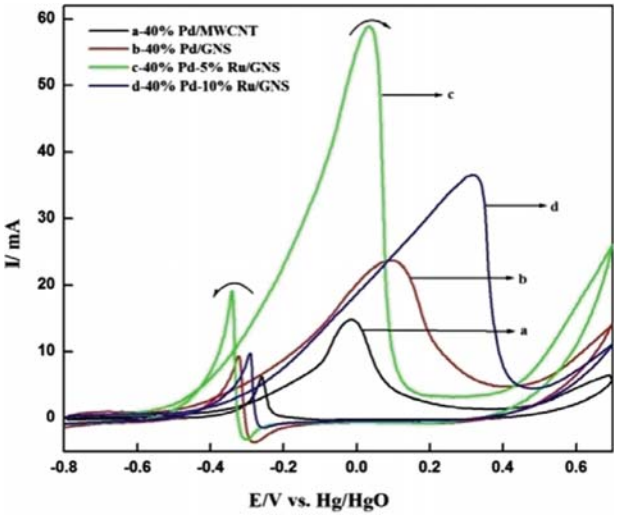

Figure 25. CVs of methanol oxidation on 40%Pd/MWCNT, 40%Pd/GNs, 40%Pd−5%Ru/GNs, and 40%Pd−10%Ru/GNs catalysts at potential scan rate of 50 mV/s in 1 M KOH + 1 M CH_3OH at 25 °C. Reprinted with permission from ref 257. Copyright 2013 Elsevier.

4.1.2. Formic Acid Oxidation Reaction (FAOR). Formic acid is liquid at room temperature, and diluted formic acid is recognized as a kind of safe fuel used in fuel cells. As compared to hydrogen fuel, aqueous solution of formic acid shows the advantages of the ease of handling, transportation, and storage. Meanwhile, direct formic acid fuel cells (DFAFCs) has a lower crossover of formic acid than that of methanol in DMFCs, which enables the use of thinner membranes and high concentration of fuel to improve the performance of fuel cells. In addition, the theoretical open circuit voltage (OCV) of DFAFC (~1.48 or 1.45 V) is higher than hydrogen−oxygen (1.23 V) and methanol−oxygen (1.18 V) fuel cells.[464] It has been generally accepted that the FAOR follows a dual-pathway mechanism: (I) direct dehydrogenation producing CO_2 pathway, which involves the removal of two hydrogen atoms (dehydrogenation) to form CO_2 directly $HCOOH \rightarrow CO_2 + 2H^+ + 2e^-$, and (II) indirect pathway, which involves the dehydration of formic acid to form a poisonous intermediate CO_{ads} species and then further oxidation to CO_2. On the basis of such a mechanism, the materials on which the dehydrogenation pathway predominantly occurs or have high CO tolerance are ideal anode catalysts for formic acid oxidation. Graphene-based catalysts are endowed with excellent catalytic performance toward formic acid electrooxidation as they are able to overcome CO poisoning through the direct pathway, and graphene is propitious to not only maximize the availability of surface area of supported nanoelectrocatalysts but also provide efficient mass transport of reactants, products, and electrolytes.[262,275] A number of mono-, bi-, and ternary metallic nanostructures supported on graphene have been fabricated as electrocatalysts for FAOR.[154,188,206,249,263,465−468]

The advantages of low cost, high tolerance to CO poisoning, and catalytic properties similar to those of Pt, Pd-based nanomaterials have been applied to FAOR as efficient anode catalysts.[263,275,278,465,469−471] Wang and co-workers[467] studied the catalytic activity of Pd nanoparticles supported on three-dimensional reduced graphene oxide (Pd/TRGO) for formic acid electrooxidation. From the CVs of formic acid oxidation shown in Figure 26, the Pd/TRGO exhibits much higher

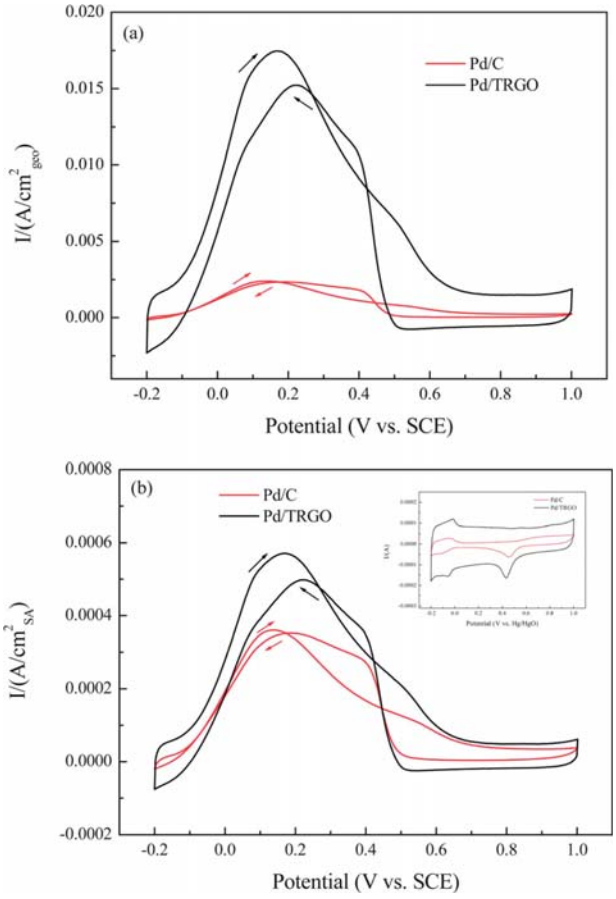

Figure 26. CVs of formic acid oxidation on Pd/C and Pd/TRGO catalysts in 0.5 M H_2SO_4 + 0.5 M HCOOH. (a) Normalized by the electrode surface area; (b) normalized by the Pd ECSA (inset: CVs in a 0.5 M H_2SO_4 solution). Reprinted with permission from ref 467. Copyright 2013 Royal Society of Chemistry.

current density of FAOR as compared to the Pd loaded on carbon black with the same amount of Pd. The enhanced catalytic activity of Pd/TRGO can be ascribed to the high specific surface area of 3D graphene oxide support, efficient Pd dispersion on the porous structured TRGO, and the improved efficiency of mass transport through the 3D graphene network with abundant macropores and mesopores. In another work, highly dispersed Pd nanoparticles supported on graphene were fabricated by a one-step electrochemical codeposition approach with reductant- and surfactant-free process.[270] Because of the clean surface of the as-synthesized Pd nanoparticles, the Pd/GNs showed remarkably improved electrocatalytic performance for FAOR. Zhao et al.[471] prepared Pd nanoparticles supported on graphene via galvanic displacement between Pd ions and the presynthesized Cu nanoparticles anchored on graphene (g-Pd/GNs). From the CV measurements, the g-Pd/GNs catalyst exhibited much higher current density of 446.3 mA/mg_{Pd}, as compared to those for the Pd/GNs synthesized by direct reduction of Pd ions (213.0 mA/mg_{Pd}) and Pd/C catalysts (191.9 mA/mg_{Pd}). The chronoamperometric curves obtained at 0.15 V showed that the residual current of FAOR at g-Pd/GNs is about 6.9 times higher than those at Pd/GNs and Pd/C. The electrochemical measurements indicated that the g-Pd/GN catalyst has excellent stability and activity, which can be ascribed to the small size (~3 nm) and high dispersion of the

dx.doi.org/10.1021/cr400523y | Chem. Rev. 2014, 114, 5117−5160

Pd nanoparticles, and the absence of stabilizers or surfactants on the particle surface.

Rao et al.[154] compared the electrocatalytic performance of graphene-supported Pt (Pt/GNs) and PtAu alloy (PtAu/GNs) toward FAOR. The voltammetric measurements indicated that the activity of PtAu/GNs for formic acid oxidation is about 10 times higher than that of Pt/GNs. Figure 27 shows the single-

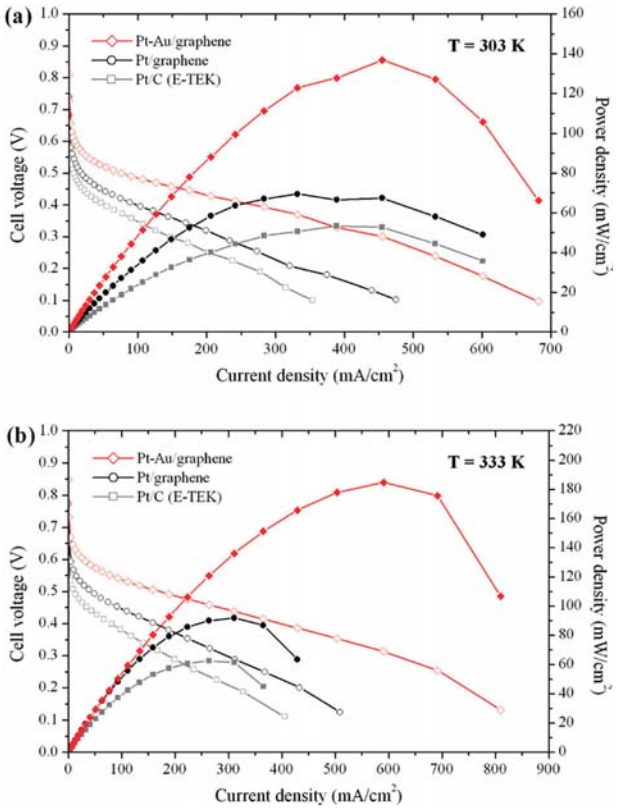

Figure 27. *I*–*V* polarization curves of Pt/GNs, PtAu/GNs, and Pt/C anodes under DFAFC conditions: (a) 303 K and 1 atm and (b) 333 K and 1 atm. Open and closed symbols corresponding to the cell voltage and power density, respectively. Reprinted with permission from ref 154. Copyright 2011 American Chemical Society.

cell DFAFC performance with the as-synthesized materials at 303 and 333 K. From the polarization curves shown in Figure 27, the Pt/GNs and PtAu/GNs show better fuel cell performance than the commercial Pt/C catalyst at both temperatures, and the PtAu/GNs anode exhibited the best performance. The open circuit voltages (OCV) of the membrane-electrode assembly (MEA) based on Pt/C, Pt/GNs, and PtAu/GNs were calculated to be 0.72, 0.77, and 0.85 V, respectively. At 303 K, the Pt/C, Pt/GNs, and PtAu/GNs showed limiting current densities of 354, 475, and 682 mA/cm^2, which correspond to the maximum power densities of 53, 70, and 136 mW/cm^2, respectively. This study clearly indicates that graphene support can enhance the catalytic performance of catalysts in a real fuel cell.

4.1.3. Ethanol Oxidation Reaction (EOR). Ethanol fueled direct alcohol fuel cells have been attracted much attention due to the higher theoretical energy density but less toxicity of ethanol as compared to methanol. For ethanol oxidation on Pt-based electrocatalysts, several reaction mechanisms have been proposed with complex processes.[472,473] On the basis of the mechanisms, acetaldehyde, acetic acid, or CO_2 can be formed through different reaction pathways. For Pd-based electrocatalysts, it has been found that they show catalytic activity for EOR only in alkaline media and on them ethanol is selectively converted to acetate. Previous studies on smooth Pt showed that the kinetics of EOR is strongly dependent on the pH value of electrolyte, and a peak current density was observed at pH = 14.[474] In NaOH solution with concentration higher and lower than 1 mol/L, the activity will decrease. It was proposed that ethanol oxidation on Pd in alkaline media has the following reaction mechanism:

$$Pd + CH_3CH_2OH + 3OH^- \rightarrow Pd{-}CH_3CO_{ads} + 3H_2O + 3e \quad (1)$$

$$Pd + OH^- \leftarrow\rightarrow Pd{-}OH_{ads} + e^- \quad (2)$$

$$Pd{-}CH_3CO_{ads} + Pd{-}OH_{ads} \rightarrow Pd{-}CH_3COOH + Pd \quad (3)$$

The removal of the adsorbed acyl by the adsorbed hydroxyl (the third step) has been suggested to be the rate-determining step.

Recently, metal nanoparticles supported on graphene have been used as catalysts for EOR. Dong et al.[212] synthesized graphene-supported Pt (Pt/GNs) and Pt–Ru nanoparticles (Pt–Ru/GNs) and studied their catalytic activity for ethanol oxidation. The electrochemical results showed that, as compared to the Vulcan XC-72R carbon black support, graphene as catalyst support can more effectively enhance the electrocatalytic activities of Pt and PtRu for EOR. Moreover, as observed previously, the introduction of Ru into nanoparticles (PtRu) can efficiently improve the CO-tolerance during EOR. Jiang et al.[475] synthesized Pt nanoparticles supported on electrochemically reduced and poly(3,4-ethylenedioxythiophene) (PEDOT) incorporated graphene oxide (ER-GO) sheets (Pt/PEDOT/ER-GO). From the CVs of ethanol oxidation on different catalysts, the forward peak current density (390 A/g) on the Pt/PEDOT/ER-GO is higher than that from the Pt/C catalyst, and 5 times greater than that of bare Pt/GC electrode. The high electrocatalytic activity of Pt/PEDOT/ER-GO is mainly due to the good electronic conductivity of PEDOT/ER-GO composites and the well-dispersed Pt nanoparticles, resulting in the large electrochemical active surface area of Pt (47.1 m^2/g).

Besides Pt, EOR has also been studied on various graphene-supported Pd-based electrocatalysts.[476] Fan and co-workers[157] reported the synthesis of Pd/GNs composites and studied their electrochemical properties toward alcohol electrooxidation in alkaline electrolyte. Figure 28 compares the CVs of ethanol oxidation on Pd/GNs and Vulcan XC-72R carbon-supported Pd nanoparticles (Pd/VXC). Obviously, higher catalytic performance of EOR was obtained on Pd/GNs with more negative onset potential (−0.65 vs −0.52 V on Pd/VXC) and 8.06 times larger peak current density than that from Pd/VXC. In another work, Chen et al.[262] reported the synthesis of "clean" and ultrafine monodispersed Pd nanoparticles on graphene oxide (PdNPs/GO) and their catalytic activity for ethanol oxidation in alkaline media. It was found that the onset potential of ethanol oxidation on PdNPs/GO is more negative than that on Pd/C. The peak current densities from the PdNPs-GO are ∼3- and 1.6-fold larger than those of commercial Pd/C catalyst in the forward and reverse potential scans, respectively. Moreover, after 100 potential cycles, the

dx.doi.org/10.1021/cr400523y | *Chem. Rev.* 2014, 114, 5117–5160

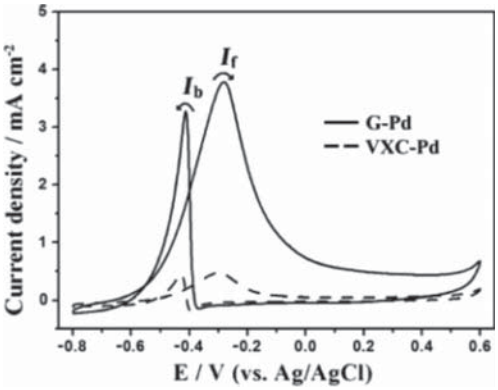

Figure 28. CVs of ethanol oxidation on Pd/GNs and Pd/VXC in 1.0 M C_2H_5OH + 1.0 M NaOH. Reprinted with permission from ref 157. Copyright 2013 American Chemical Society.

drop of the current density is only ~6.3%, suggesting that the PdNPs/GO catalyst has great stability in EOR. Recently, Lee and co-workers[203] synthesized bimetallic PtPd alloy nanoparticles on Nafion−graphene film by a simple electrochemical method. The hybrid exhibited efficient electrocatalytic activity and stability toward ethanol oxidation in alkaline media.

4.1.4. Hydrogen Oxidation Reaction (HOR). Hydrogen is a kind of zero-emission and high-energy fuel for fuel cells. A hydrogen-fed fuel cell can produce electricity, heat, and very clean product of water. Therefore, a lot of work has been done on the HOR with different electrocatalysts.[477−484] Similar to other small organic molecular fuels, platinum-based catalysts show the best catalytic properties for HOR. It should be noted that the kinetics of HOR in a PEMFC is much faster than that of the ORR; therefore, only very low Pt loading is needed for the HOR. Although different types of carbon materials have been used as catalyst supports for HOR,[479] only a few of studies have been reported about the graphene-supported catalysts for HOR.

For HOR, the CO tolerance is an important parameter to evaluate the properties of a catalyst. Graphene nanosheets show a high CO tolerance performance in HOR. Yoo et al.[184] reported that subnano Pt clusters supported on graphene nanosheets (Pt/GNs) showed a higher CO tolerance performance in the HOR than the Pt clusters dispersed on carbon black (Pt/CB). It was found that in pure H_2 atmosphere, Pt/GNs, Pt/CB, and PtRu/CB showed similar electrocatalytic activities for the HOR despite the different types of carbon material used. However, the activity of the Pt/GNs for the HOR can remain 52% in the presence of H_2 and 500 ppm CO, while that of the Pt/CB is only 11%.

4.2. Oxygen Reduction Reaction (ORR) at Cathode

Oxygen reduction reaction (ORR) on cathode plays a critical role in determining the performance of a fuel cell. Although substantial progress has been achieved on cathodic catalysts in the past decades, the sluggish electron-transfer kinetics of ORR and the large overpotential still remarkably limit the wide commercialization of fuel cells. The ORR has complicated reaction pathways and proceeds through an efficient four-electron reduction of O_2 to water as the end product ($O_2 + 4H^+ + 4e^- \rightarrow 2H_2O$), or a less efficient two-step, two-electron reduction pathway, involving the formation of hydrogen peroxide as an intermediate ($O_2 + 4H^+ + 2e^- \rightarrow H_2O_2 + 2H^+ + 2e^- \rightarrow 2H_2O$).[485] Pt and Pt alloys have been accepted as the most active and effective cathodic catalysts for ORR. However, a number of challenges remain for the Pt-based catalysts, such as low durability, easy poisoning from methanol crossover, high cost, and so on. To resolve these problems, low-Pt or non-Pt and metal-free electrocatalysts with low-cost, high electrocatalytic activity, and stability have been extensively studied as efficient ORR electrocatalysts in recent years (Tables 2−4).[10,65,81,382,435]

The kinetic parameters of ORR can be determined using the rotating disk electrode (RDE) technique. The kinetic current density and the electron transfer numbers can be derived from the following equations:[486]

$$\frac{1}{J} = \frac{1}{J_K} + \frac{1}{J_L} = \frac{1}{J_K} + \frac{1}{B\omega^{1/2}} \quad (4)$$

$$B = 0.62nFC_O D_O^{2/3} \nu^{-1/6} \quad (5)$$

$$J_K = nFkC_O \quad (6)$$

where J is the measured current density, J_K and J_L are the kinetic and diffusion limiting current densities, respectively, ω is the electrode rotation rate, n is the overall number of electron transferred, F is the Faraday constant, C_O is the bulk concentration of O_2 dissolved in the electrolyte, D_O is the diffusion coefficient for O_2, ν is the kinematic viscosity of the electrolyte, and k is the electron transfer rate constant. In addition, rotation ring-disk electrode (RRDE) can also be used to evaluate the ORR performance of a catalyst. Electron transfer number (n) can be obtained from the ring and disk current as the equation of $n = 4I_D/(I_D + (I_R/N))$. I_D and I_R represent the disk and ring current, and N is the RRDE collection efficiency. The H_2O_2 percentage generated at the disk electrode can also be calculated according to the equation of $\%H_2O_2 = (2I_R/N)/(I_D + (I_R/N))$.

As described above, graphene as substrate would enhance the catalytic performance of electrocatalysts supported on it due to its high surface area, excellent conductivity, and improved durability. In recent years, Pt-based catalysts supported on graphene nanosheets have been fabricated for ORR.[166,170,181,194,201,225,237,244,487] Kou et al.[181] found that Pt nanoparticles (~2 nm) supported on the functionalized graphene sheets exhibit enhanced electrochemical surface area (ECSA), higher ORR activity, and improved stability in acid solution as compared to commercial E-TEK catalyst. As is reported by Ha and co-workers in another work,[170] Pt nanoparticles (~2.9 nm) embedded on reduced graphene oxide platelets also showed much larger electrochemically active surface area and greater catalytic activity toward ORR in 0.1 M H_2SO_4 as compared to Johnson Matthey (JM) Pt/C (75 wt % Pt) catalyst. To improve the stability and reduce the chemical/physical defects of graphene support, Shao et al.[166] prepared Pt nanoparticles supported on poly(diallyldimethylammonium chloride) (PDDA)-functionalized graphene nanoplatelets as ORR electrocatalysts. It was found that the synthesized hybrid exhibited improved durability with 2−3 times over commercial Etek Pt/C and Pt/CNT catalysts. In a recent report from Huang's group,[195] the stacking of rGO can be effectively avoided by inserting carbon black (CB) particles between rGO sheets. The unique stable Pt/rGO/CN composite showed greatly enhanced ORR activity and durability as compared to the simple Pt/rGO hybrid. Because of the lower cost and greater resistance to CO over Pt catalysts, graphene-supported low-Pt bimetallic hybrids have also been studied as potential

dx.doi.org/10.1021/cr400523y | Chem. Rev. 2014, 114, 5117−5160

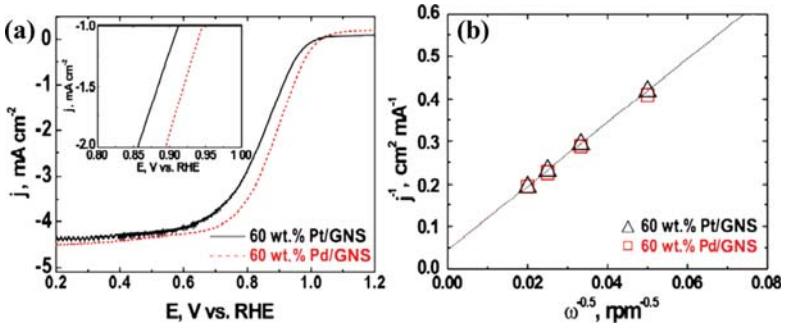

Figure 29. Polarization curves (a) and the Levich–Koutecky plots (b) of the ORR obtained from Pt/GNs and Pd/GNs in O_2-saturated 0.1 M NaOH solution with a sweep rate of 10 mV/s and rotating speed of 1600 rpm. Reprinted with permission from ref 265. Copyright 2011 Elsevier.

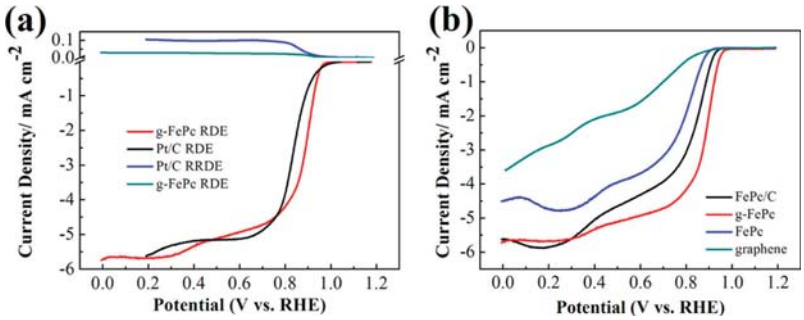

Figure 30. (a) RDE and RRDE measurements of ORR at graphene-supported iron phthalocyanine (g-FePc) and commercial Pt/C catalyst in O_2-saturated 0.1 M KOH. The ring electrode is polarized at 0.5 V (vs Ag/AgCl) with a rotation rate of 1600 rpm and a potential scan rate of 10 mV/s. (b) Comparison of the RDE polarization curves of FePc, graphene, g-FePc, and FePc supported on carbon (FePc/C) in O_2-saturated 0.1 M KOH at 1600 rpm. Reprinted with permission from ref 431. Copyright 2013 American Chemical Society.

ORR electrocatalysts. Yue et al.[228] reported that the PtCo nanoparticles supported on graphene (PtCo/graphene) exhibited higher ORR catalytic activity over pure Pt in alkaline solutions. Moreover, the ORR activity of the PtCo/graphene and the generation of OH radicals showed a volcano dependence upon the alloy compositions. The authors also studied the ORR activity of the acid-treated PtNi alloy supported on graphene (PtNi/graphene) with different compositions.[233] The PtNi/graphene catalysts were found to have higher ORR activity than that of pure Pt catalysts in both acidic and alkaline solutions, and the PtNi alloy with 50 atom % Ni content gave the highest ORR activity. It is interesting that after acid treatment, the composites demonstrated enhanced ORR catalytic performance.

To reduce the Pt loading and the cost of electrocatalysts in fuel cells, graphene-supported non-Pt catalysts were also developed in recent years. Pd-based nanomaterials have attracted special interest as cathode catalysts.[488] For instance, Kim and co-workers[265] studied the ORR electrocatalytic activities of Pt/GNs and Pd/GNs in alkaline solution. As shown in Figure 29, the uniformly dispersed Pd/GNS catalyst shows higher mass and specific catalytic activities toward ORR than does the Pt/GNS catalyst. Also, efficient four-electron reduction processes occur on both the Pt/GNs and the Pd/GNs catalysts. Recently, we prepared PdAg nanorings supported on graphene nanosheets (PdAg/GNs) and studied their ORR performance in alkaline solution.[276] The graphene-supported PdAg nanorings demonstrated the advantages as ORR catalysts, including efficient usage of noble metals, high surface area, and high ORR electrocatalytic performance. Moreover, the prepared PdAg/GNs have higher methanol tolerance even at a high concentration as compared to Pd/C and Pt/C catalysts.

Although bulk coinage metals, such as Au, Ag, are electrocatalytically inert for ORR, their materials on nanoscale exhibit relative high catalytic activities.[49] Tang and co-workers[50] synthesized small surfactant-free gold nanoclusters (less than ~2 nm) supported on rGO (Au/rGO) and studied their catalytic activity for ORR. It was found that the ORR onset potential on Au/rGO is at ca. −0.08 V (vs Ag/AgCl) with a reduction current peak at ca. −0.19 V, which are very close to those obtained from commercial Pt/C catalyst. The Au/rGO catalysts exhibited improved methanol-tolerance and electrocatalytic stability as compared to commercial Pt/C catalyst. Other studies also indicated that graphene-supported gold and silver nanoparticles have high electrocatalytic activities for ORR.[285,290,306,489]

Because of the high cost of noble metal electrocatalysts, nonprecious metal-based catalysts supported on graphene or doped graphene sheets have been investigated extensively as efficient ORR catalysts.[254,332,334−337,490] Fe (or Co)−N−C catalysts have been found to be a class of promising non-noble metal catalysts for ORR.[63,491] Byon et al.[337] prepared Fe-based catalyst on rGO (Fe−N-rGO), which contains the pyridinic N-dominant heterocyclic N. The Fe−N-rGO exhibited higher ORR mass activity and improved stability than the Fe−N−C catalysts prepared from carbon black (CB) or oxidized CB in acid solution. Recently, graphene nanosheets functionalized with iron phthalocyanine (g-FePc) through $\pi-\pi$ interaction were studied as a kind of noble metal-free catalyst for ORR in alkaline media.[431] It can be seen from Figure 30 that the graphene support can remarkably improve the ORR perform-

dx.doi.org/10.1021/cr400523y | Chem. Rev. 2014, 114, 5117−5160

ance of the FePc catalyst, and the g-FePc has better ORR activity than the carbon-supported FePc electrocatalyst (FePc/C). Moreover, the g-FePc exhibited comparable ORR activity, long-term operation stability, and better tolerance to methanol crossover and CO poisoning compared with commercial Pt/C. Transition metal oxides or sulfides supported on graphene have also been studied as non-noble metal catalysts for ORR.[253,255,341,368,373,378,380] The strong and intimate electrical and chemical couplings between metal oxide nanomaterials and graphene can enhance the charge transport through interfaces. Moreover, the high intrinsic structural stability of graphene and the strong interactions among the hybrids can largely improve the stability and durability of the inorganic/graphene hybrids.[372]

In recent years, a large number of surface-functionalized graphene and heteroatom-doped graphene materials have been reported as metal-free electrocatalysts for ORR.[81,116,131,404,435,439,492−498] Wang et al.[492] reported graphene modified with PDDA (PDDA-graphene) as metal-free catalyst toward ORR. The PDDA-graphene exhibited excellent ORR electrocatalytic performance with better selectivity, higher CO tolerance, and longer durability than that of graphene and the commercial Pt/C catalyst. In electrochemical studies, the ORR proceeds via a nearly four-electron pathway within the range of the electron transfer number from 3.5 to 4. The excellent ORR electrocatalytic activity of the PDDA-graphene is attributed to the intermolecular charge-transfer that creates a net positive charge on carbon atoms in the graphene sheets.[492]

For N-doped graphene, its ORR catalytic activity is strongly dependent on the nitrogen types and doping concentration. Geng et al.[106] prepared N-doped graphene with different content of three types of nitrogen at different temperatures (Figure 31). From the polarization curves of ORR at different

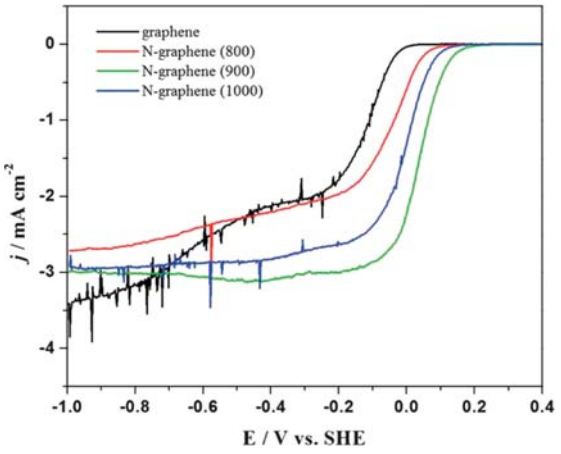

Figure 31. (a) Linear-sweep voltammograms of ORR on graphene and N-doped graphene prepared under different temperatures in O_2-saturated 0.1 M KOH. Potential scan rate, 5 mV/s; rotation speed, 1600 rpm. Reprinted with permission from ref 106. Copyright 2011 Royal Society of Chemistry.

N-graphene, their catalytic performances are much different. On the basis of the detailed analysis, the authors found that there is no obvious dependence of the ORR activity on the content of pyridine-like and pyrrole-like N species. However, the quaternary type of nitrogen may play a decisive role for the ORR catalytic activity. In another study,[97] the N-graphene with pure pyridinic nitrogen doping exhibited inefficient $2e^-$ ORR process, indicating that pyridinic N may not be an effective doping for ORR. Recently, Li et al.[434] synthesized nitrogen-doped graphene quantum dots (N-GQDs) with oxygen-rich functional groups. The N-GQDs with N/C atomic ratio of ca. 4.3% exhibited electrocatalytic activity for ORR comparable to that of commercial Pt/C catalyst. The transferred electron number per O_2 molecule (n) was calculated to be in the range of 3.6−4.4, suggesting an efficient four-electron process.

5. CONCLUSIONS AND FUTURE OUTLOOK

Carbon materials are the most widely used supports for electrocatalysts in fuel cells. Since being obtained with Scotch tape for the first time, graphene has aroused an intense research interest due to its unique structure and novel chemical and physical properties. Although graphene is still a relatively new member in carbon material family, its novel properties, such as large surface area, ultrahigh electrical conductivity, excellent mechanical properties, and high chemical stability, render it an ideal electrocatalyst support for fuel cells. Moreover, the defects and functional groups present on graphene surface can immobilize the nanocatalysts, resulting in improved stability of the graphene-based hybrid catalysts. Graphene-based fuel cell catalysts at both anode and cathode have been very successfully fabricated and developed by many research groups in the past decade. Thanks to the efforts of researchers in the related fields, a huge increasing number of studies in the synthesis and characterization of graphene-based nanomaterials as electrocatalysts for fuel cells have been performed, and impressive progress has been achieved.

In this Review, the recent development of graphene-supported nanoelectrocatalysts for fuel cells, including synthesis, characterizations, properties, and application at anode and cathode of fuel cells, has been extensively reviewed. Up to now, graphene-based structures, such as zero-dimensional graphene quantum dots (GQD), two-dimensinoal graphene nanosheets (GNs), and three-dimensional graphene aerogel (GA) structures have been developed as catalyst supports. Overall, graphene-based nanoelectrocatalysts can be classified into the following types according to the composition of catalysts: (1) metal-free electrocatalysts, including surface-functionalized graphene and heteroatom-doped graphene; (2) graphene-supported non-noble metal electrocatalysts, including transition metal and their oxide, sulfide nanomaterials, and metal complex; (3) graphene-supported Pt-free electrocatalysts, including Pd, Au, Ag monometallic and alloy nanomaterials; and (4) graphene-supported Pt-based nanocatalysts. On the basis of the reported results, graphene-supported nanoelectrocatalysts exhibit excellent catalytic performance for fuel oxidation or oxygen reduction with optimized structures. Especially, single- or codoped graphene with N, S, B, and P is promising as a cost-efficient cathode catalyst for fuel cells. The nitrogen types and doping concentration in graphene have been found to significantly influence their catalytic performance in ORR.

It should be noted that, despite substantial progress that has been made in constructing graphene-based advanced electrocatalysts and understanding their electrocatalytic mechanism, a lot of scientific and technical challenges still remain to realize commercialization of graphene-supported electrocatalysts in fuel cells. First, shape-controlled synthesis methods should be developed for depositing metal nanocrystals on graphene nanosheets. It is well-known that the catalytic activity of metal

dx.doi.org/10.1021/cr400523y | Chem. Rev. 2014, 114, 5117−5160

nanocrystal is closely related to the structures, such as size, composition, and exposed crystal facet (shape), etc. Although nonsupported metal crystals with well-controlled size and shape can be synthesized easily through various chemical and physical synthetic strategies, most of the graphene-supported metal crystals are sphere in shape, and only a few kinds of graphene-supported nanocrystals with controlled shape have been reported. Therefore, to further improve the catalytic performance, how to synthesize morphology-tunable and graphene-supported nanocatalysts is a critical issue in this field. Second, the catalytic properties of graphene-based nanocatalysts are also strongly dependent on the quality of graphene. From the literature, similar graphene-based electrocatalysts may exhibit different catalytic performance, which is at least partly ascribed to the different quality of the used graphene support. It is anticipated that the electrocatalytic properties of graphene-based catalysts can be further enhanced by improving the quality of graphene nanosheets. Third, the enhancement effect of graphene support for the activity of catalysts and the catalytic mechanism of heteroatom-doped graphene materials need to be elucidated from both experimental and theoretical investigations. Currently, catalytic properties of graphene-based electrocatalysts have been studied extensively, and it has been found that graphene nanosheets can enhance the catalytic activity of the supported nanocatalysts. However, the enhancement mechanism, including the improved stability of nanoparticles on graphene surface and the electronic interactions between graphene and nanocatalysts, is still not clear. On the other hand, a lot of studies have illustrated that the heteroatoms doped in graphene, such as N, S, P, B, can effectively enhance the ORR catalytic activity, and nitrogen types and doping concentration have an obvious effect on the catalytic performance on N-graphene. However, contradictory results were obtained from different research groups about the effects of nitrogen types on their catalytic performance. To design high-performance electrocatalysts, more research on the catalytic mechanism of heteroatom-doped graphene is required. Moreover, the durability of graphene-based catalysts is of crucial importance for their practical application in real fuel cells. Therefore, how to improve the electrochemical stability of graphene-based catalysts is another critical issue. In addition to the intrinsic stability of catalysts, the durability of graphene-supported electrocatalysts is also influenced by the following factors. First, the structure stability of graphene can affect the durability of the graphene-based catalysts.[372] Previous studies have shown that the unique graphitic basal plane structure of graphene could guarantee its electrochemical durability.[106] It was proposed that the corrosion of carbon starts from the defects, and carbon materials with more graphitic phase usually exhibit less structure defects.[166] Therefore, the intrinsically high graphitization degree of graphene could improve the durability of metal/graphene composites. Second, the interaction strength between graphene support and composites can also affect the stability of the graphene-based electrocatalysts. For instance, the strong coupling between N-doping sites in graphene nanosheet and metal nanoparticles can lead to enhanced durability of the hybrid catalysts.[253]

Overall, graphene-supported electrocatalysts have promising applications in fuel cells, and much progress has been made in recent years on their synthesis, characterization, and property studies. However, there is still a long way to realize their applications into commercial entities. More efforts have to be devoted to the scalable and reproducible synthesis with controlled composition and morphology, and investigations on properties and catalytic mechanism.

AUTHOR INFORMATION

Corresponding Author

*E-mail: weichen@ciac.ac.cn.

Author Contributions

§These authors contributed equally.

Notes

The authors declare no competing financial interest.

Biographies

Minmin Liu was born in Shandong Province, China. She obtained her B.S. degree in chemistry in 2010 from the College of Chemistry and Chemical Engineering, Liao Cheng University. She is currently pursuing a Ph.D. in Electroanalytical Chemistry under the supervision of Prof. Wei Chen at Changchun Institute of Applied Chemistry, Chinese Academy of Sciences. Her current research includes the design and application of graphene-based nanoelectrocatalysts in fuel cells.

Ruizhong Zhang is currently pursuing her Ph.D. under the direction of Professor Wei Chen at Changchun Institute of Applied Chemistry (CIAC), Chinese Academy of Sciences. She received her B.S. in chemistry from Northwest Normal University, China, in 2011. Her current research interests mainly focus on the design and synthesis of carbonous and noble metal-free nanomaterials, as well as their applications in fuel cells and sensors.

Wei Chen received his Ph.D. in electrochemistry from Xiamen University in 2003. Following his graduate studies, he began working as a postdoctoral associate in the area of synthesis and the property studies of metal nanoclusters at the University of California−Santa Cruz. He is currently a full professor at Changchun Institute of Applied Chemistry, Chinese Academy of Sciences. His research interests include electroanalytical chemistry, surface electrochemistry, electrocatalysis, photoelectrocatalysis, and the controlled synthesis, characterization, and application of nanomaterials, especially metal nanoclusters, in fuel cells, solar cells, and optical devices.

ACKNOWLEDGMENTS

This work is supported by grants from the National Natural Science Foundation of China (nos. 21275136, 21043013), the Natural Science Foundation of Jilin Province, China (no. 201215090), the State Key Laboratory of Electroanalytical Chemistry, and the Changchun Institute of Applied Chemistry, Chinese Academy of Sciences.

ABBREVIATIONS

AA	ascorbic acid
AFM	atomic force microscopy
CB	carbon black
CNTs	carbon nanotubes
CoTAPP	cobalt [tetrakis(*o*-aminophenyl)porphyrin]
CTAB	hexadecyltrimethylammonium bromide
CVD	chemical vapor deposition
DCDA	dicyandiamide
DDS	diphenyldisulfide
DDSe	diphenyldiselenide
DFAFCs	direct formic acid fuel cells
DFT	density functional theory
DMFCs	direct methanol fuel cells
DOE	Department of Energy
ECSA	electrochemical surface area
EDC	*N*-ethyl-*N*′-(3-dimethyl aminopropyl)carbodiimide
EDOT	ethylenedioxythiophene
EDS	energy dispersive spectroscopy
EELS	electron energy loss spectroscopy
EG	ethylene glycol
EOR	ethanol oxidation reaction
ESFDA	electrostatic force directed assembly
FAOR	formic acid oxidation reaction
FePc	iron(II) phthalocyanine
FeTsPc	iron tetrasulfophthalocyanine
FTIR	Fourier transform infrared spectroscopy
fwhm	full-width at half-maximum
GNs	graphene nanosheets
GC	glassy carbon
GO	graphene oxide
GQDs	graphene quantum dots
HER	hydrogen evolution reaction
HOMO	highest-occupied molecular orbital
HOPG	highly oriented pyrolitic graphite
HOR	hydrogen oxidation reaction
ITO	indium tin oxide
LUMO	lowest-unoccupied molecular orbital
MEA	membrane-electrode assembly
MOR	methanol oxidation reaction
OCV	open circuit voltage
ODT	1-octadecanethiol
ORR	oxygen reduction reaction
PDAC	poly (diallyldimethylammonium chloride)
PDDA	poly (diallyldimethylammonium chloride)
PEDOT	poly (3,4-ethylenedioxythiophene)
PEMFCs	proton exchange membrane fuel cells
PMAA	poly (methacrylic acid)
PMMA	polymethylmethacrylate
PSS	poly(sodium 4-styrene sulfonate)
PTCA	3,4,9,10-perylene tetracarboxylic acid
PVP	polyvinylpyrrolidone
RDE	rotating disk electrode
rGO	reduced graphene oxide
RRDE	rotation ring-disk electrode
SCE	saturated calomel electrode
SEM	scanning electron microscopy
SSA	specific surface area
STM	scanning tunneling microscopy
STEM	scanning transmission electron microscopy
TAA	thioacetamide
TCPP	5,10,15,20-tetrakis (4-carboxyl)-21*H*,23*H*-porphyrin
TDMAC	tridodecylmethylammonium chloride
TEM	transmission electron microscopy
UHV	ultrahigh vacuum
XANES	X-ray absorption near edge structure
XPS	X-ray photoelectron spectroscopic
XRD	X-ray diffraction

REFERENCES

(1) Armand, M.; Tarascon, J. M. *Nature* **2008**, *451*, 652.
(2) Potocnik, J. *Science* **2007**, *315*, 810.
(3) Cook, T. R.; Dogutan, D. K.; Reece, S. Y.; Surendranath, Y.; Teets, T. S.; Nocera, D. G. *Chem. Rev.* **2010**, *110*, 6474.
(4) Acres, G. J. K. *J. Power Sources* **2001**, *100*, 60.
(5) Antolini, E. *J. Power Sources* **2007**, *170*, 1.
(6) Lamy, C.; Lima, A.; LeRhun, V.; Delime, F.; Coutanceau, C.; Leger, J. M. *J. Power Sources* **2002**, *105*, 283.
(7) Vigier, F.; Rousseau, S.; Coutanceau, C.; Leger, J. M.; Lamy, C. *Top. Catal.* **2006**, *40*, 111.
(8) James, B. D.; Kalinoski, J. A. Mass Production Cost Estimation for Direct H_2 PEM Fuel Cell System for Automotive Applications: 2008 Update, 2009.
(9) Steele, B. C. H.; Heinzel, A. *Nature* **2001**, *414*, 345.
(10) Chen, A. C.; Holt-Hindle, P. *Chem. Rev.* **2010**, *110*, 3767.
(11) Lu, Y. Z.; Chen, W. *Chem. Commun.* **2011**, *47*, 2541.
(12) Chen, W.; Xu, L. P.; Chen, S. W. *J. Electroanal. Chem.* **2009**, *631*, 36.
(13) Chen, W.; Kim, J. M.; Xu, L. P.; Sun, S. H.; Chen, S. W. *J. Phys. Chem. C* **2007**, *111*, 13452.
(14) Chen, W.; Kim, J. M.; Sun, S. H.; Chen, S. W. *Langmuir* **2007**, *23*, 11303.
(15) Chen, W.; Kim, J. M.; Sun, S. H.; Chen, S. W. *J. Phys. Chem. C* **2008**, *112*, 3891.

(16) Chen, W.; Kim, J.; Sun, S. H.; Chen, S. W. *Phys. Chem. Chem. Phys.* **2006**, *8*, 2779.
(17) Zhang, J.; Yang, H. Z.; Yang, K. K.; Fang, J.; Zou, S. Z.; Luo, Z. P.; Wang, H.; Bae, I. T.; Jung, D. Y. *Adv. Funct. Mater.* **2010**, *20*, 3727.
(18) Stamenkovic, V. R.; Fowler, B.; Mun, B. S.; Wang, G. F.; Ross, P. N.; Lucas, C. A.; Markovic, N. M. *Science* **2007**, *315*, 493.
(19) Xia, B. Y.; Wu, H. B.; Wang, X.; Lou, X. W. *J. Am. Chem. Soc.* **2012**, *134*, 13934.
(20) Yang, H. Z.; Zhang, J.; Sun, K.; Zou, S. Z.; Fang, J. Y. *Angew. Chem., Int. Ed.* **2010**, *49*, 6848.
(21) Kang, Y. J.; Murray, C. B. *J. Am. Chem. Soc.* **2010**, *132*, 7568.
(22) Chen, W.; Chen, S. W. *J. Mater. Chem.* **2011**, *21*, 9169.
(23) Zhang, H.; Jin, M. S.; Xia, Y. N. *Chem. Soc. Rev.* **2012**, *41*, 8035.
(24) Gasteiger, H. A.; Markovic, N.; Ross, P. N.; Cairns, E. J. *J. Electrochem. Soc.* **1994**, *141*, 1795.
(25) Goodenough, J. B.; Hamnett, A.; Kennedy, B. J.; Manoharan, R.; Weeks, S. A. *J. Electroanal. Chem.* **1988**, *240*, 133.
(26) Oetjen, H. F.; Schmidt, V. M.; Stimming, U.; Trila, F. *J. Electrochem. Soc.* **1996**, *143*, 3838.
(27) Frelink, T.; Visscher, W.; vanVeen, J. A. R. *Langmuir* **1996**, *12*, 3702.
(28) Dinh, H. N.; Ren, X. M.; Garzon, F. H.; Zelenay, P.; Gottesfeld, S. *J. Electroanal. Chem.* **2000**, *491*, 222.
(29) Antolini, E. *Energy Environ. Sci.* **2009**, *2*, 915.
(30) Bianchini, C.; Shen, P. K. *Chem. Rev.* **2009**, *109*, 4183.
(31) Fernandez, J. L.; Walsh, D. A.; Bard, A. J. *J. Am. Chem. Soc.* **2005**, *127*, 357.
(32) Schmidt, T. J.; Jusys, Z.; Gasteiger, H. A.; Behm, R. J.; Endruschat, U.; Boennemann, H. *J. Electroanal. Chem.* **2001**, *501*, 132.
(33) Jiang, L.; Hsu, A.; Chu, D.; Chen, R. *Electrochim. Acta* **2010**, *55*, 4506.
(34) Shao, M. H.; Sasaki, K.; Adzic, R. R. *J. Am. Chem. Soc.* **2006**, *128*, 3526.
(35) Jung, C. H.; Sanchez-Sanchez, C. M.; Lin, C. L.; Rodriguez-Lopez, J.; Bard, A. J. *Anal. Chem.* **2009**, *81*, 7003.
(36) Fernandez, J. L.; Raghuveer, V.; Manthiram, A.; Bard, A. J. *J. Am. Chem. Soc.* **2005**, *127*, 13100.
(37) Maiyalagan, T.; Scott, K. *J. Power Sources* **2010**, *195*, 5246.
(38) Koenigsmann, C.; Sutter, E.; Chiesa, T. A.; Adzic, R. R.; Wong, S. S. *Nano Lett.* **2012**, *12*, 2013.
(39) Xu, C. X.; Zhang, Y.; Wang, L. Q.; Xu, L. Q.; Bian, X. F.; Ma, H. Y.; Ding, Y. *Chem. Mater.* **2009**, *21*, 3110.
(40) Lu, Y. Z.; Chen, W. *J. Phys. Chem. C* **2010**, *114*, 21190.
(41) Wang, H.; Xu, C. W.; Cheng, F. L.; Zhang, M.; Wang, S. Y.; Jiang, S. P. *Electrochem. Commun.* **2008**, *10*, 1575.
(42) Li, W. Z.; Haldar, P. *Electrochem. Commun.* **2009**, *11*, 1195.
(43) Zhang, Z. Y.; More, K. L.; Sun, K.; Wu, Z. L.; Li, W. Z. *Chem. Mater.* **2011**, *23*, 1570.
(44) Chen, Z. W.; Waje, M.; Li, W. Z.; Yan, Y. S. *Angew. Chem., Int. Ed.* **2007**, *46*, 4060.
(45) Lu, Y. Z.; Chen, W. *ACS Catal.* **2012**, *2*, 84.
(46) Alia, S. M.; Jensen, K. O.; Pivovar, B. S.; Yan, Y. S. *ACS Catal.* **2012**, *2*, 858.
(47) Wei, W. T.; Chen, W. *J. Power Sources* **2012**, *204*, 85.
(48) Wei, W. T.; Lu, Y. Z.; Chen, W.; Chen, S. W. *J. Am. Chem. Soc.* **2011**, *133*, 2060.
(49) Chen, W.; Chen, S. W. *Angew. Chem., Int. Ed.* **2009**, *48*, 4386.
(50) Yin, H. J.; Tang, H. J.; Wang, D.; Gao, Y.; Tang, Z. Y. *ACS Nano* **2012**, *6*, 8288.
(51) Lu, Y. Z.; Chen, W. *Chem. Soc. Rev.* **2012**, *41*, 3594.
(52) Lu, Y. Z.; Chen, W. *J. Power Sources* **2012**, *197*, 107.
(53) Liu, Y.; Ishihara, A.; Mitsushima, S.; Kamiya, N.; Ota, K. *J. Electrochem. Soc.* **2007**, *154*, B664.
(54) Mentus, S. V. *Electrochim. Acta* **2004**, *50*, 27.
(55) El-Deab, M. S.; Ohsaka, T. *Angew. Chem., Int. Ed.* **2006**, *45*, 5963.
(56) Liang, Y. Y.; Wang, H. L.; Diao, P.; Chang, W.; Hong, G. S.; Li, Y. G.; Gong, M.; Xie, L. M.; Zhou, J. G.; Wang, J.; Regier, T. Z.; Wei, F.; Dai, H. J. *J. Am. Chem. Soc.* **2012**, *134*, 15849.
(57) Chen, W.; Ny, D.; Chen, S. W. *J. Power Sources* **2010**, *195*, 412.
(58) Reeve, R. W.; Christensen, P. A.; Hamnett, A.; Haydock, S. A.; Roy, S. C. *J. Electrochem. Soc.* **1998**, *145*, 3463.
(59) Liu, H. S.; Song, C. J.; Tang, Y. H.; Zhang, J. L.; Zhang, H. J. *Electrochim. Acta* **2007**, *52*, 4532.
(60) Zhang, L.; Zhang, J. J.; Wilkinson, D. P.; Wang, H. J. *J. Power Sources* **2006**, *156*, 171.
(61) Holze, R.; Vogel, I.; Vielstich, W. *J. Electrochem. Soc.* **1986**, *133*, C115.
(62) Wu, G.; More, K. L.; Johnston, C. M.; Zelenay, P. *Science* **2011**, *332*, 443.
(63) Lefevre, M.; Proietti, E.; Jaouen, F.; Dodelet, J. P. *Science* **2009**, *324*, 71.
(64) Wu, H. B.; Chen, W. *J. Am. Chem. Soc.* **2011**, *133*, 15236.
(65) Gong, K. P.; Du, F.; Xia, Z. H.; Durstock, M.; Dai, L. M. *Science* **2009**, *323*, 760.
(66) Tang, Y. F.; Allen, B. L.; Kauffman, D. R.; Star, A. *J. Am. Chem. Soc.* **2009**, *131*, 13200.
(67) Yang, L. J.; Jiang, S. J.; Zhao, Y.; Zhu, L.; Chen, S.; Wang, X. Z.; Wu, Q.; Ma, J.; Ma, Y. W.; Hu, Z. *Angew. Chem., Int. Ed.* **2011**, *50*, 7132.
(68) Wang, Y. J.; Wilkinson, D. P.; Zhang, J. J. *Chem. Rev.* **2011**, *111*, 7625.
(69) Novoselov, K. S.; Geim, A. K.; Morozov, S. V.; Jiang, D.; Zhang, Y.; Dubonos, S. V.; Grigorieva, I. V.; Firsov, A. A. *Science* **2004**, *306*, 666.
(70) Fampiou, I.; Ramasubramaniam, A. *J. Phys. Chem. C* **2012**, *116*, 6543.
(71) Kou, R.; Shao, Y. Y.; Mei, D. H.; Nie, Z. M.; Wang, D. H.; Wang, C. M.; Viswanathan, V. V.; Park, S.; Aksay, I. A.; Lin, Y. H.; Wang, Y.; Liu, J. *J. Am. Chem. Soc.* **2011**, *133*, 2541.
(72) Lu, Y. Z.; Jiang, Y. Y.; Wu, H. B.; Chen, W. *J. Phys. Chem. C* **2013**, *117*, 2926.
(73) Chen, D.; Feng, H. B.; Li, J. H. *Chem. Rev.* **2012**, *112*, 6027.
(74) Allen, M. J.; Tung, V. C.; Kaner, R. B. *Chem. Rev.* **2010**, *110*, 132.
(75) Georgakilas, V.; Otyepka, M.; Bourlinos, A. B.; Chandra, V.; Kim, N.; Kemp, K. C.; Hobza, P.; Zboril, R.; Kim, K. S. *Chem. Rev.* **2012**, *112*, 6156.
(76) Guo, S. J.; Dong, S. J. *Chem. Soc. Rev.* **2011**, *40*, 2644.
(77) Pumera, M. *Chem. Soc. Rev.* **2010**, *39*, 4146.
(78) Huang, X.; Qi, X. Y.; Boey, F.; Zhang, H. *Chem. Soc. Rev.* **2012**, *41*, 666.
(79) Brownson, D. A. C.; Kampouris, D. K.; Banks, C. E. *Chem. Soc. Rev.* **2012**, *41*, 6944.
(80) Zhu, Y. W.; Murali, S.; Cai, W. W.; Li, X. S.; Suk, J. W.; Potts, J. R.; Ruoff, R. S. *Adv. Mater.* **2010**, *22*, 3906.
(81) Wang, H. B.; Maiyalagan, T.; Wang, X. *ACS Catal.* **2012**, *2*, 781.
(82) Viculis, L. M.; Mack, J. J.; Mayer, O. M.; Hahn, H. T.; Kaner, R. B. *J. Mater. Chem.* **2005**, *15*, 974.
(83) Si, Y. C.; Samulski, E. T. *Chem. Mater.* **2008**, *20*, 6792.
(84) Kosynkin, D. V.; Higginbotham, A. L.; Sinitskii, A.; Lomeda, J. R.; Dimiev, A.; Price, B. K.; Tour, J. M. *Nature* **2009**, *458*, 872.
(85) Jiao, L. Y.; Zhang, L.; Wang, X. R.; Diankov, G.; Dai, H. J. *Nature* **2009**, *458*, 877.
(86) Subrahmanyam, K. S.; Panchakarla, L. S.; Govindaraj, A.; Rao, C. N. R. *J. Phys. Chem. C* **2009**, *113*, 4257.
(87) Panchokarla, L. S.; Subrahmanyam, K. S.; Saha, S. K.; Govindaraj, A.; Krishnamurthy, H. R.; Waghmare, U. V.; Rao, C. N. R. *Adv. Mater.* **2009**, *21*, 4726.
(88) Wei, D. C.; Liu, Y. Q.; Wang, Y.; Zhang, H. L.; Huang, L. P.; Yu, G. *Nano Lett.* **2009**, *9*, 1752.
(89) Reina, A.; Jia, X. T.; Ho, J.; Nezich, D.; Son, H. B.; Bulovic, V.; Dresselhaus, M. S.; Kong, J. *Nano Lett.* **2009**, *9*, 30.
(90) Hass, J.; de Heer, W. A.; Conrad, E. H. *J. Phys.: Condens. Matter* **2008**, *20*, 323202.
(91) Li, X. S.; Cai, W. W.; An, J. H.; Kim, S.; Nah, J.; Yang, D. X.; Piner, R.; Velamakanni, A.; Jung, I.; Tutuc, E.; Banerjee, S. K.; Colombo, L.; Ruoff, R. S. *Science* **2009**, *324*, 1312.

(92) Gao, T.; Xie, S. B.; Gao, Y. B.; Liu, M. X.; Chen, Y. B.; Zhang, Y. F.; Liu, Z. F. *ACS Nano* **2011**, *5*, 9194.
(93) Kim, K. S.; Zhao, Y.; Jang, H.; Lee, S. Y.; Kim, J. M.; Kim, K. S.; Ahn, J. H.; Kim, P.; Choi, J. Y.; Hong, B. H. *Nature* **2009**, *457*, 706.
(94) Qu, L. T.; Liu, Y.; Baek, J. B.; Dai, L. M. *ACS Nano* **2010**, *4*, 1321.
(95) Reddy, A. L. M.; Srivastava, A.; Gowda, S. R.; Gullapalli, H.; Dubey, M.; Ajayan, P. M. *ACS Nano* **2010**, *4*, 6337.
(96) Imamura, G.; Saiki, K. *J. Phys. Chem. C* **2011**, *115*, 10000.
(97) Luo, Z. Q.; Lim, S. H.; Tian, Z. Q.; Shang, J. Z.; Lai, L. F.; MacDonald, B.; Fu, C.; Shen, Z. X.; Yu, T.; Lin, J. Y. *J. Mater. Chem.* **2011**, *21*, 8038.
(98) Jin, Z.; Yao, J.; Kittrell, C.; Tour, J. M. *ACS Nano* **2011**, *5*, 4112.
(99) Cattelan, M.; Agnoli, S.; Favaro, M.; Garoli, D.; Romanato, F.; Meneghetti, M.; Barinov, A.; Dudin, P.; Granozzi, G. *Chem. Mater.* **2013**, *25*, 1490.
(100) Wu, T. R.; Shen, H. L.; Sun, L.; Cheng, B.; Liu, B.; Shen, J. C. *New J. Chem.* **2012**, *36*, 1385.
(101) Gao, H.; Liu, Z.; Song, L.; Guo, W. H.; Gao, W.; Ci, L. J.; Rao, A.; Quan, W. J.; Vajtai, R.; Ajayan, P. M. *Nanotechnology* **2012**, *23*, 275605.
(102) Wu, Z. S.; Ren, W. C.; Gao, L. B.; Zhao, J. P.; Chen, Z. P.; Liu, B. L.; Tang, D. M.; Yu, B.; Jiang, C. B.; Cheng, H. M. *ACS Nano* **2009**, *3*, 411.
(103) Wu, Y. P.; Wang, B.; Ma, Y. F.; Huang, Y.; Li, N.; Zhang, F.; Chen, Y. S. *Nano Res.* **2010**, *3*, 661.
(104) Volotskova, O.; Levchenko, I.; Shashurin, A.; Raitses, Y.; Ostrikov, K.; Keidar, M. *Nanoscale* **2010**, *2*, 2281.
(105) Guo, B. D.; Liu, Q. A.; Chen, E. D.; Zhu, H. W.; Fang, L. A.; Gong, J. R. *Nano Lett.* **2010**, *10*, 4975.
(106) Geng, D. S.; Chen, Y.; Chen, Y. G.; Li, Y. L.; Li, R. Y.; Sun, X. L.; Ye, S. Y.; Knights, S. *Energy Environ. Sci.* **2011**, *4*, 760.
(107) Geng, D. S.; Yang, S. L.; Zhang, Y.; Yang, J. L.; Liu, J.; Li, R. Y.; Sham, T. K.; Sun, X. L.; Ye, S. Y.; Knights, S. *Appl. Surf. Sci.* **2011**, *257*, 9193.
(108) Wang, X. R.; Li, X. L.; Zhang, L.; Yoon, Y.; Weber, P. K.; Wang, H. L.; Guo, J.; Dai, H. J. *Science* **2009**, *324*, 768.
(109) Zhang, L. S.; Liang, X. Q.; Song, W. G.; Wu, Z. Y. *Phys. Chem. Chem. Phys.* **2010**, *12*, 12055.
(110) Zhang, C.; Fu, L.; Liu, N.; Liu, M.; Wang, Y.; Liu, Z. *Adv. Mater.* **2011**, *23*, 1020.
(111) Yao, Z.; Nie, H. G.; Yang, Z.; Zhou, X. M.; Liu, Z.; Huang, S. M. *Chem. Commun.* **2012**, *48*, 1027.
(112) Zhang, C. Z.; Mahmood, N.; Yin, H.; Liu, F.; Hou, Y. L. *Adv. Mater.* **2013**, *25*, 4932.
(113) Liu, Z. W.; Peng, F.; Wang, H. J.; Yu, H.; Zheng, W. X.; Yang, J. *Angew. Chem., Int. Ed.* **2011**, *50*, 3257.
(114) Lin, Z. Y.; Waller, G. H.; Liu, Y.; Liu, M. L.; Wong, C. P. *Nano Energy* **2013**, *2*, 241.
(115) Pan, F. P.; Jin, J. T.; Fu, X. G.; Liu, Q.; Zhang, J. Y. *ACS Appl. Mater. Interfaces* **2013**, *5*, 11108.
(116) Sheng, Z. H.; Shao, L.; Chen, J. J.; Bao, W. J.; Wang, F. B.; Xia, X. H. *ACS Nano* **2011**, *5*, 4350.
(117) Sheng, Z. H.; Gao, H. L.; Bao, W. J.; Wang, F. B.; Xia, X. H. *J. Mater. Chem.* **2012**, *22*, 390.
(118) Kim, Y. A.; Fujisawa, K.; Muramatsu, H.; Hayashi, T.; Endo, M.; Fujimori, T.; Kaneko, K.; Terrones, M.; Behrends, J.; Eckmann, A.; Casiraghi, C.; Novoselov, K. S.; Saito, R.; Dresselhaus, M. S. *ACS Nano* **2012**, *6*, 6293.
(119) Li, X. L.; Wang, H. L.; Robinson, J. T.; Sanchez, H.; Diankov, G.; Dai, H. J. *J. Am. Chem. Soc.* **2009**, *131*, 15939.
(120) Yang, Z.; Yao, Z.; Li, G. F.; Fang, G. Y.; Nie, H. G.; Liu, Z.; Zhou, X. M.; Chen, X.; Huang, S. M. *ACS Nano* **2012**, *6*, 205.
(121) Yang, S. B.; Zhi, L. J.; Tang, K.; Feng, X. L.; Maier, J.; Mullen, K. *Adv. Funct. Mater.* **2012**, *22*, 3634.
(122) Wang, S. Y.; Zhang, L. P.; Xia, Z. H.; Roy, A.; Chang, D. W.; Baek, J. B.; Dai, L. M. *Angew. Chem., Int. Ed.* **2012**, *51*, 4209.
(123) Liang, J.; Jiao, Y.; Jaroniec, M.; Qiao, S. Z. *Angew. Chem., Int. Ed.* **2012**, *51*, 11496.
(124) Su, Y. Z.; Zhang, Y.; Zhuang, X. D.; Li, S.; Wu, D. Q.; Zhang, F.; Feng, X. L. *Carbon* **2013**, *62*, 296.
(125) Choi, C. H.; Chung, M. W.; Kwon, H. C.; Park, S. H.; Woo, S. I. *J. Mater. Chem. A* **2013**, *1*, 3694.
(126) Choi, C. H.; Chung, M. W.; Jun, Y. J.; Woo, S. I. *RSC Adv.* **2013**, *3*, 12417.
(127) Dato, A.; Radmilovic, V.; Lee, Z.; Phillips, J.; Frenklach, M. *Nano Lett.* **2008**, *8*, 2012.
(128) Hazra, K. S.; Rafiee, J.; Rafiee, M. A.; Mathur, A.; Roy, S. S.; McLauhglin, J.; Koratkar, N.; Misra, D. S. *Nanotechnology* **2011**, *22*, 025704.
(129) Wang, Y.; Shao, Y. Y.; Matson, D. W.; Li, J. H.; Lin, Y. H. *ACS Nano* **2010**, *4*, 1790.
(130) Shao, Y. Y.; Zhang, S.; Engelhard, M. H.; Li, G. S.; Shao, G. C.; Wang, Y.; Liu, J.; Aksay, I. A.; Lin, Y. H. *J. Mater. Chem.* **2010**, *20*, 7491.
(131) Jafri, R. I.; Rajalakshmi, N.; Ramaprabhu, S. *J. Mater. Chem.* **2010**, *20*, 7114.
(132) Jeong, H. M.; Lee, J. W.; Shin, W. H.; Choi, Y. J.; Shin, H. J.; Kang, J. K.; Choi, J. W. *Nano Lett.* **2011**, *11*, 2472.
(133) Lin, Y. C.; Lin, C. Y.; Chiu, P. W. *Appl. Phys. Lett.* **2010**, *96*, 133110.
(134) Kumar, N. A.; Nolan, H.; McEvoy, N.; Rezvani, E.; Doyle, R. L.; Lyons, M.; Duesberg, G. S. *J. Mater. Chem. A* **2013**, *1*, 4431.
(135) Wang, C. D.; Yuen, M. F.; Ng, T. W.; Jha, S. K.; Lu, Z. Z.; Kwok, S. Y.; Wong, T. L.; Yang, X.; Lee, C. S.; Lee, S. T.; Zhang, W. J. *Appl. Phys. Lett.* **2012**, *100*, 253107.
(136) Chen, W. F.; Yan, L. F. *Nanoscale* **2010**, *2*, 559.
(137) Dubin, S.; Gilje, S.; Wang, K.; Tung, V. C.; Cha, K.; Hall, A. S.; Farrar, J.; Varshneya, R.; Yang, Y.; Kaner, R. B. *ACS Nano* **2010**, *4*, 3845.
(138) Nethravathi, C.; Rajamathi, M. *Carbon* **2008**, *46*, 1994.
(139) Gao, X. F.; Jang, J.; Nagase, S. *J. Phys. Chem. C* **2010**, *114*, 832.
(140) Deng, D. H.; Pan, X. L.; Yu, L. A.; Cui, Y.; Jiang, Y. P.; Qi, J.; Li, W. X.; Fu, Q. A.; Ma, X. C.; Xue, Q. K.; Sun, G. Q.; Bao, X. H. *Chem. Mater.* **2011**, *23*, 1188.
(141) Wang, R. H.; Wang, Y.; Xu, C. H.; Sun, J.; Gao, L. *RSC Adv.* **2013**, *3*, 1194.
(142) Long, D. H.; Li, W.; Ling, L. C.; Miyawaki, J.; Mochida, I.; Yoon, S. H. *Langmuir* **2010**, *26*, 16096.
(143) Berger, C.; Song, Z. M.; Li, X. B.; Wu, X. S.; Brown, N.; Naud, C.; Mayou, D.; Li, T. B.; Hass, J.; Marchenkov, A. N.; Conrad, E. H.; First, P. N.; de Heer, W. A. *Science* **2006**, *312*, 1191.
(144) Shivaraman, S.; Barton, R. A.; Yu, X.; Alden, J.; Herman, L.; Chandrashekhar, M. V. S.; Park, J.; McEuen, P. L.; Parpia, J. M.; Craighead, H. G.; Spencer, M. G. *Nano Lett.* **2009**, *9*, 3100.
(145) Sutter, P. W.; Flege, J. I.; Sutter, E. A. *Nat. Mater.* **2008**, *7*, 406.
(146) Lu, X. K.; Yu, M. F.; Huang, H.; Ruoff, R. S. *Nanotechnology* **1999**, *10*, 269.
(147) Shao, Y. Y.; Wang, J.; Engelhard, M.; Wang, C. M.; Lin, Y. H. *J. Mater. Chem.* **2010**, *20*, 743.
(148) Guo, H. L.; Wang, X. F.; Qian, Q. Y.; Wang, F. B.; Xia, X. H. *ACS Nano* **2009**, *3*, 2653.
(149) Murugan, A. V.; Muraliganth, T.; Manthiram, A. *Chem. Mater.* **2009**, *21*, 5004.
(150) Hirsch, A. *Angew. Chem., Int. Ed.* **2009**, *48*, 6594.
(151) Wang, G. M.; Qian, F.; Saltikov, C.; Jiao, Y. Q.; Li, Y. *Nano Res.* **2011**, *4*, 563.
(152) Salas, E. C.; Sun, Z. Z.; Luttge, A.; Tour, J. M. *ACS Nano* **2010**, *4*, 4852.
(153) Liu, Z. L.; Ling, X. Y.; Su, X. D.; Lee, J. Y. *J. Phys. Chem. B* **2004**, *108*, 8234.
(154) Rao, C. V.; Cabrera, C. R.; Ishikawa, Y. *J. Phys. Chem. C* **2011**, *115*, 21963.
(155) Hsieh, C. T.; Chen, W. Y.; Tzou, D. Y.; Roy, A. K.; Hsiao, H. T. *Int. J. Hydrogen Energy* **2012**, *37*, 17837.
(156) Chen, X. J.; Zang, W. Z.; Vimalanathan, K.; Iyer, K. S.; Raston, C. L. *Chem. Commun.* **2013**, *49*, 1160.

(157) Gao, L. N.; Yue, W. B.; Tao, S. S.; Fan, L. Z. *Langmuir* **2013**, *29*, 957.
(158) Jang, B.; Choi, E.; Piao, Y. *Mater. Res. Bull.* **2013**, *48*, 834.
(159) Qiu, H. J.; Dong, X. C.; Sana, B.; Peng, T.; Paramelle, D.; Chen, P.; Lim, S. *ACS Appl. Mater. Interfaces* **2013**, *5*, 782.
(160) Huang, C. C.; Li, C.; Shi, G. Q. *Energy Environ. Sci.* **2012**, *5*, 8848.
(161) Seger, B.; Kamat, P. V. *J. Phys. Chem. C* **2009**, *113*, 7990.
(162) Jafri, R. I.; Arockiados, T.; Rajalakshmi, N.; Ramaprabhu, S. *J. Electrochem. Soc.* **2010**, *157*, B874.
(163) Li, Y. M.; Tang, L. H.; Li, J. H. *Electrochem. Commun.* **2009**, *11*, 846.
(164) Qian, Y.; Wang, C. Y.; Le, Z. G. *Appl. Surf. Sci.* **2011**, *257*, 10758.
(165) Li, Y. J.; Gao, W.; Ci, L. J.; Wang, C. M.; Ajayan, P. M. *Carbon* **2010**, *48*, 1124.
(166) Shao, Y. Y.; Zhang, S.; Wang, C. M.; Nie, Z. M.; Liu, J.; Wang, Y.; Lin, Y. H. *J. Power Sources* **2010**, *195*, 4600.
(167) Huang, H. J.; Chen, H. Q.; Sun, D. P.; Wang, X. *J. Power Sources* **2012**, *204*, 46.
(168) Grinou, A.; Yun, Y. S.; Cho, S. Y.; Park, H. H.; Jin, H. J. *Materials* **2012**, *5*, 2927.
(169) Wang, L.; Tian, C. G.; Mu, G.; Zhang, H. X.; Fu, H. G. *Mater. Res. Bull.* **2012**, *47*, 4311.
(170) Ha, H. W.; Kim, I. Y.; Hwang, S. J.; Ruoff, R. S. *Electrochem. Solid-State Lett.* **2011**, *14*, B70.
(171) Meng, H.; Wang, C. X.; Shen, P. K.; Wu, G. *Energy Environ. Sci.* **2011**, *4*, 1522.
(172) Tian, N.; Zhou, Z. Y.; Sun, S. G.; Ding, Y.; Wang, Z. L. *Science* **2007**, *316*, 732.
(173) Favier, F.; Walter, E. C.; Zach, M. P.; Benter, T.; Penner, R. M. *Science* **2001**, *293*, 2227.
(174) Zhou, Y. G.; Chen, J. J.; Wang, F. B.; Sheng, Z. H.; Xia, X. H. *Chem. Commun.* **2010**, *46*, 5951.
(175) Maiyalagan, T.; Dong, X. C.; Chen, P.; Wang, X. *J. Mater. Chem.* **2012**, *22*, 5286.
(176) Liu, X. W.; Mao, J. J.; Liu, P. D.; Wei, X. W. *Carbon* **2011**, *49*, 477.
(177) Tu, W. X.; Lin, H. F. *Chem. Mater.* **2000**, *12*, 564.
(178) Gerbec, J. A.; Magana, D.; Washington, A.; Strouse, G. F. *J. Am. Chem. Soc.* **2005**, *127*, 15791.
(179) Sharma, S.; Ganguly, A.; Papakonstantinou, P.; Miao, X. P.; Li, M. X.; Hutchison, J. L.; Delichatsios, M.; Ukleja, S. *J. Phys. Chem. C* **2010**, *114*, 19459.
(180) Kundu, P.; Nethravathi, C.; Deshpande, P. A.; Rajamathi, M.; Madras, G.; Ravishankar, N. *Chem. Mater.* **2011**, *23*, 2772.
(181) Kou, R.; Shao, Y. Y.; Wang, D. H.; Engelhard, M. H.; Kwak, J. H.; Wang, J.; Viswanathan, V. V.; Wang, C. M.; Lin, Y. H.; Wang, Y.; Aksay, I. A.; Liu, J. *Electrochem. Commun.* **2009**, *11*, 954.
(182) Giovanni, M.; Poh, H. L.; Ambrosi, A.; Zhao, G. J.; Sofer, Z.; Sanek, F.; Khezri, B.; Webster, R. D.; Pumera, M. *Nanoscale* **2012**, *4*, 5002.
(183) Zhang, H.; Chen, S.; Quan, X.; Yu, H. T.; Zhao, H. M. *J. Mater. Chem.* **2011**, *21*, 12986.
(184) Yoo, E.; Okada, T.; Akita, T.; Kohyama, M.; Honma, I.; Nakamura, J. *J. Power Sources* **2011**, *196*, 110.
(185) Siburian, R.; Nakamura, J. *J. Phys. Chem. C* **2012**, *116*, 22947.
(186) Guo, S. J.; Wen, D.; Zhai, Y. M.; Dong, S. J.; Wang, E. K. *ACS Nano* **2010**, *4*, 3959.
(187) Yang, D. Q.; Rochette, J. F.; Sacher, E. *J. Phys. Chem. B* **2005**, *109*, 4481.
(188) Wang, S. Y.; Wang, X.; Jiang, S. P. *Phys. Chem. Chem. Phys.* **2011**, *13*, 7187.
(189) Wang, Z. H.; Xia, J. F.; Guo, X. M.; Xia, Y. Z.; Yao, S. Y.; Zhang, F. F.; Li, Y. H.; Xia, L. H. *Anal. Methods* **2013**, *5*, 483.
(190) Qiu, J. D.; Wang, G. C.; Liang, R. P.; Xia, X. H.; Yu, H. W. *J. Phys. Chem. C* **2011**, *115*, 15639.
(191) Zhang, S.; Shao, Y. Y.; Liao, H. G.; Engelhard, M. H.; Yin, G. P.; Lin, Y. H. *ACS Nano* **2011**, *5*, 1785.
(192) Ahmed, M. S.; Kim, D.; Han, H. S.; Jeong, H.; Jeon, S. *J. Nanosci. Nanotechnol.* **2012**, *12*, 8349.
(193) Mayavan, S.; Jang, H. S.; Lee, M. J.; Choi, S. H.; Choi, S. M. *J. Mater. Chem. A* **2013**, *1*, 3489.
(194) Nam, K. W.; Song, J.; Oh, K. H.; Choo, M. J.; Park, H. A.; Park, J. K.; Choi, J. W. *J. Solid State Electrochem.* **2013**, *17*, 767.
(195) Li, Y. J.; Li, Y. J.; Zhu, E. B.; McLouth, T.; Chiu, C. Y.; Huang, X. Q.; Huang, Y. *J. Am. Chem. Soc.* **2012**, *134*, 12326.
(196) Yuan, Q.; Zhuang, J.; Wang, X. *Chem. Commun.* **2009**, 6613.
(197) Lim, B.; Jiang, M. J.; Camargo, P. H. C.; Cho, E. C.; Tao, J.; Lu, X. M.; Zhu, Y. M.; Xia, Y. N. *Science* **2009**, *324*, 1302.
(198) Peng, Z. M.; Yang, H. *J. Am. Chem. Soc.* **2009**, *131*, 7542.
(199) Lu, Y. Z.; Jiang, Y. Y.; Chen, W. *Nano Energy* **2013**, *2*, 836.
(200) Guo, S. J.; Dong, S. J.; Wang, E. K. *ACS Nano* **2010**, *4*, 547.
(201) He, W.; Jiang, H. J.; Zhou, Y.; Yang, S. D.; Xue, X. Z.; Zou, Z. Q.; Zhang, X. G.; Akins, D. L.; Yang, H. *Carbon* **2012**, *50*, 265.
(202) Ji, H. Q.; Li, M. G.; Wang, Y. L.; Gao, F. *Electrochem. Commun.* **2012**, *24*, 17.
(203) Yang, X.; Yang, Q. D.; Xu, J.; Lee, C. S. *J. Mater. Chem.* **2012**, *22*, 8057.
(204) Lu, Y. Z.; Jiang, Y. Y.; Chen, W. *Nanoscale* **2014**, *6*, 3309.
(205) Zhao, D.; Xu, B. Q. *Angew. Chem., Int. Ed.* **2006**, *45*, 4955.
(206) Zhang, S.; Shao, Y. Y.; Liao, H. G.; Liu, J.; Aksay, I. A.; Yin, G. P.; Lin, Y. H. *Chem. Mater.* **2011**, *23*, 1079.
(207) Hu, Y. J.; Zhang, H.; Wu, P.; Zhang, H.; Zhou, B.; Cai, C. X. *Phys. Chem. Chem. Phys.* **2011**, *13*, 4083.
(208) Yang, G. H.; Li, Y. J.; Rana, R. K.; Zhu, J. J. *J. Mater. Chem. A* **2013**, *1*, 1754.
(209) Rolison, D. R.; Hagans, P. L.; Swider, K. E.; Long, J. W. *Langmuir* **1999**, *15*, 774.
(210) Lu, Y. Z.; Jiang, Y. Y.; Zhang, R. Z.; Chen, W. *Sci. Adv. Mater.* **2013**, *5*, 1718.
(211) Cong, H. P.; Ren, X. C.; Yu, S. H. *ChemCatChem* **2012**, *4*, 1555.
(212) Dong, L. F.; Gari, R. R. S.; Li, Z.; Craig, M. M.; Hou, S. F. *Carbon* **2010**, *48*, 781.
(213) Galal, A.; Atta, N. F.; Hassan, H. K. *Int. J. Electrochem. Sci.* **2012**, *7*, 768.
(214) Nethravathi, C.; Anumol, E. A.; Rajamathi, M.; Ravishankar, N. *Nanoscale* **2011**, *3*, 569.
(215) Zhao, J.; Zhang, L.; Xue, H.; Wang, Z. B.; Hu, H. Q. *RSC Adv.* **2012**, *2*, 9651.
(216) Zhao, J.; Xue, H.; Zhang, L.; Yu, J. H.; Hu, H. Q. *J. Nanopart. Res.* **2012**, *14*.
(217) Kim, H. J.; Choi, S. M.; Seo, M. H.; Green, S.; Huber, G. W.; Kim, W. B. *Electrochem. Commun.* **2011**, *13*, 890.
(218) Li, H. Y.; Zhang, X. H.; Pang, H. L.; Huang, C. T.; Chen, J. H. *J. Solid State Electrochem.* **2010**, *14*, 2267.
(219) Wang, Y. S.; Yang, S. Y.; Li, S. M.; Tien, H. W.; Hsiao, S. T.; Liao, W. H.; Liu, C. H.; Chang, K. H.; Ma, C. C. M.; Hu, C. C. *Electrochim. Acta* **2013**, *87*, 261.
(220) Lv, R. T.; Cui, T. X.; Jun, M. S.; Zhang, Q.; Cao, A. Y.; Su, D. S.; Zhang, Z. J.; Yoon, S. H.; Miyawaki, J.; Mochida, I.; Kang, F. Y. *Adv. Funct. Mater.* **2011**, *21*, 999.
(221) Woo, S.; Lee, J.; Park, S. K.; Kim, H.; Chung, T. D.; Piao, Y. *J. Power Sources* **2013**, *222*, 261.
(222) Huang, H. J.; Sun, D. P.; Wang, X. *Chin. Sci. Bull.* **2012**, *57*, 3071.
(223) Yang, P.; Jin, S. Y.; Xu, Q. Z.; Yu, S. H. *Small* **2013**, *9*, 199.
(224) Shi, G. Y.; Wang, Z. H.; Xia, J. F.; Zhang, F. F.; Xia, Y. Z.; Li, Y. H. *Acta Chim. Sin.* **2013**, *71*, 227.
(225) Yan, Z. H.; Wang, M.; Huang, B. X.; Liu, R. M.; Zhao, J. S. *Int. J. Electrochem. Sci.* **2013**, *8*, 149.
(226) Ma, Y. W.; Liu, Z. R.; Wang, B. L.; Zhu, L.; Yang, J. P.; Li, X. A. *New Carbon Mater.* **2012**, *27*, 250.
(227) Shen, J. F.; Yan, B.; Shi, M.; Ma, H. W.; Li, N.; Ye, M. X. *Mater. Res. Bull.* **2012**, *47*, 1486.
(228) Yue, Q. L.; Zhang, K.; Chen, X. M.; Wang, L.; Zhao, J. S.; Liu, J. F.; Jia, J. B. *Chem. Commun.* **2010**, *46*, 3369.

(229) Nam, K. W.; Song, J.; Oh, K. H.; Choo, M. J.; Park, H.; Park, J. K.; Choi, J. W. *Carbon* **2012**, *50*, 3739.
(230) Luo, B. M.; Xu, S.; Yan, X. B.; Xue, Q. J. *J. Electrochem. Soc.* **2013**, *160*, F262.
(231) Luo, B. M.; Xu, S.; Yan, X. B.; Xue, Q. J. *Electrochem. Commun.* **2012**, *23*, 72.
(232) Gao, H. C.; Xiao, F.; Ching, C. B.; Duan, H. W. *ACS Appl. Mater. Interfaces* **2011**, *3*, 3049.
(233) Zhang, K.; Yue, Q. L.; Chen, G. F.; Zhai, Y. L.; Wang, L.; Wang, H. S.; Zhao, J. S.; Liu, J. F.; Jia, J. B.; Li, H. B. *J. Phys. Chem. C* **2011**, *115*, 379.
(234) Hu, Y. J.; Wu, P.; Yin, Y. J.; Zhang, H.; Cai, C. X. *Appl. Catal., B* **2012**, *111*, 208.
(235) Zhang, C.; Lv, W.; Yang, Q. H.; Liu, Y. *Appl. Surf. Sci.* **2012**, *258*, 7795.
(236) Hu, Y. J.; Wu, P.; Zhang, H.; Cai, C. X. *Electrochim. Acta* **2012**, *85*, 314.
(237) Guo, S. J.; Sun, S. H. *J. Am. Chem. Soc.* **2012**, *134*, 2492.
(238) Wei, G.; Zhang, Y.; Steckbeck, S.; Su, Z. Q.; Li, Z. *J. Mater. Chem.* **2012**, *22*, 17190.
(239) Ji, Z. Y.; Zhu, G. X.; Shen, X. P.; Zhou, H.; Wu, C. M.; Wang, M. *New J. Chem.* **2012**, *36*, 1774.
(240) Yang, H.; Kwon, Y.; Kwon, T.; Lee, H.; Kim, B. J. *Small* **2012**, *8*, 3161.
(241) Liu, Y. J.; Huang, Y. Q.; Xie, Y.; Yang, Z. H.; Huang, H. L.; Zhou, Q. Y. *Chem. Eng. J.* **2012**, *197*, 80.
(242) Anandan, S.; Manivel, A.; Ashokkumar, M. *Fuel Cells* **2012**, *12*, 956.
(243) Han, F.; Wang, X. M.; Lian, J.; Wang, Y. Z. *Carbon* **2012**, *50*, 5498.
(244) Rao, C. V.; Reddy, A. L. M.; Ishikawa, Y.; Ajayan, P. M. *Carbon* **2011**, *49*, 931.
(245) Feng, L. L.; Gao, G.; Huang, P.; Wang, X. S.; Zhang, C. L.; Zhang, J. L.; Guo, S. W.; Cui, D. X. *Nanoscale Res. Lett.* **2011**, *6*, 551.
(246) Cunci, L.; Rao, C. V.; Velez, C.; Ishikawa, Y.; Cabrera, C. R. *Electrocatalysis* **2013**, *4*, 61.
(247) Ji, Z. Y.; Shen, X. P.; Zhu, G. X.; Chen, K. M.; Fu, G. H.; Tong, L. *J. Electroanal. Chem.* **2012**, *682*, 95.
(248) Sun, C. L.; Hsu, Y. K.; Lin, Y. G.; Chen, K. H.; Bock, C.; MacDougall, B.; Wu, X. H.; Chen, L. C. *J. Electrochem. Soc.* **2009**, *156*, B1249.
(249) Hu, C. G.; Zhao, Y.; Cheng, H. H.; Hu, Y.; Shi, G. Q.; Dai, L. M.; Qu, L. T. *Chem. Commun.* **2012**, *48*, 11865.
(250) Ye, F.; Cao, X. R.; Yu, L.; Chen, S. Z.; Lin, W. M. *Int. J. Electrochem. Sci.* **2012**, *7*, 1251.
(251) Zhang, Y. Z.; Gu, Y. E.; Lin, S. X.; Wei, J. P.; Wang, Z. H.; Wang, C. M.; Du, Y. L.; Ye, W. C. *Electrochim. Acta* **2011**, *56*, 8746.
(252) Hu, C. G.; Cheng, H. H.; Zhao, Y.; Hu, Y.; Liu, Y.; Dai, L. M.; Qu, L. T. *Adv. Mater.* **2012**, *24*, 5493.
(253) Liang, Y. Y.; Li, Y. G.; Wang, H. L.; Zhou, J. G.; Wang, J.; Regier, T.; Dai, H. J. *Nat. Mater.* **2011**, *10*, 780.
(254) Wu, Z. S.; Yang, S. B.; Sun, Y.; Parvez, K.; Feng, X. L.; Mullen, K. *J. Am. Chem. Soc.* **2012**, *134*, 9082.
(255) Wang, H. L.; Liang, Y. Y.; Li, Y. G.; Dai, H. J. *Angew. Chem., Int. Ed.* **2011**, *50*, 10969.
(256) Liang, Y. Y.; Wang, H. L.; Zhou, J. G.; Li, Y. G.; Wang, J.; Regier, T.; Dai, H. J. *J. Am. Chem. Soc.* **2012**, *134*, 3517.
(257) Awasthi, R.; Singh, R. N. *Carbon* **2013**, *51*, 282.
(258) Khomyakov, P. A.; Giovannetti, G.; Rusu, P. C.; Brocks, G.; van den Brink, J.; Kelly, P. J. *Phys. Rev. B* **2009**, *79*, 195425.
(259) Wang, Q. J.; Che, J. G. *Phys. Rev. Lett.* **2009**, *103*, 066802.
(260) Scheuermann, G. M.; Rumi, L.; Steurer, P.; Bannwarth, W.; Mulhaupt, R. *J. Am. Chem. Soc.* **2009**, *131*, 8262.
(261) Li, Y.; Fan, X. B.; Qi, J. J.; Ji, J. Y.; Wang, S. L.; Zhang, G. L.; Zhang, F. B. *Nano Res.* **2010**, *3*, 429.
(262) Chen, X. M.; Wu, G. H.; Chen, J. M.; Chen, X.; Xie, Z. X.; Wang, X. R. *J. Am. Chem. Soc.* **2011**, *133*, 3693.
(263) Yang, J.; Tian, C. G.; Wang, L.; Fu, H. G. *J. Mater. Chem.* **2011**, *21*, 3384.
(264) Xi, P. X.; Chen, F. J.; Xie, G. Q.; Ma, C.; Liu, H. Y.; Shao, C. W.; Wang, J.; Xu, Z. H.; Xu, X. M.; Zeng, Z. Z. *Nanoscale* **2012**, *4*, 5597.
(265) Seo, M. H.; Choi, S. M.; Kim, H. J.; Kim, W. B. *Electrochem. Commun.* **2011**, *13*, 182.
(266) Zhao, Y. C.; Zhan, L.; Tian, J. N.; Nie, S. L.; Ning, Z. *Electrochim. Acta* **2011**, *56*, 1967.
(267) Liu, R.; Zhou, H. H.; Liu, J.; Yao, Y.; Huang, Z. Y.; Fu, C. P.; Kuang, Y. F. *Electrochem. Commun.* **2013**, *26*, 63.
(268) Chen, X. J.; Yasin, F. M.; Eggers, P. K.; Boulos, R. A.; Duan, X. F.; Lamb, R. N.; Iyer, K. S.; Raston, C. L. *RSC Adv.* **2013**, *3*, 3213.
(269) Yang, J.; Deng, S. Y.; Lei, J. P.; Ju, H. X.; Gunasekaran, S. *Biosens. Bioelectron.* **2011**, *29*, 159.
(270) Jiang, Y. Y.; Lu, Y. Z.; Li, F. H.; Wu, T. S.; Niu, L.; Chen, W. *Electrochem. Commun.* **2012**, *19*, 21.
(271) Wang, Y. X.; Balbuena, P. B. *J. Phys. Chem. B* **2005**, *109*, 18902.
(272) Wang, Y.; Sheng, Z. M.; Yang, H. B.; Jiang, S. P.; Li, C. M. *Int. J. Hydrogen Energy* **2010**, *35*, 10087.
(273) Awasthi, R.; Singh, R. N. *Int. J. Hydrogen Energy* **2012**, *37*, 2103.
(274) Wang, J.; Qin, Y. L.; Liu, X.; Zhang, X. B. *J. Mater. Chem.* **2012**, *22*, 12468.
(275) Chai, J.; Li, F. H.; Hu, Y. W.; Zhang, Q. X.; Han, D. X.; Niu, L. *J. Mater. Chem.* **2011**, *21*, 17922.
(276) Liu, M. M.; Lu, Y. Z.; Chen, W. *Adv. Funct. Mater.* **2013**, *23*, 1289.
(277) Awasthi, R.; Singh, R. N. *Catal. Sci. Technol.* **2012**, *2*, 2428.
(278) Bong, S.; Uhm, S.; Kim, Y. R.; Lee, J.; Kim, H. *Electrocatalysis* **2010**, *1*, 139.
(279) Choi, S. M.; Seo, M. H.; Kim, H.; Kim, W. B. *Synth. Met.* **2011**, *161*, 2405.
(280) Li, Y. Z.; Yu, Y.; Wang, J. G.; Song, J.; Li, Q.; Dong, M. D.; Liu, C. J. *Appl. Catal., B* **2012**, *125*, 189.
(281) Seo, M. H.; Choi, S. M.; Seo, J. K.; Noh, S. H.; Kim, W. B.; Han, B. *Appl. Catal., B* **2013**, *129*, 163.
(282) Herzing, A. A.; Kiely, C. J.; Carley, A. F.; Landon, P.; Hutchings, G. J. *Science* **2008**, *321*, 1331.
(283) Wei, W. T.; Chen, W. *Int. J. Smart Nano Mater.* **2013**, *4*, 62.
(284) Lu, Y. Z.; Wei, W. T.; Chen, W. *Chin. Sci. Bull.* **2012**, *57*, 41.
(285) Lim, E. J.; Choi, S. M.; Seo, M. H.; Kim, Y.; Lee, S.; Kim, W. B. *Electrochem. Commun.* **2013**, *28*, 100.
(286) Liu, X.; Wang, X. Y.; He, P. Y.; Yi, L. H.; Liu, Z. L.; Yi, X. *J. Solid State Electrochem.* **2012**, *16*, 3929.
(287) Xiong, Z. G.; Zhang, L. L.; Ma, J. Z.; Zhao, X. S. *Chem. Commun.* **2010**, *46*, 6099.
(288) Liu, S.; Tian, J. Q.; Wang, L.; Li, H. L.; Zhang, Y. W.; Sun, X. P. *Macromolecules* **2010**, *43*, 10078.
(289) Li, Y.; Fan, X. B.; Qi, J. J.; Ji, J. Y.; Wang, S. L.; Zhang, G. L.; Zhang, F. B. *Mater. Res. Bull.* **2010**, *45*, 1413.
(290) Hu, Y. J.; Jin, J. A.; Wu, P.; Zhang, H.; Cai, C. X. *Electrochim. Acta* **2010**, *56*, 491.
(291) Zhou, K. F.; Zhu, Y. H.; Yang, X. L.; Li, C. Z. *Electroanalysis* **2010**, *22*, 259.
(292) Cho, S. J.; Suri, A.; Mei, X. G.; Ouyang, J. Y. *RSC Adv.* **2013**, *3*, 1201.
(293) Chen, Y.; Shen, Y. Y.; Sun, D.; Zhang, H. Y.; Tian, D. B.; Zhang, J. R.; Zhu, J. J. *Chem. Commun.* **2011**, *47*, 11733.
(294) Yang, X.; Xu, M. S.; Qiu, W. M.; Chen, X. Q.; Deng, M.; Zhang, J. L.; Iwai, H.; Watanabe, E.; Chen, H. Z. *J. Mater. Chem.* **2011**, *21*, 8096.
(295) Li, J.; Liu, C. Y. *Eur. J. Inorg. Chem.* **2010**, 1244.
(296) Kong, B. S.; Geng, J. X.; Jung, H. T. *Chem. Commun.* **2009**, 2174.
(297) Vinodgopal, K.; Neppolian, B.; Lightcap, I. V.; Grieser, F.; Ashokkumar, M.; Kamat, P. V. *J. Phys. Chem. Lett.* **2010**, *1*, 1987.
(298) Goncalves, G.; Marques, P. A. A. P.; Granadeiro, C. M.; Nogueira, H. I. S.; Singh, M. K.; Gracio, J. *Chem. Mater.* **2009**, *21*, 4796.
(299) Pasricha, R.; Gupta, S.; Srivastava, A. K. *Small* **2009**, *5*, 2253.

(300) Shen, J. F.; Shi, M.; Li, N.; Yan, B.; Ma, H. W.; Hu, Y. Z.; Ye, M. X. *Nano Res.* **2010**, *3*, 339.
(301) Li, J.; Liu, C. Y.; Liu, Y. *J. Mater. Chem.* **2012**, *22*, 8426.
(302) Le, Z. G.; Liu, Z. R.; Qian, Y.; Wang, C. Y. *Appl. Surf. Sci.* **2012**, *258*, 5348.
(303) Zhang, Q. X.; Ren, Q. Q.; Miao, Y. Q.; Yuan, J. H.; Wang, K. K.; Li, F. H.; Han, D. X.; Niu, L. *Talanta* **2012**, *89*, 391.
(304) Lu, Y. Z.; Jiang, Y. Y.; Wei, W. T.; Wu, H. B.; Liu, M. M.; Niu, L.; Chen, W. *J. Mater. Chem.* **2012**, *22*, 2929.
(305) Zhang, Z.; Xu, F. G.; Yang, W. S.; Guo, M. Y.; Wang, X. D.; Zhang, B. L.; Tang, J. L. *Chem. Commun.* **2011**, *47*, 6440.
(306) Li, F. H.; Yang, H. F.; Shan, C. S.; Zhang, Q. X.; Han, D. X.; Ivaska, A.; Niu, L. *J. Mater. Chem.* **2009**, *19*, 4022.
(307) Huang, J.; Zhang, L. M.; Chen, B. A.; Ji, N.; Chen, F. H.; Zhang, Y.; Zhang, Z. J. *Nanoscale* **2010**, *2*, 2733.
(308) Gong, J. M.; Zhou, T.; Song, D. D.; Zhang, L. Z. *Sens. Actuators, B* **2010**, *150*, 491.
(309) Lu, G.; Li, H.; Liusman, C.; Yin, Z. Y.; Wu, S. X.; Zhang, H. *Chem. Sci.* **2011**, *2*, 1817.
(310) Huang, X.; Zhou, X. Z.; Wu, S. X.; Wei, Y. Y.; Qi, X. Y.; Zhang, J.; Boey, F.; Zhang, H. *Small* **2010**, *6*, 513.
(311) Fu, C. P.; Kuang, Y. F.; Huang, Z. Y.; Wang, X.; Du, N. N.; Chen, J. H.; Zhou, H. H. *Chem. Phys. Lett.* **2010**, *499*, 250.
(312) Zhao, B.; Liu, Z. R.; Fu, W. Y.; Yang, H. B. *Electrochem. Commun.* **2013**, *27*, 1.
(313) Zhou, Y. Z.; Yang, J.; Cheng, X. N.; Zhao, N.; Sun, H. B.; Li, D. *RSC Adv.* **2013**, *3*, 3391.
(314) Lu, G. H.; Mao, S.; Park, S.; Ruoff, R. S.; Chen, J. H. *Nano Res.* **2009**, *2*, 192.
(315) Lefevre, M.; Dodelet, J. P.; Bertrand, P. *J. Phys. Chem. B* **2002**, *106*, 8705.
(316) Lee, J. S.; Park, G. S.; Kim, S. T.; Liu, M. L.; Cho, J. *Angew. Chem., Int. Ed.* **2013**, *52*, 1026.
(317) Wiesener, K. *Electrochim. Acta* **1986**, *31*, 1073.
(318) Schulenburg, H.; Stankov, S.; Schunemann, V.; Radnik, J.; Dorbandt, I.; Fiechter, S.; Bogdanoff, P.; Tributsch, H. *J. Phys. Chem. B* **2003**, *107*, 9034.
(319) Gojkovic, S. L.; Gupta, S.; Savinell, R. F. *Electrochim. Acta* **1999**, *45*, 889.
(320) Sawaguchi, T.; Itabashi, T.; Matsue, T.; Uchida, I. *J. Electroanal. Chem.* **1990**, *279*, 219.
(321) Hung, T. F.; Tu, M. H.; Tsai, C. W.; Chen, C. J.; Liu, R. S.; Liu, W. R.; Lo, M. Y. *Int. J. Hydrogen Energy* **2013**, *38*, 3956.
(322) Gupta, S.; Tryk, D.; Bae, I.; Aldred, W.; Yeager, E. *J. Appl. Electrochem.* **1989**, *19*, 19.
(323) Koslowski, U. I.; Abs-Wurmbach, I.; Fiechter, S.; Bogdanoff, P. *J. Phys. Chem. C* **2008**, *112*, 15356.
(324) Bae, I. T.; Tryk, D. A.; Scherson, D. A. *J. Phys. Chem. B* **1998**, *102*, 4114.
(325) Bezerra, C. W. B.; Zhang, L.; Lee, K. C.; Liu, H. S.; Marques, A. L. B.; Marques, E. P.; Wang, H. J.; Zhang, J. J. *Electrochim. Acta* **2008**, *53*, 4937.
(326) Ye, S. Y.; Vijh, A. K. *Electrochem. Commun.* **2003**, *5*, 272.
(327) Choi, J. Y.; Hsu, R. S.; Chen, Z. W. *J. Phys. Chem. C* **2010**, *114*, 8048.
(328) Wang, H.; Cote, R.; Faubert, G.; Guay, D.; Dodelet, J. P. *J. Phys. Chem. B* **1999**, *103*, 2042.
(329) Lefevre, M.; Dodelet, J. P.; Bertrand, P. *J. Phys. Chem. B* **2000**, *104*, 11238.
(330) Chung, H. T.; Johnston, C. M.; Artyushkova, K.; Ferrandon, M.; Myers, D. J.; Zelenay, P. *Electrochem. Commun.* **2010**, *12*, 1792.
(331) Zhang, Y. Z.; Mo, G. Q.; Li, X. W.; Ye, J. S. *J. Power Sources* **2012**, *197*, 93.
(332) Parvez, K.; Yang, S. B.; Hernandez, Y.; Winter, A.; Turchanin, A.; Feng, X. L.; Mullen, K. *ACS Nano* **2012**, *6*, 9541.
(333) Morozan, A.; Campidelli, S.; Filoramo, A.; Jousselme, B.; Palacin, S. *Carbon* **2011**, *49*, 4839.
(334) Zhang, C. Z.; Hao, R.; Yin, H.; Liu, F.; Hou, Y. L. *Nanoscale* **2012**, *4*, 7326.
(335) Kamiya, K.; Hashimoto, K.; Nakanishi, S. *Chem. Commun.* **2012**, *48*, 10213.
(336) Tsai, C. W.; Tu, M. H.; Chen, C. J.; Hung, T. F.; Liu, R. S.; Liu, W. R.; Lo, M. Y.; Peng, Y. M.; Zhang, L.; Zhang, J. J.; Shy, D. S.; Xing, X. K. *RSC Adv.* **2011**, *1*, 1349.
(337) Byon, H. R.; Suntivich, J.; Shao-Horn, Y. *Chem. Mater.* **2011**, *23*, 3421.
(338) Li, S. Z.; Hu, Y. Y.; Xu, Q.; Sun, J.; Hou, B.; Zhang, Y. P. *J. Power Sources* **2012**, *213*, 265.
(339) Choi, J. Y.; Higgins, D.; Chen, Z. W. *J. Electrochem. Soc.* **2012**, *159*, B87.
(340) Jahan, M.; Bao, Q. L.; Loh, K. P. *J. Am. Chem. Soc.* **2012**, *134*, 6707.
(341) Guo, S. J.; Zhang, S.; Wu, L. H.; Sun, S. H. *Angew. Chem., Int. Ed.* **2012**, *51*, 11770.
(342) Tributsch, H.; Koslowski, U. I.; Dorbandt, I. *Electrochim. Acta* **2008**, *53*, 2198.
(343) Warner, J. H.; Rummeli, M. H.; Bachmatiuk, A.; Wilson, M.; Buchner, B. *ACS Nano* **2010**, *4*, 470.
(344) Mao, Y.; Yuan, J.; Zhong, J. *J. Phys.: Condens. Matter* **2008**, *20*, 115209.
(345) Olson, T. S.; Pylypenko, S.; Kattel, S.; Atanassov, P.; Kiefer, B. *J. Phys. Chem. C* **2010**, *114*, 15190.
(346) Wang, J.; Zhou, J.; Hu, Y. F.; Regier, T. *Energy Environ. Sci.* **2013**, *6*, 926.
(347) Chen, S.; Zhu, J. W.; Wang, X. *J. Phys. Chem. C* **2010**, *114*, 11829.
(348) Wu, J. J.; Zhang, D.; Wang, Y.; Wan, Y.; Hou, B. R. *J. Power Sources* **2012**, *198*, 122.
(349) Yang, S. B.; Cui, G. L.; Pang, S. P.; Cao, Q.; Kolb, U.; Feng, X. L.; Maier, J.; Mullen, K. *ChemSusChem* **2010**, *3*, 236.
(350) Wang, Z. H.; Du, Y. L.; Zhang, F. Y.; Zheng, Z. X.; Zhang, Y. Z.; Wang, C. M. *J. Solid State Electrochem.* **2013**, *17*, 99.
(351) Yuasa, M.; Yamaguchi, A.; Itsuki, H.; Tanaka, K.; Yamamoto, M.; Oyaizu, K. *Chem. Mater.* **2005**, *17*, 4278.
(352) Yuan, X. X.; Zeng, X.; Zhang, H. J.; Ma, Z. F.; Wang, C. Y. *J. Am. Chem. Soc.* **2010**, *132*, 1754.
(353) Kim, S. K.; Jeon, S. *Electrochem. Commun.* **2012**, *22*, 141.
(354) Fleischm, M.; Korinek, K.; Pletcher, D. *J. Electroanal. Chem.* **1971**, *31*, 39.
(355) Amjad, M.; Pletcher, D.; Smith, C. *J. Electrochem. Soc.* **1977**, *124*, 203.
(356) Singh, R. N.; Singh, A.; Anindita; Mishra, D. *Int. J. Hydrogen Energy* **2008**, *33*, 6878.
(357) Tehrani, R. M. A.; Ab Ghani, S. *Fuel Cells* **2009**, *9*, 579.
(358) Stradiotto, N. R.; Toghill, K. E.; Xiao, L.; Moshar, A.; Compton, R. G. *Electroanalysis* **2009**, *21*, 2627.
(359) Martinez-Huerta, M. V.; Rojas, S.; de la Fuente, J. L. G.; Terreros, P.; Pena, M. A.; Fierro, J. L. G. *Appl. Catal., B* **2006**, *69*, 75.
(360) Zhao, X. H.; Fuji, M.; Shirai, T.; Watanabe, H.; Takahashi, M. *J. Am. Ceram. Soc.* **2011**, *94*, 1167.
(361) Danaee, I.; Jafarian, M.; Forouzandeh, F.; Gobal, F.; Mahjani, M. G. *Int. J. Hydrogen Energy* **2008**, *33*, 4367.
(362) Lv, X. Y.; Xu, Z. H.; Yan, Z. X.; Li, X. H. *Electrocatalysis* **2011**, *2*, 82.
(363) Liu, Q.; Jin, J. T.; Zhang, J. Y. *ACS Appl. Mater. Interfaces* **2013**, *5*, 5002.
(364) Yang, J. H.; Tan, J.; Yang, F.; Li, X. Y.; Liu, X. H.; Ma, D. *Electrochem. Commun.* **2012**, *23*, 13.
(365) Jafarian, M.; Mahjani, M. G.; Heli, H.; Gobal, F.; Heydarpoor, M. *Electrochem. Commun.* **2003**, *5*, 184.
(366) Zhang, L. R.; Zhao, J.; Li, M.; Ni, H. T.; Zhang, J. L.; Feng, X. M.; Ma, Y. W.; Fan, Q. L.; Wang, X. Z.; Hu, Z.; Huang, W. *New J. Chem.* **2012**, *36*, 1108.
(367) Elzatahry, A. A.; Abdullah, A. M.; El-Din, T. A. S.; Al-Enizi, A. M.; Maarouf, A. A.; Galal, A.; Hassan, H. K.; El-Ads, E. H.; Al-Theyab, S. S.; Al-Ghamdi, A. A. *Int. J. Electrochem. Sci.* **2012**, *7*, 3115.

(368) Lambert, T. N.; Davis, D. J.; Lu, W.; Limmer, S. J.; Kotula, P. G.; Thuli, A.; Hungate, M.; Ruan, G. D.; Jin, Z.; Tour, J. M. *Chem. Commun.* **2012**, *48*, 7931.
(369) Tian, X. K.; Zhao, X. Y.; Zhang, L. D.; Yang, C.; Pi, Z. B.; Zhang, S. X. *Nanotechnology* **2008**, *19*, 215711.
(370) Tehrani, R. M. A.; Ab Ghani, S. *J. Electrochem. Soc.* **2008**, *155*, K199.
(371) Zhou, R. F.; Zheng, Y.; Hulicova-Jurcakova, D.; Qiao, S. Z. *J. Mater. Chem. A* **2013**, *1*, 13179.
(372) Liang, Y. Y.; Li, Y. G.; Wang, H. L.; Dai, H. J. *J. Am. Chem. Soc.* **2013**, *135*, 2013.
(373) Yan, X. Y.; Tong, X. L.; Zhang, Y. F.; Han, X. D.; Wang, Y. Y.; Jin, G. Q.; Qin, Y.; Guo, X. Y. *Chem. Commun.* **2012**, *48*, 1892.
(374) Cheng, F. Y.; Zhang, T. R.; Zhang, Y.; Du, J.; Han, X. P.; Chen, J. *Angew. Chem., Int. Ed.* **2013**, *52*, 2474.
(375) Yang, C. C.; Hsu, S. T.; Chien, W. C.; Shih, M. C.; Chiu, S. J.; Lee, K. T.; Wang, C. L. *Int. J. Hydrogen Energy* **2006**, *31*, 2076.
(376) Roche, I.; Chainet, E.; Chatenet, M.; Vondrak, J. *J. Phys. Chem. C* **2007**, *111*, 1434.
(377) Cheng, F. Y.; Su, Y.; Liang, J.; Tao, Z. L.; Chen, J. *Chem. Mater.* **2010**, *22*, 898.
(378) Qian, Y.; Lu, S. B.; Gao, F. L. *Mater. Lett.* **2011**, *65*, 56.
(379) Lee, J. S.; Lee, T.; Song, H. K.; Cho, J.; Kim, B. S. *Energy Environ. Sci.* **2011**, *4*, 4148.
(380) Wu, J. J.; Zhang, D.; Wang, Y.; Wan, Y. *Electrochim. Acta* **2012**, *75*, 305.
(381) Zhang, R. Z.; Chen, W. *J. Mater. Chem. A* **2013**, *1*, 11457.
(382) Paraknowitsch, J. P.; Thomas, A. *Energy Environ. Sci.* **2013**, *6*, 2839.
(383) Liu, Y.; Wu, P. Y. *ACS Appl. Mater. Interfaces* **2013**, *5*, 3362.
(384) Lai, L. F.; Potts, J. R.; Zhan, D.; Wang, L.; Poh, C. K.; Tang, C. H.; Gong, H.; Shen, Z. X.; Jianyi, L. Y.; Ruoff, R. S. *Energy Environ. Sci.* **2012**, *5*, 7936.
(385) Lu, Z. J.; Bao, S. J.; Gou, Y. T.; Cai, C. J.; Ji, C. C.; Xu, M. W.; Song, J.; Wang, R. Y. *RSC Adv.* **2013**, *3*, 3990.
(386) Park, J. E.; Jang, Y. J.; Kim, Y. J.; Song, M. S.; Yoon, S.; Kim, D. H.; Kim, S. J. *Phys. Chem. Chem. Phys.* **2014**, *16*, 103.
(387) Seredych, M.; Bandosz, T. J. *Carbon* **2014**, *66*, 227.
(388) Seredych, M.; Idrobo, J. C.; Bandosz, T. J. *J. Mater. Chem. A* **2013**, *1*, 7059.
(389) Ma, Y. W.; Sun, L. Y.; Huang, W.; Zhang, L. R.; Zhao, J.; Fan, Q. L.; Huang, W. *J. Phys. Chem. C* **2011**, *115*, 24592.
(390) Lee, J. S.; Jo, K.; Lee, T.; Yun, T.; Cho, J.; Kim, B. S. *J. Mater. Chem. A* **2013**, *1*, 9603.
(391) Chen, P.; Xiao, T. Y.; Qian, Y. H.; Li, S. S.; Yu, S. H. *Adv. Mater.* **2013**, *25*, 3192.
(392) Jin, Z. P.; Nie, H. G.; Yang, Z.; Zhang, J.; Liu, Z.; Xu, X. J.; Huang, S. M. *Nanoscale* **2012**, *4*, 6455.
(393) Lyth, S. M.; Nabae, Y.; Islam, N. M.; Kuroki, S.; Kakimoto, M.; Miyata, S. *J. Nanosci. Nanotechnol.* **2012**, *12*, 4887.
(394) Lyth, S. M.; Nabae, Y.; Islam, N. M.; Kuroki, S.; Kakimoto, M.; Miyata, S. *J. Electrochem. Soc.* **2011**, *158*, B194.
(395) Lyth, S. M.; Nabae, Y.; Moriya, S.; Kuroki, S.; Kakimoto, M.; Ozaki, J.; Miyata, S. *J. Phys. Chem. C* **2009**, *113*, 20148.
(396) Zhai, H. S.; Cao, L.; Xia, X. H. *Chin. Chem. Lett.* **2013**, *24*, 103.
(397) Feng, Y. X.; Yao, X. L.; Wang, M.; Hu, Z. P.; Luo, X. G.; Wang, H. T.; Zhang, L. X. *J. Chem. Phys.* **2013**, *138*, 164706.
(398) Ma, Y. W.; Zhang, L. R.; Li, J. J.; Ni, H. T.; Li, M.; Zhang, J. L.; Feng, X. M.; Fan, Q. L.; Hu, Z.; Huang, W. *Chin. Sci. Bull.* **2011**, *56*, 3583.
(399) Yang, S. B.; Feng, X. L.; Wang, X. C.; Mullen, K. *Angew. Chem., Int. Ed.* **2011**, *50*, 5339.
(400) Zhou, Y. F.; Zhang, G. Q.; Chen, J.; Yuan, G. E.; Xu, L.; Liu, L. F.; Yang, F. L. *Electrochem. Commun.* **2012**, *22*, 69.
(401) Unni, S. M.; Bhange, S. N.; Anothumakkool, B.; Kurungot, S. *ChemPlusChem* **2013**, *78*, 1296.
(402) Unni, S. M.; Devulapally, S.; Karjule, N.; Kurungot, S. *J. Mater. Chem.* **2012**, *22*, 23506.
(403) Jeon, I. Y.; Choi, H. J.; Jung, S. M.; Seo, J. M.; Kim, M. J.; Dai, L. M.; Baek, J. B. *J. Am. Chem. Soc.* **2013**, *135*, 1386.
(404) Ahmed, M. S.; Jeon, S. *J. Power Sources* **2012**, *218*, 168.
(405) Wang, L.; Ambrosi, A.; Pumera, M. *Angew. Chem., Int. Ed.* **2013**, *52*, 13818.
(406) Huang, J. Y.; Ding, F.; Yakobson, B. I.; Lu, P.; Qi, L.; Li, J. *Proc. Natl. Acad. Sci. U.S.A.* **2009**, *106*, 10103.
(407) Gass, M. H.; Bangert, U.; Bleloch, A. L.; Wang, P.; Nair, R. R.; Geim, A. K. *Nat. Nanotechnol.* **2008**, *3*, 676.
(408) Gomez-Navarro, C.; Meyer, J. C.; Sundaram, R. S.; Chuvilin, A.; Kurasch, S.; Burghard, M.; Kern, K.; Kaiser, U. *Nano Lett.* **2010**, *10*, 1144.
(409) Meyer, J. C.; Geim, A. K.; Katsnelson, M. I.; Novoselov, K. S.; Booth, T. J.; Roth, S. *Nature* **2007**, *446*, 60.
(410) Mkhoyan, K. A.; Contryman, A. W.; Silcox, J.; Stewart, D. A.; Eda, G.; Mattevi, C.; Miller, S.; Chhowalla, M. *Nano Lett.* **2009**, *9*, 1058.
(411) Jung, I.; Vaupel, M.; Pelton, M.; Piner, R.; Dikin, D. A.; Stankovich, S.; An, J.; Ruoff, R. S. *J. Phys. Chem. C* **2008**, *112*, 8499.
(412) Gunther, S.; Danhardt, S.; Ehrensperger, M.; Zeller, P.; Schmitt, S.; Wintterlin, J. *ACS Nano* **2013**, *7*, 154.
(413) Gunther, S.; Danhardt, S.; Wang, B.; Bocquet, M. L.; Schmitt, S.; Wintterlin, J. *Nano Lett.* **2011**, *11*, 1895.
(414) Ferrari, A. C.; Meyer, J. C.; Scardaci, V.; Casiraghi, C.; Lazzeri, M.; Mauri, F.; Piscanec, S.; Jiang, D.; Novoselov, K. S.; Roth, S.; Geim, A. K. *Phys. Rev. Lett.* **2006**, *97*, 187401.
(415) Cancado, L. G.; Jorio, A.; Ferreira, E. H. M.; Stavale, F.; Achete, C. A.; Capaz, R. B.; Moutinho, M. V. O.; Lombardo, A.; Kulmala, T. S.; Ferrari, A. C. *Nano Lett.* **2011**, *11*, 3190.
(416) Dresselhaus, M. S.; Jorio, A.; Hofmann, M.; Dresselhaus, G.; Saito, R. *Nano Lett.* **2010**, *10*, 751.
(417) Ferrari, A. C. *Solid State Commun.* **2007**, *143*, 47.
(418) Obraztsov, A. N.; Tyurnina, A. V.; Obraztsova, E. A.; Zolotukhin, A. A.; Liu, B. H.; Chin, K. C.; Wee, A. T. S. *Carbon* **2008**, *46*, 963.
(419) Casiraghi, C. *Phys. Status Solidi RRL* **2009**, *3*, 175.
(420) Das, A.; Pisana, S.; Chakraborty, B.; Piscanec, S.; Saha, S. K.; Waghmare, U. V.; Novoselov, K. S.; Krishnamurthy, H. R.; Geim, A. K.; Ferrari, A. C.; Sood, A. K. *Nat. Nanotechnol.* **2008**, *3*, 210.
(421) Hassan, H. M. A.; Abdelsayed, V.; Khder, A. E. R. S.; AbouZeid, K. M.; Terner, J.; El-Shall, M. S.; Al-Resayes, S. I.; El-Azhary, A. A. *J. Mater. Chem.* **2009**, *19*, 3832.
(422) Shin, H. J.; Kim, K. K.; Benayad, A.; Yoon, S. M.; Park, H. K.; Jung, I. S.; Jin, M. H.; Jeong, H. K.; Kim, J. M.; Choi, J. Y.; Lee, Y. H. *Adv. Funct. Mater.* **2009**, *19*, 1987.
(423) Sun, Z. Z.; Yan, Z.; Yao, J.; Beitler, E.; Zhu, Y.; Tour, J. M. *Nature* **2010**, *468*, 549.
(424) Liu, M. M.; Liu, R.; Chen, W. *Biosens. Bioelectron.* **2013**, *45*, 206.
(425) Liu, M. M.; Chen, W. *Biosens. Bioelectron.* **2013**, *46*, 68.
(426) Schultz, B. J.; Patridge, C. J.; Lee, V.; Jaye, C.; Lysaght, P. S.; Smith, C.; Barnett, J.; Fischer, D. A.; Prendergast, D.; Banerjee, S. *Nat. Commun.* **2011**, *2*, 372.
(427) Dennis, R. V.; Schultz, B. J.; Jaye, C.; Wang, X.; Fischer, D. A.; Cartwright, A. N.; Banerjee, S. *J. Vac. Sci. Technol., B* **2013**, *31*, 041204.
(428) Zhao, L. Y.; He, R.; Rim, K. T.; Schiros, T.; Kim, K. S.; Zhou, H.; Gutierrez, C.; Chockalingam, S. P.; Arguello, C. J.; Palova, L.; Nordlund, D.; Hybertsen, M. S.; Reichman, D. R.; Heinz, T. F.; Kim, P.; Pinczuk, A.; Flynn, G. W.; Pasupathy, A. N. *Science* **2011**, *333*, 999.
(429) Shang, N. G.; Papakonstantinou, P.; McMullan, M.; Chu, M.; Stamboulis, A.; Potenza, A.; Dhesi, S. S.; Marchetto, H. *Adv. Funct. Mater.* **2008**, *18*, 3506.
(430) Zhou, X. H.; Chen, Z. X.; Yan, D. H.; Lu, H. B. *J. Mater. Chem.* **2012**, *22*, 13506.
(431) Jiang, Y. Y.; Lu, Y. Z.; Lv, X. Y.; Han, D. X.; Zhang, Q. X.; Niu, L.; Chen, W. *ACS Catal.* **2013**, *3*, 1263.
(432) Xu, Y. X.; Bai, H.; Lu, G. W.; Li, C.; Shi, G. Q. *J. Am. Chem. Soc.* **2008**, *130*, 5856.
(433) Sun, Y. Q.; Li, C.; Shi, G. Q. *J. Mater. Chem.* **2012**, *22*, 12810.

(434) Li, Q. Q.; Zhang, S.; Dai, L. M.; Li, L. S. *J. Am. Chem. Soc.* **2012**, *134*, 18932.
(435) Yang, Z.; Nie, H. G.; Chen, X.; Chen, X. H.; Huang, S. M. *J. Power Sources* **2013**, *236*, 238.
(436) Park, M.; Lee, T.; Kim, B. S. *Nanoscale* **2013**, *5*, 12255.
(437) Zheng, Y.; Jiao, Y.; Ge, L.; Jaroniec, M.; Qiao, S. Z. *Angew. Chem., Int. Ed.* **2013**, *52*, 3110.
(438) Zhang, L. P.; Xia, Z. H. *J. Phys. Chem. C* **2011**, *115*, 11170.
(439) Zhang, L. P.; Niu, J. B.; Dai, L.; Xia, Z. H. *Langmuir* **2012**, *28*, 7542.
(440) Boukhvalov, D. W.; Son, Y. W. *Nanoscale* **2012**, *4*, 417.
(441) Kong, X. K.; Chen, Q. W.; Sun, Z. Y. *ChemPhysChem* **2013**, *14*, 514.
(442) Johll, H.; Wu, J.; Ong, S. W.; Kang, H. C.; Tok, E. S. *Phys. Rev. B* **2011**, *83*, 205408.
(443) Li, Y. G.; Wang, H. L.; Xie, L. M.; Liang, Y. Y.; Hong, G. S.; Dai, H. J. *J. Am. Chem. Soc.* **2011**, *133*, 7296.
(444) Okamoto, Y. *Chem. Phys. Lett.* **2006**, *420*, 382.
(445) Zhou, M.; Zhang, A. H.; Dai, Z. X.; Zhang, C.; Feng, Y. P. *J. Chem. Phys.* **2010**, *132*, 194704.
(446) Groves, M. N.; Chan, A. S. W.; Malardier-Jugroot, C.; Jugroot, M. *Chem. Phys. Lett.* **2009**, *481*, 214.
(447) Akturk, O. U.; Tomak, M. *Phys. Rev. B* **2009**, *80*, 085417.
(448) Liu, X.; Meng, C. G.; Han, Y. *J. Phys. Chem. C* **2013**, *117*, 1350.
(449) Frank, I. W.; Tanenbaum, D. M.; Van der Zande, A. M.; McEuen, P. L. *J. Vac. Sci. Technol., B* **2007**, *25*, 2558.
(450) Lee, C.; Wei, X. D.; Kysar, J. W.; Hone, J. *Science* **2008**, *321*, 385.
(451) Bolotin, K. I.; Sikes, K. J.; Jiang, Z.; Klima, M.; Fudenberg, G.; Hone, J.; Kim, P.; Stormer, H. L. *Solid State Commun.* **2008**, *146*, 351.
(452) Kuila, T.; Bose, S.; Khanra, P.; Mishra, A. K.; Kim, N. H.; Lee, J. H. *Biosens. Bioelectron.* **2011**, *26*, 4637.
(453) Liu, Y. X.; Dong, X. C.; Chen, P. *Chem. Soc. Rev.* **2012**, *41*, 2283.
(454) Zhu, S. J.; Zhang, J. H.; Tang, S. J.; Qiao, C. Y.; Wang, L.; Wang, H. Y.; Liu, X.; Li, B.; Li, Y. F.; Yu, W. L.; Wang, X. F.; Sun, H. C.; Yang, B. *Adv. Funct. Mater.* **2012**, *22*, 4732.
(455) Pan, D. Y.; Guo, L.; Zhang, J. C.; Xi, C.; Xue, Q.; Huang, H.; Li, J. H.; Zhang, Z. W.; Yu, W. J.; Chen, Z. W.; Li, Z.; Wu, M. H. *J. Mater. Chem.* **2012**, *22*, 3314.
(456) Wu, Z. S.; Zhou, G. M.; Yin, L. C.; Ren, W.; Li, F.; Cheng, H. M. *Nano Energy* **2012**, *1*, 107.
(457) Leger, J. M. *J. Appl. Electrochem.* **2001**, *31*, 767.
(458) Yoo, E.; Okata, T.; Akita, T.; Kohyama, M.; Nakamura, J.; Honma, I. *Nano Lett.* **2009**, *9*, 2255.
(459) Xin, Y. C.; Liu, J. G.; Zhou, Y.; Liu, W. M.; Gao, J. A.; Xie, Y.; Yin, Y.; Zou, Z. G. *J. Power Sources* **2011**, *196*, 1012.
(460) Kakaei, K.; Zhiani, M. *J. Power Sources* **2013**, *225*, 356.
(461) Bong, S.; Kim, Y. R.; Kim, I.; Woo, S.; Uhm, S.; Lee, J.; Kim, H. *Electrochem. Commun.* **2010**, *12*, 129.
(462) Wang, S. Y.; Jiang, S. P.; Wang, X. *Electrochim. Acta* **2011**, *56*, 3338.
(463) Jha, N.; Jafri, R. I.; Rajalakshmi, N.; Ramaprabhu, S. *Int. J. Hydrogen Energy* **2011**, *36*, 7284.
(464) Yu, X. W.; Pickup, P. G. *J. Power Sources* **2008**, *182*, 124.
(465) Yang, S. D.; Shen, C. M.; Lu, X. J.; Tong, H.; Zhu, J. J.; Zhang, X. G.; Gao, H. J. *Electrochim. Acta* **2012**, *62*, 242.
(466) Huang, H. J.; Wang, X. *J. Mater. Chem.* **2012**, *22*, 22533.
(467) Wang, Y.; Liu, H. L.; Wang, L.; Wang, H. B.; Du, X.; Wang, F.; Qi, T.; Lee, J. M.; Wang, X. *J. Mater. Chem. A* **2013**, *1*, 6839.
(468) Jin, T.; Guo, S. J.; Zuo, J. L.; Sun, S. H. *Nanoscale* **2013**, *5*, 160.
(469) Pandey, R. K.; Lakshminarayanan, V. *J. Phys. Chem. C* **2009**, *113*, 21596.
(470) Wang, S. Y.; Manthiram, A. *Electrochim. Acta* **2013**, *88*, 565.
(471) Zhao, H.; Yang, J.; Wang, L.; Tian, C. G.; Jiang, B. J.; Fu, H. G. *Chem. Commun.* **2011**, *47*, 2014.
(472) Lamy, C.; Rousseau, S.; Belgsir, E. M.; Coutanceau, C.; Leger, J. M. *Electrochim. Acta* **2004**, *49*, 3901.
(473) Simoes, F. C.; dos Anjos, D. M.; Vigier, F.; Leger, J. M.; Hahn, F.; Coutanceau, C.; Gonzalez, E. R.; Tremiliosi, G.; de Andrade, A. R.; Olivi, P.; Kokoh, K. B. *J. Power Sources* **2007**, *167*, 1.
(474) Fang, X.; Wang, L. Q.; Shen, P. K.; Cui, G. F.; Bianchini, C. *J. Power Sources* **2010**, *195*, 1375.
(475) Jiang, F. X.; Yao, Z. Q.; Yue, R. R.; Du, Y. K.; Xu, J. K.; Yang, P.; Wang, C. Y. *Int. J. Hydrogen Energy* **2012**, *37*, 14085.
(476) Singh, R. N.; Awasthi, R. *Catal. Sci. Technol.* **2011**, *1*, 778.
(477) Sheng, W. C.; Gasteiger, H. A.; Shao-Horn, Y. *J. Electrochem. Soc.* **2010**, *157*, B1529.
(478) Neyerlin, K. C.; Gu, W. B.; Jorne, J.; Gasteiger, H. A. *J. Electrochem. Soc.* **2007**, *154*, B631.
(479) Carmo, M.; Paganin, V. A.; Rosolen, J. M.; Gonzalez, E. R. *J. Power Sources* **2005**, *142*, 169.
(480) Genorio, B.; Strmcnik, D.; Subbaraman, R.; Tripkovic, D.; Karapetrov, G.; Stamenkovic, V. R.; Pejovnik, S.; Markovic, N. M. *Nat. Mater.* **2010**, *9*, 998.
(481) Izhar, S.; Nagai, M. *Catal. Today* **2009**, *146*, 172.
(482) Elezovic, N. R.; Babic, B. M.; Vracar, L. M.; Radmilovic, V. R.; Krstajic, N. V. *Phys. Chem. Chem. Phys.* **2009**, *11*, 5192.
(483) Uchida, H.; Izumi, K.; Aoki, K.; Watanabe, M. *Phys. Chem. Chem. Phys.* **2009**, *11*, 1771.
(484) Gotz, M.; Wendt, H. *Electrochim. Acta* **1998**, *43*, 3637.
(485) Yeager, E. *Electrochim. Acta* **1984**, *29*, 1527.
(486) Coutanceau, C.; Crouigneau, P.; Leger, J. M.; Lamy, C. *J. Electroanal. Chem.* **1994**, *379*, 389.
(487) Sato, J.; Higurashi, K.; Fukuda, K.; Sugimoto, W. *Electrochemistry* **2011**, *79*, 337.
(488) Wang, D. L.; Xin, H. L.; Wang, H. S.; Yu, Y. C.; Rus, E.; Muller, D. A.; DiSalvo, F. J.; Abruna, H. D. *Chem. Mater.* **2012**, *24*, 2274.
(489) Gotoh, K.; Kinumoto, T.; Fujii, E.; Yamamoto, A.; Hashimoto, H.; Ohkubo, T.; Itadani, A.; Kuroda, Y.; Ishida, H. *Carbon* **2011**, *49*, 1118.
(490) Toh, R. J.; Poh, H. L.; Sofer, Z.; Pumera, M. *Chem.-Asian J.* **2013**, *8*, 1295.
(491) Bashyam, R.; Zelenay, P. *Nature* **2006**, *443*, 63.
(492) Wang, S. Y.; Yu, D. S.; Dai, L. M.; Chang, D. W.; Baek, J. B. *ACS Nano* **2011**, *5*, 6202.
(493) Zhang, C. Z.; Hao, R.; Liao, H. B.; Hou, Y. L. *Nano Energy* **2013**, *2*, 88.
(494) He, C. Y.; Li, Z. S.; Cai, M. L.; Cai, M.; Wang, J. Q.; Tian, Z. Q.; Zhang, X.; Shen, P. K. *J. Mater. Chem. A* **2013**, *1*, 1401.
(495) Zhao, Y.; Hu, C. G.; Hu, Y.; Cheng, H. H.; Shi, G. Q.; Qu, L. T. *Angew. Chem., Int. Ed.* **2012**, *51*, 11371.
(496) Wu, J. J.; Zhang, D.; Wang, Y.; Hou, B. R. *J. Power Sources* **2013**, *227*, 185.
(497) Lee, K. R.; Lee, K. U.; Lee, J. W.; Ahn, B. T.; Woo, S. I. *Electrochem. Commun.* **2010**, *12*, 1052.
(498) Lin, Z. Y.; Waller, G.; Liu, Y.; Liu, M. L.; Wong, C. P. *Adv. Energy Mater.* **2012**, *2*, 884.